TUNABLE ENCAPSULATIONS: DROPLET-BASED MICROFLUIDICS FOR THE
EXPANSION OF BIODEGRADABLE POLYMER TECHNOLOGIES

BY

DANIELLE D. HARRIER

DISSERTATION

Submitted in partial fulfillment of the requirements
for the degree of Doctor of Philosophy in Chemical Engineering
in the Graduate College of the
University of Illinois Urbana-Champaign, 2022

Urbana, Illinois

Doctoral Committee:

       Associate Professor Damien S. Guironnet, Chair
       Professor Paul J. A. Kenis, Co-Chair
       Associate Professor Cecilia Leal
       Professor Charles M. Schroeder

ABSTRACT

Environmental plastic pollution has become a cause for concern over the past decades, motivated by an alarming accumulation of plastics in landfills and oceans. Biodegradable polymers have been gaining momentum as substitutes for non-biodegradable plastics as more sustainable and environmentally-friendly alternatives. Biodegradable polymers are synthetic compounds susceptible to degradation over time into environmentally acceptable substances. Despite the successful commercialization of many biodegradable thermoplastics, to date, there are still limitations in the applications. For example, aqueous polymer dispersions (i.e. emulsions) of biodegradable polymers are inaccessible due to the incompatibility of the emulsion polymerization process and the polymerization chemistry of biodegradable polymers. Biodegradable polymers are synthesized via a ring-opening polymerization (ROP) process which is water-sensitive. The water sensitivity of the polymerization chemistry prevents any technique using water as a solvent or dispersion media, which ultimately sets a limit on the polymeric material accessible. This thesis describes a droplet-based microfluidic encapsulation strategy that protects the water-sensitive catalyst from the aqueous phase, allowing the ROP to proceed in an aqueous dispersion. The success of this approach relies on simultaneous precise control of the kinetics of polymerization, the rate of mass transfer rates, and fluid mechanics. We report, for the first time, the production of biodegradable polymer particles dispersed in water. In this work, we systematically investigated the process and formulation parameters that govern the stability of the micro-droplets during generation, flow, and collection. More specifically, we tune droplet viscosity, surface tension, and hydrophobicity to further shield the ROP catalyst in the aqueous dispersion. Herein, a set of design rules for the tuning of catalyst protection efficiency within the aqueous dispersion are detailed, which ultimately allowed us to perform another water-sensitive ROP to produce polyether particles

in water. To demonstrate the power and versatility of the encapsulation methodology, we crosslinked both chemistries to produce biodegradable elastomers and crosslinked polyethers in continuous flow. This project identifies the fundamental guiding principles to encapsulate water-sensitive polymerization catalysts to yield novel spherical polymer particles dispersed in water.

ACKNOWLEDGMENTS

Graduate school has been such a transformative, challenging, and overall exciting five years. The work in this thesis would not have been possible without my amazing support system including mentors, family, and friends. First, I would like to thank my research advisor, Damien Guironnet, who fostered an environment where I could grow as an independent researcher. Our relationship changed a lot over time, but I learned so much and developed a diverse set of skills with his help and guidance. Thank you, Damien, for letting me ask a million questions, listening to me, challenging me, and helping me build my confidence. I would also like to thank my co-advisor, Paul Kenis, whose door was always open to guide me personally and professionally. In addition to my current advisors here at UIUC, I have had many other advisors along my academic journey from the University of New Mexico, Los Alamos National Laboratory, and the Wyss at Harvard Medical- Dr. Gabriel Montaño, Dr. Julianna Fessenden-Rahn, Dr. Jaimie Gomez, and Dr. Adama Sesay-your guidance through my scientific trajectory has fostered a sense of curiosity and love for science. I would also like to thank my thesis committee members, Cecilia Leal and Charles Schroeder, who always came with thought-provoking questions and constructive feedback.

To the past and present members of the Guironnet Group, aka G Gang, thank you so much for making the lab a supportive and collaborative environment. Dr. Nicholas Wang, Dr. Alexander Horn, Keelee McCleary-Petersen, Susannah Miller, Yash Kamble, Vanessa DaSilva, Kaitlyn Wiegand, Brian Van Dyke, Jerry Rong, Dr. Micheal Hyatt, Dr. Tianwei Yan, Dr. Dylan Walsh, and Dr. Camille Boucher-Jacobs. The lab culture that we have created over the years is something to be proud of, and I cannot wait to see what each one of you accomplishes in the future. I

specifically would like to thank Nick and Alex for being amazing friends inside and outside of the lab. Your optimism and humor made the tough days in the lab a little better!

My most important support system was 1,199 miles away in Espanola, New Mexico. Thank you to my parents, Debbie and Harvie Harrier, I would not be the woman I am today if I wasn't your daughter. Thank you, Mom, for teaching me how to be a loving and genuine woman and always reminding me to "be sweet". Thank you, Dad, for always being my number one role model; you are the smartest man I know! Thank you to my siblings, Colin, Cameron, Joseph, Jovanna, and Devon, for always being interested in my work and telling me millions of times that you are proud of me. To my nieces, Kianna, Alyissa, and Jadzia, being a good role model for you girls has motivated me more than you know. To my best friend, Carolina Cecilia Martinez, I wish you could have been here to see me finish my Ph.D. Since we were little girls, you were my biggest fan and believed in me when I didn't believe in myself. I feel all your love and support shining through your family- Jimena, Cami, Lorena, and Gene. To Jimena, you bring pieces of Caro back to me with your advice, words of wisdom, and friendship. Family is everything to me—and without it, I would be lost.

To all my friends that have supported me throughout this journey, I could have never done it without you! To my New Mexico crew, Maia, Peter, CJ, Kyra, Olivia, Elyse, Kristin, Danielle, Tracy, Analisa, Estevan, Zach, Rachel, Cris, Valeria, Nick, Daniel, and Sammi, thank you for always making time to see me over the holidays, checking in on me to make sure that I was still sane in graduate school, and for encouraging me when I had my doubts. To Maia and Peter specifically, you two held my heart together when I lost Caro and your love and support helped me through the toughest year of my life. To my Illinois crew, Raul, Aleczandria, Rose, Nick, Hanna, James, Ale, Zeynep, Chris, Eddie, Isamar, Howard, DJ, Tony, and Uzoma, you all made

graduate school way more fun than it had any business being. From wine nights, Star Karaoke, Halloween disco, toga parties, to weekends escaping to Chicago, I have so many fond memories of my time in Illinois thanks to each one of you. To Raul, thank you for helping me to grow, laugh, and be happy-you have balanced and brightened my whole world. To Alec, thank you for always being an inspiration to me and motivating me to push for social change, stand up for myself, and fight for things I believe in. To Rose, I know I can always trust you to be in my corner, buy the plane ticket for all the last-minute vacations, and be a solid rock for me to fall back on. To Nick and Hanna, thank you for being the therapists I needed, always opening the next bottle of wine, and enriching my cooking skills. I feel so lucky to have so many people to help me celebrate good times and provide support during bad times. You have increased my sense of belonging and purpose.

They say it takes a village to raise a child, well the same can be said for a Ph.D. I am so excited for my next steps into an exciting future, especially because I know I have the best support system behind me. I love you all.

to Carolina Cecilia Martinez

"Long live all the mountains we moved..."

TABLE OF CONTENTS

CHAPTER 1: Ring-Opening Polymerization in Flow

1.1 Chapter Overview

Herein, I will give a brief overview of the theory surrounding the ring-opening polymerization (ROP) of heterocyclic monomers, including the general mechanisms, the thermodynamics and kinetics governing ROP, and the effect of monomer ring-strain. Then I will focus more specifically on the organocatalyzed ROP of cyclic esters and how these polymerizations have been implemented in flow. I will give a brief overview of current microflow technologies being employed to expand the field of polymer science and catalysis. Lastly, I will call attention to the current limitations of performing ROP in flow and outline the efforts we have made to overcome some of the limitations and broaden the types of polymeric materials attainable with ROP in flow with the dissertation overview.

1.2 Introduction to Ring-Opening Polymerization of Heterocyclic Monomers

The ring-opening polymerization (ROP) of heterocyclic monomers is a form of chain-growth polymerization. Heterocyclic monomers have at least two different elements within their ring structure and whose polymerization results in polymers containing at least one heteroatom within the polymer backbone. The most common elements found in heterocycles are oxygen, nitrogen, sulfur, phosphorous, and silicon, *Figure 1.1a*. A diverse range of commercially important polymers that we use in our daily lives relies on the ROP of heterocycles, including biodegradable plastics, polyethylene glycol for PEGylation of pharmaceuticals, and silicon materials.[1–9] Many different catalysts facilitate the ROP process of these monomers, including organic, inorganic, organometallic, and enzymes.[10,11] Given the large family of heterocyclic monomers and corresponding ROP catalysts, there are many mechanisms by which ROP can

proceed. The three most common mechanisms are anionic, cationic, and coordination insertion, *Figure 1.1b*.

Figure 1.1: a) Common heterolytic monomers containing oxygen, nitrogen, sulfur, phosphorous, and silicon atoms in their rings. The opening of these cyclic monomer rings results from a bond cleavage denoted by the dashed lines. b) Ring-opening polymerization mechanisms include anionic, cationic, and coordination-insertion, shown here with the ROP of lactones. *Figure reproduced from Guironnet et al. ACS Catal. 2019.*[12]

The driving force for the polymerization of the majority of cyclic monomers is their ring strain, which stems from bond stretching, bond compression, non-disordered bond angles, repulsion, and nonbonding interactions between substituents.[13] Polymerization of cyclic monomers leads to the loss of translational degrees of freedom resulting in an entropy decrease.

Three and four-membered rings are the most strained cyclic monomers, as they experience the most severe angle and bond deformations. Five and six-membered rings experience a minor strain from conformation interactions, some of which are ultimately unable to undergo ROP. As ring size increases to larger membered rings, the resulting ring strain is decreased due to the flexibility of the ring, leading to an increase in polymerization entropy. The polymerization rate of different cyclic monomers can depend on the steric hindrance of the monomers, the additional strain imposed on the cyclic monomer via interactions, and the polymerization mechanism.[14]

The conversion of monomers into macromolecules, both linear and more complex topologies, must be allowed thermodynamically and kinetically. In other words, the monomer-macromolecule equilibrium has to be shifted to the right-hand side (macromolecule), and the corresponding polymerization mechanism enables the conversion of monomer molecules to polymer repeating units within a feasible polymerization time.[15] Simply, the reaction of a monomer with an initiator should lead to an active species capable of adding new monomer molecules faster than any side reactions, terminations, or transfers, ***Scheme 1.1***. Polymerizations that can reliably control molecular weight (MW, where M_n=number average MW, M_w=weighted average MW, and M_0=monomer MW) and produce a narrow molecular weight distribution $(Đ = \frac{M_w}{M_n} < 1.2)$ are generally desired because it offers precision and control in macromolecular synthesis. Usually, MW control can be obtained from a living polymerization. The IUPAC definition of a living polymerization is "a chain polymerization from which chain transfer and chain termination are absent. In many cases, the rate of chain initiation is fast compared with the rate of chain propagation, so that the number of kinetic-chain carriers is essentially constant throughout the polymerization."[16] Several ROPs can be realized as living polymerization, where they generally exhibit first-order kinetics, a MW versus degree of polymerization (DP, $DP = \frac{MW_{polymer}}{MW_{monomer}}$) that

follows a linear regression, and the DP is proportional to conversion ($X = \frac{M_n - M_0}{M_0}$). If there are any

deviations from the linear dependence, it is a sign of slow initiation or undesired side reactions.

Scheme 1.1: General ring-opening polymerization reaction scheme showing initiation, propagation, termination, and transfer of the polymer chain.
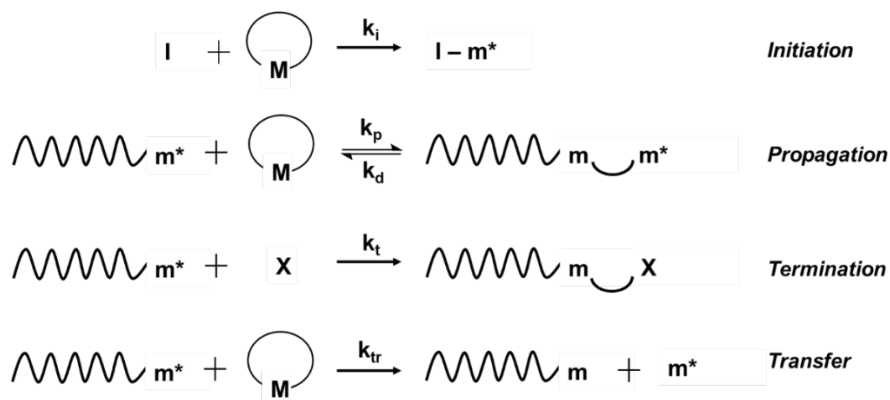
Accessing a living ROP has enabled the controlled synthesis of advanced architecture, including graft, branched, and star polymers.[17] When compared to step-growth polymerizations, for example, high MW is only obtained at the end of the process by long oligomers reacting with one another, and molecular species of any length exist throughout the reaction leading to an increase in dispersity. Additionally, step-growth polymerization depends on the conversion and stoichiometric balance, which is difficult to control. In a living ROP, where the rates of termination (k_t) and transfer (k_{tr}) are negligible, there is an invariant number of propagating chains which results in the generation of nearly monodisperse polymers at a high DP.[18] The catalyst of choice plays a critical role in controlling the selectivity of the reaction for macromolecule production over side reactions and in enhancing the reaction rate. A living polymerization will enable excellent

control over molecular weight, polymer dispersity, architecture, stereochemistry and topology, functionality, and the number of polymer end groups.

Organocatalytic ROP of Cyclic Esters

Organocatalysts for ROP have gained much momentum due to their commercial availability, lower toxicity, ease-of-use, and competitive rates and selectivities to metal-based systems.[19,20] This low toxicity suppresses the need for the removal of the metal impurities from the resulting polymers, which has opened up many applications in biomedical and microelectronic applications.[21] These catalysts also have enhanced substrate tolerance and are stable in the presence of trace impurities.[22] The substance tolerance helps prevent expensive and harsh reaction conditions.[23] Additionally, these organic catalysts are tolerant to a range of solvents, reaction conditions, and monomers which provide new opportunities for the controlled synthesis of macromolecules.[24]

For simplicity, we will focus on the organocatalytic ROP of lactones that produce polymers for the entirety of this chapter, ***Figure 1.2***. The ROPs of these cyclic monomers produce polyesters, which give rise to an important class of polymers with a wide range of applications including biomedical applications, food packaging, composite materials, coatings, and adhesives.[2,25–28] Polylactide (PLA), polyglycolide (PGA), polycaprolactone (PCL), and polylactide-co-glycolide (PLGA) have been identified as an essential class of biomaterials due to their excellent biodegradability and biocompatibility.[1] These sustainable and environmentally responsible polymeric materials offer alternatives to traditional non-biodegradable polymers as they have been shown to have similar material characteristics.[3] Overall, the precision of organocatalyzed ROP of

lactones has enabled the synthesis of polymers with controlled composition, topology, and incorporation of a wide range of functionalities.[29–37]
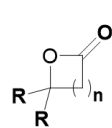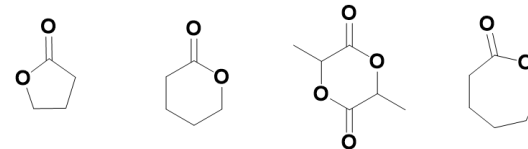

Figure 1.2: List of popular ether and ester monomers and their typical ROP mechanisms. A few of the most commercially relevant cyclic esters include γ-butyrolactone, δ-valerolactone, L-lactide, and ε-caprolactone.

Many organocatalysts are utilized for ROP, including guanidine, amidine, thiourea, and urea catalysts, which are very effective for enhancing ROP rate and selectivity and have provided a new strategy for macromolecular design, **_Figure 1.3_**. Guanidine and amidine organocatalysts like 1,5,7-Triazabicyclo[4.4.0]dec-5-ene (TBD), N-methyl-TBD (MTBD), and 1,8-diazabicyclo[5.4.0]undec-7-ene (DBU) are effective at ROP and produce polymers with high end-group fidelity, predictable molecular weight, and livingness.[38–46] TBD has enhanced activity over MTBD and DBU which is attributed to its bifunctionality. Various thioureas and ureas also perform bifunctional activation of the cyclic ester by an electrophile and the initiator by a nucleophile to activate ring-opening and produce polymers with very narrow dispersity.[47–50] Specifically, several typical monomers, δ-valerolactone, L-lactide, and ε-caprolactone have been polymerization via urea anion catalysts and shown to reach high conversion in seconds with excellent control.[50] In conclusion, the organocatalyzed ROP of cyclic esters produces a variety of important polymers with controlled molecular weights, narrow dispersity, and architectural control.

ORGANOCATALYSTS AND PRECISION POLYMER SYNTHESIS

Guanidine and Amidine

Thio(urea) anion catalysts

well-defined linear

block copolymers

heteroatam backbones

architecture control

functionalized

$M^{\oplus} = K^{\oplus}$ or $Na^{\oplus}$
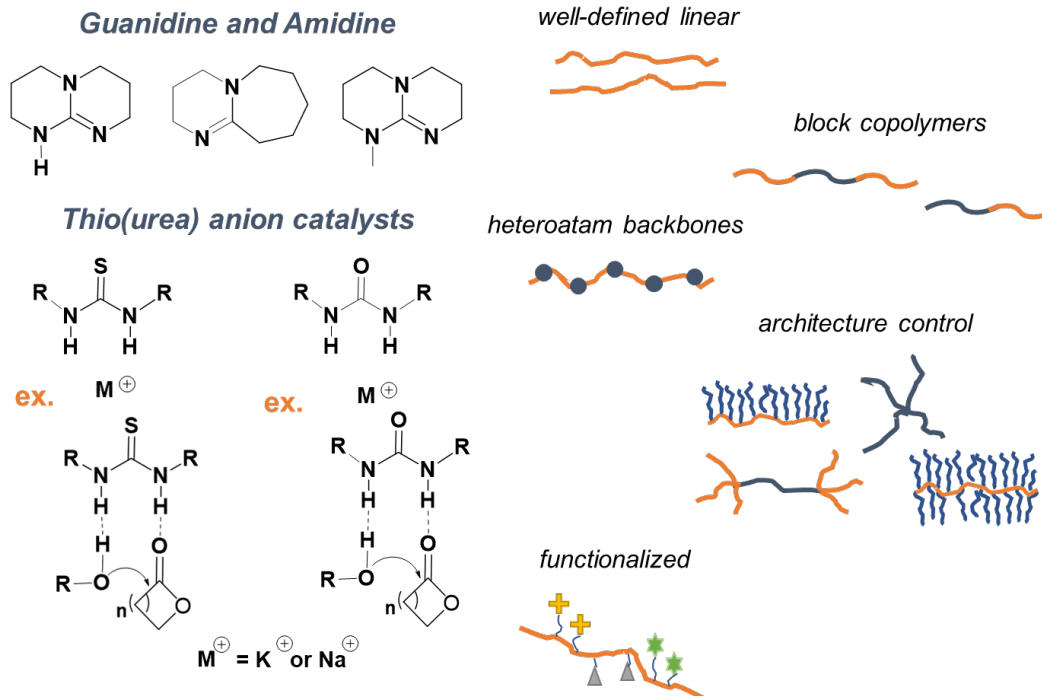
Figure 1.3: A few organocatalysts for the ring-opening polymerization of cyclic esters. These catalysts can produce a diverse range of polymers including well-defined linear, block copolymers, functionalized, and complex architecture.

1.3 Microflow Reactors and Ring-Opening Polymerization

Flow chemistry within microflow reactors is the process of performing chemical reactions within a micron-scale (i.e. ID < 1mm) tube or pipe in a continuously flowing stream. A simplified microflow system is depicted in *Figure 1.4*, where the reaction components are supplied to a mixing junction, come in contact with one another, and react along the length of the reactor. The combination of ROP and microflow technology is increasingly relevant to industry and academia. Improved reaction condition control can be achieved when employing ROP in flow because the surface area to volume ratio is dramatically increased when the dimensions of a reactor are <1mm. The improved heat and mass transfer enable the implementation of faster ROP formulations, where heat transfer management within a traditional batch reactor (i.e. vials, bound-bottom flasks, etc.)

7

would result in a loss of reaction condition control due to exothermic dissipation.[51,52] The continuous flow aspect of these microflow reactors permits high-throughput applications that can be employed on an industrial scale. As an additional advantage, the small reaction volume (i.e. device internal volume) improves reaction process safety, which allows highly toxic or exothermic reactions to be performed safely at the benchtop.[53]
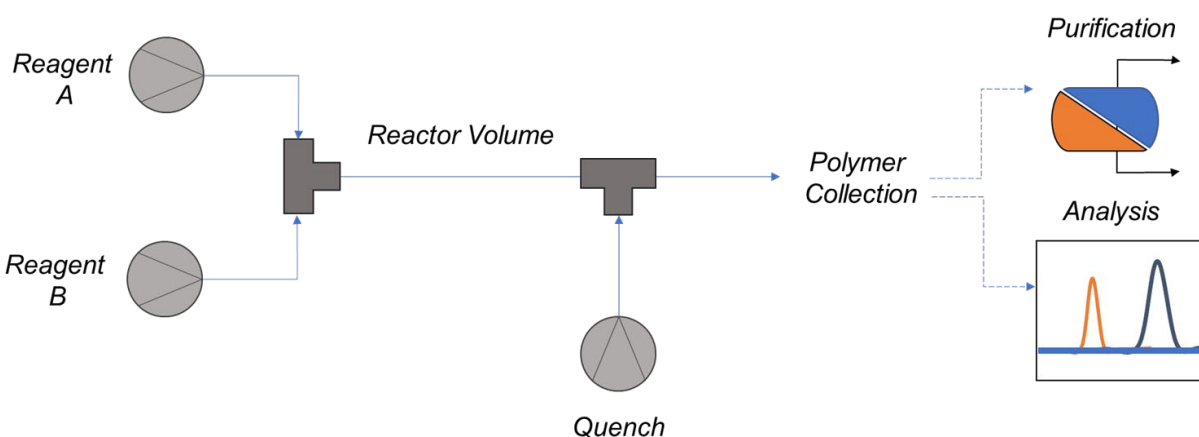
Figure 1.4: Basic components necessary to perform ring-opening polymerization in flow. Multiple reagent streams can be supplied separately until they meet a junction where they come in contact and mix along the reactor volume before reaching the quenching solution. Post polymer collection the polymer can be purified if needed and analyzed.

Understanding dispersion and mixing within the volume of microflow reactors is a crucial factor in ensuring the process's success. Most microflow systems operate at small Reynolds numbers and exhibit laminar flow with a parabolic velocity profile.[54] Fluid at the center of the channel spends half as much time in the reactor compared to the fluid near the walls. When co-flowing solutions within the microreactor volume, the lack of turbulence and eddies when operating in laminar flow means mixing within the small tubing diameters relies on diffusion rather than convection. The Damkohler number ($Da = \frac{rate\ of\ reaction}{rate\ of\ diffusion}$) describes the relative rates of

reaction and mass transfer via diffusion.[55] When the Da is greater than one, the rate of reaction is faster and the system will experience a concentration gradient. In microflow systems, the rate of diffusion can be modulated by optimizing the distance of diffusion (i.e. tubing diameter), length of tubing, and/or residence time within the reactor. The smaller the tubing diameter the shorter the axial diffusion time, and if the tubing length is long it allows a fully developed plug flow to be achieved.[56] The residence time $\left(rt = \frac{Reactor\ Volume\ (V)}{Flow\ Rate\ (Q)} \right)$ of the reagents within the reactor is easily controlled in the microflow system by changing the flow rate of the reagents into the reactor volume. Through a deep understanding of reactor design and fluid dynamics heat transfer, reaction time, and reactant mixing can be easily controlled within microflow systems, which allows unique polymerization conditions unaccessible in batch.

ROP of Polyesters in Microflow

Research utilizing ROP in flow has shown improved chemistry control and precise macromolecular synthesis. Simple tubular reactors have been utilized for ROP in continuous flow since the early 2000s. The first example of ROP in the literature was the ROP of n-carboxyanhydride (NCA).[57] In batch, the ROP of NCA is very sensitive to concentration gradients of reagents, which leads to an increase in dispersity of the polymer product (Mn= 40.2 kg mol^{-1} Đ =1.56). It was shown that moving from batch to flow enabled strict control of the chemical reaction to produce a polymer with high molecular weight (Mn=40 kg mol^{-1}) and low dispersity (Đ =1.17). Regarding cyclic esters, our monomers of interest, the ROP of CL in a microflow, was first performed with tin(II)trifluoromethanesulfonate showing better polymerization control compared to batch and improved reaction rates.[57] Similarly, organocatalyzed ROP of CL and VL via TBD in microflow resulted in a 4-7 times increase of the apparent rate constants compared to batch.[57] Well-

defined functional polyesters with high end-group fidelity were also achieved under microflow conditions.[58] The use of microflow reactors allows rapid, extensive screening of reaction conditions and formulations.[59] Next-generation microflow reactors aimed to expand the complexity of the polymeric materials attainable and to enable the production of novel materials by employing engineering principles to ROP chemistry.[53]

Our group has explicitly exploited the ROP of cyclic esters in microflow to generate bottlebrush polymers (i.e. large cylindrical macromolecules with polymer side chains densely grafted to a linear backbone).[60] The precise control over the bottlebrush macromolecular chemical composition and shape was only possible using a microflow reactor where $L \gg R$ (L=length of the reactor, R=radius of the reactor). The design and synthesis of macromolecules with 3D geometries were possible through a deep understanding of fluid mechanics and reactor engineering. For example, when you have a very long tubular reactor, you can access a Taylor dispersion regime where the diffusion in the axial direction is insignificant and radial diffusion causes homogenization of the solutes within the tube yielding a plug flow.[61] This work is a leading example of how bringing together engineering principles to microflow and reactor design can push the boundaries of polymer science.

Similarly, other groups have applied reactor design principles to microflow reactors to perform block copolymerization of lactones via sequential monomer introduction.[62–64] They could produce well-defined block copolymers more easily and rapidly within microflow tubular reactors than batch reactors and alter molecular weight and dispersity through fluid flow optimization. However, flow rates are not the only parameter that influences the molecular weight and dispersity of the polymer. Tubing diameter, tubing length, residence time, and viscosity have all been shown

to impact the ROP of cyclic esters in microflow reactors.[65] Increasing tubing diameter, decreasing retention time, and increasing viscosity all result in the broadening of the dispersity of the polymer.

1.4 Limitations and Areas for Improvement for the ROP of Polyesters in Flow

Even with all of the current advances on the ROP of polyesters in flow, some limitations in polymer topology and/or morphology remain. For instance, we aim to tackle the lack of synthetic techniques allowing the ROP of cyclic esters in an aqueous dispersion and the lack of processability of viscous polymer solutions to access novel crosslinked polymeric materials.

ROP of Cyclic Esters in an Aqueous Dispersion

Biodegradable plastics seem an obvious solution to the plastic waste problem; however, their current properties lag behind fossil fuel-based polymers, limiting their applications. Designing polymers and developing green polymerization processes that are safe, decrease pollution, and increase energy efficiency is an important topic in modern chemistry.[66] All organocatalyzed ROPs in flow use organic solvents instead of a benign solvent like water, which is environmentally and biologically friendly. However, the ROP of cyclic esters is very water-sensitive, and excess water quenches the polymerization. Without the possibility of using water as a reaction solvent, there is a range of polymerization techniques that remain incompatible with ROP; for example, emulsion polymerization of cyclic esters (i.e. biodegradable latex).

The need for biodegradable polymers has been gaining momentum over the past decade, motivated by the alarming accumulation of plastics in landfills and our oceans.[8,67] Despite the great synthetic achievements made, highlighted by the commercialization of many different biodegradable thermoplastics, there has been one area of plastic material that has been untouched

by the shift to biodegradability, and that is polymer latex. The main technical challenge lies in the water incompatibility of the catalytic ring-opening polymerization (ROP) of a cyclic ester with emulsion polymerization (the traditional method to synthesize biodegradable polymers). Emulsion polymerization is a key industrial process that offers unique technological advantages over other polymerization methods; thus, it is frequently used to manufacture several commercial polymers for applications in coatings, paints, synthetic rubber, and thermoplastic elastomers. Emulsion polymerization production accounts for over 21 million tons of polymers produced globally per year and has a global growth rate between 3-6% annually.[68] Today none of the polymers produced via emulsion polymerization are biodegradable, which means that they eventually accumulate in landfills.[69] The end-of-life fate of these materials has led to the question of how we can meet the needs of the polymer industry without compromising the environment for future generations.

Protecting the ROP catalyst from water during emulsification appears as a simple way to synthesize biodegradable latex. Miniemulsion polymerization has previously been successfully implemented for performing catalytic polymerization in water with catalysts that are only moderately compatible with water.[70,71] In the miniemulsion process, the catalyst and the monomer are dissolved in a hydrophobic solvent mixture that is dispersed using high shear into nanodroplets stabilized by a large amount of surfactant. The polymerization proceeds independently in each droplet to yield the desired nanoparticle dispersion. During the emulsification process, the catalyst/initiator is exposed to both the water, which will lead to deactivation, and to the monomer, which will initiate polymerization.[72] Consequentially, it is necessary to ensure that the catalysts are water-compatible and that the polymerization remains slow or completely stalled during the emulsification phase.[73,74] These two requirements make performing ROP in miniemulsion inherently impossible, which motivated us to develop an alternative encapsulation strategy for

performing the ROP in the presence of water. Our approach utilizes a microflow encapsulation strategy where the dispersed phase, comprised of both a monomer and a catalyst solution, is mixed inline before meeting the immiscible continuous phase at a junction to form micrometer size reactive droplets, **Chapter 2**. The polymerization starts directly upon the catalyst and monomer solutions coming in contact and continues in the droplet until water diffuses throughout the organic layer and fully deactivates the catalyst, *Figure 1.5*.
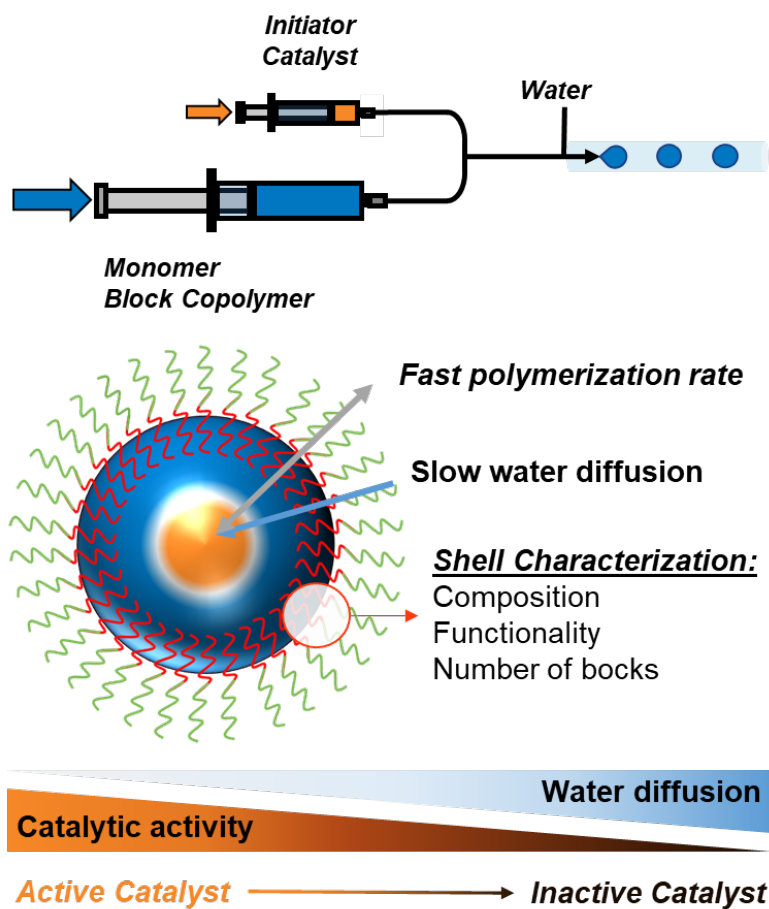

Figure 1.5: Methodology of a microfluidic device that produces droplet reactors for ring-opening polymerization in water. The rate of polymerization must be faster than the diffusion of water to promote polymerization while in the aqueous phase. The shell of the droplet can be tuned to form a protective barrier.

The encapsulation of the water-sensitive catalyst within the core of hydrophobic droplets allows polymerization to progress a small extent before the droplets are formed. The polymerization time is thus directly limited by the rate of diffusion of water after droplet formation. Therefore, this approach requires the use of a fast polymerization catalyst, as we want the polymerization to proceed to completion before the water diffuses to the core of the droplet deactivating the catalyst. We utilize a co-flow microfluidic technique for its consistent microdroplet formation and high throughput production capabilities to demonstrate that the ROP of cyclic esters can be performed in an aqueous dispersion.[6,75–77] By exploiting the unparalleled control over particle size and encapsulation efficiency intrinsic to droplet-based microfluidics[78–84] we have been able to efficiently encapsulate and adequately protect the ROP catalyst promoting temporary sustainment in catalyst activity in the presence of water.

Accessing Novel Crosslinked Polymeric Materials

During a polymerization that yields crosslinked material, there is a continuous increase in the macromolecular chain length resulting in a rapid increase in the viscosity of the reaction mixture by several orders of magnitude.[85] In the most severe case, the drastic increase in viscosity of the reaction mixture can lead to clogging within the reactor volume. The high viscosity drastically changes the heat and mass transport and significantly shifts the polymerization kinetics.[86] High degrees of crosslinking within the microflow reactors can also lead to clogging within the small channels of the device. However, despite many adverse effects from the decrease in processability, there is still much interest in producing crosslinked polyesters.

Crosslinking polyesters leads to a class of polymers called biodegradable elastomers.[87,88] These materials are analogous to vulcanized rubber, in that it forms a crosslinked, three-

dimensional network of random coils and has very good elastic properties.[89–91] The elastomeric properties are particularly important to various applications in the biomedical field including tissue engineering and controlled drug delivery.[92,93] Being able to employ similar ROP crosslinking strategies in flow provides an easy way to drastically increase the molecular weight of the polymer without significantly changing the composition of the solutions we are using in the flow device. Generating crosslinked polyesters in flow would also allow us to access novel materials and polymer topologies that could not be made by any other means.

1.5 Dissertation Overview

The focus of this dissertation is the fabrication and implementation of a continuous flow droplet-based microfluidic device for the encapsulation of ring-opening polymerization catalysts. **Chapter 2** will dive into the design, development, and theory behind our microflow reactor. This reactor is droplet-based and allows us to produce monodispersed droplets in an aqueous dispersion continuously. Through a deep understanding of the fluid mechanics of droplet formation, we can create particles with a wide range of molecular weights. In **Chapter 3**, we establish a protocol for performing the ring-opening polymerization of δ-valerolactone via urea-anion organocatalysts in an aqueous dispersion. The efficient encapsulation of the water-sensitive catalyst in the center of microparticles allows the polymerization to proceed while in an aqueous dispersion temporarily. We apply this methodology to produce biodegradable elastomer particles through the addition of a crosslinker within the particles. Next, in **Chapter 4**, we systematically investigated the process and formulation parameters that govern the stability of the micro-droplets during generation, flow, and collection. More specifically, we tune droplet viscosity, surface tension, and hydrophobicity by adding amphiphilic block copolymers and hydrophobes to further shield the ROP catalyst in

the aqueous dispersion. We further expand this methodology to other water-sensitive ROP chemistries to produce polyether particles in flow. Finally, in **Chapter 5**, we utilize these guiding principles to shift into drug delivery by initiating our ROP from secondary alcohols on chemotherapeutics. The preliminary results show that as we tether and subsequently crosslink the particles, we can slow the release of the drugs over a more extended period of time. **Chapter 6** concludes the work and outlines some potential future directions for this droplet-based encapsulation microfluidic methodology.

CHAPTER 2: Droplet-Based Microfluidic Encapsulation Device

2.1 Chapter Overview

In order to perform the ring-opening polymerization (ROP) of cyclic esters in an aqueous dispersion, we must protect the water-sensitive catalyst from the aqueous phase. Traditional methods for emulsification would expose the catalyst and initiator to water, which will lead to deactivation. Therefore, we implemented a microfluidic technique to methodically encapsulate the catalyst within the center of micron-sized droplets. This chapter will detail the design and development of a droplet-based microfluidic device that produces monodisperse droplets in which the water-sensitive ROP catalyst is protected within the core. The theory behind droplet generation and dynamics is discussed, in addition to the fluid mechanics within micron-sized channels. Next, I discuss the three types of forces that influence droplet generation (i.e. velocity, viscosity, and surface tension) and how we plan to tune each parameter with our system. Lastly, I cover device design considerations, including device materials and geometry, and give a comprehensive overview of our final "off-the-shelf" droplet-based microfluidic system that can be utilized to polymerize cyclic esters in an aqueous dispersion to yield a biodegradable polyester particle aqueous dispersion.

2.2 Introduction to Microfluidics

Traditional methods for making droplets use mechanical agitation of multiphase fluids, including high shear and sonication. For our application, implementing a shear or sonication technique would expose our catalyst to the aqueous phase, which further solidified our aspiration to utilize microfluidics. Microfluidic technology has been experiencing rapid growth due to its vast applications in many scientific disciplines ranging from chemistry and biology to information

technology and optics.[94] We have seen a huge impact of microfluidics in microanalysis,[95,96] pharmaceutical and drug development,[97,98] drug delivery systems,[99] material discovery,[100] and many other fields since the 1950s, *Figure 2.1a*.[101] The advantage of choosing microfluidics over conventional macroscale technologies stems largely from the reduced scale, tunability, smaller sample sizes and reagent volumes, and the unparalleled control of fluid flow. A microfluidic system, in the most basic terms, must have a component that introduces reagents and samples, a component in which the reagents flow/mix/react/separate within micron-sized channels, and any other components for collection, detection, and/or analysis work *Figure 2.1b*.

Merging microfluidics and catalysis possesses a series of distinct advantages. Firstly, inside a microfluidic reactor, there is spatial confinement, which leads to the reactants having higher reactivity.[102] Secondly, mass and heat transfer within these confined reactor volumes can also contribute to a higher and controlled reaction rate.[103] Lastly, the small reaction volumes allow swift screening for catalyst optimization and catalytic mechanistic studies.[104] When one compares microfluidic technology with macroscopic reactors for catalyst research, the microfluidics results in easy and safe handling, high yield and throughput, short reaction times, scalable and reproducible results, and low consumption of reagents making it more economical.[105]

a) Microfluidic Applications

Nano & Micron Particle Formation

Catalyst

Monomer(s)

Polymerizations

Organ-on-a-chip

Drug Design and Drug Delivery
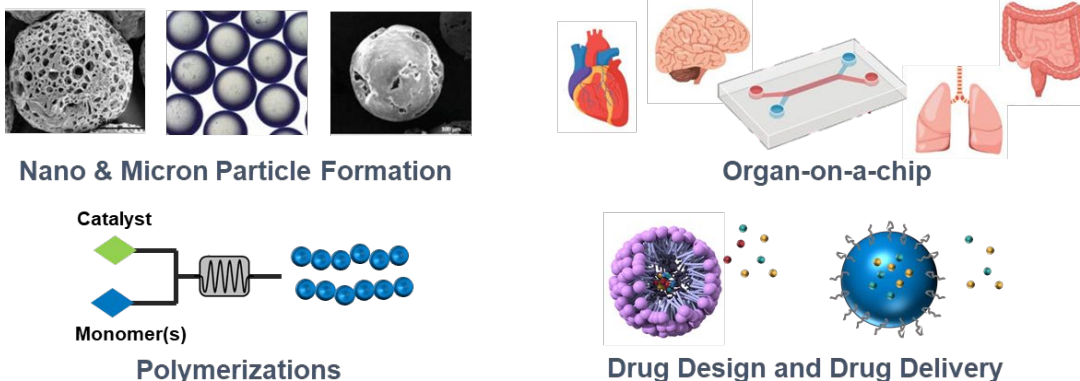
b) Basic Components of Microfluidics

Fluid Supply → **Reaction Volume** → Fluid Outlet → **Collection/ Detection/Analysis**

Figure 2.1: a) Depiction of the various microfluidic applications including nano and micron particle formation, polymerizations in flow, organ-on-a-chip, and drug delivery and design. b) Simplified components of a microfluidic device include a means for fluid supply, a reaction volume, fluid outlet, and addition collection, detection, and/or analysis techniques.

Biphasic microfluidics is a subset of microfluidic research that utilizes one or more discrete phases that are immiscible with the carrier fluid phase.[106] Droplet-based microfluidics exploits this immiscibility to form a droplet of the 'dispersed phase' fluid inside another immiscible fluid called the 'continuous phase'. The power of droplet-based microfluidics lies in forming uniform droplets and particles, with precise control over the size, shape, and monodispersity.[107,108] This technique rapidly produces predictable, periodic, and highly monodisperse droplets between the nanometer to micron diameter range. Droplet-based microfluidics has been used successfully to enhance the control over catalytic nanoparticle synthesis. By precisely controlling temperature, reaction time, and reactant concentration, one can produce very homogeneous particles with varying shapes, sizes, and compositions.[109] Additionally, a variety of work has been done producing polymer micro

and nano-particles for biomaterial and drug-delivery research. These particles are made via precipitation of the polymers and drugs dissolved in organic solvents with nonsolvents.[82,110,111]

Inspired by the success of catalytic particle and polymer particle production via microfluidics, we were interested in utilizing droplet-based microfluidics to encapsulate water-sensitive catalysts within droplet microreactors to form polymer particles dispersed in water. The water-sensitive catalysts of interest are the ring-opening polymerization (ROP) catalysts we discussed in **Chapter 1**. A successful catalyst encapsulation would allow us to make polyester particles dispersed in water that could not be made any other way. By developing a new polyester synthesis technology, we can further expand the types of polyesters accessible and thus broaden the applications of biodegradable plastics. We hypothesized that if we could encapsulate the ROP catalyst, we could slow catalyst deactivation, increase catalyst activity, and/or improve catalyst selectivity.[112] We have seen the power of catalyst encapsulation from the compartmentalization of catalysts via block copolymers,[113] metal-organic-frameworks,[114] Pickering emulsions,[115] porous materials,[116] microgels,[117] and polymers[118], which have been proven successful in serving as micro/nanoreactors and improving catalyst systems. These different encapsulation technologies inspired our design and development of a new encapsulation methodology utilizing microfluidics to continue expanding and improving catalytic limitations in the field of biodegradable polymers. Herein, I will discuss the theory behind our droplet-based microfluidics utilized to perform a water-sensitive polymerization in an aqueous dispersion.

2.3 Droplet Generation and Dimensionless Numbers

Many techniques have been developed for droplet generation, yet they all follow the same basic principles. To achieve fine control over the size, shape, and dispersity of the droplets and

particles formed, we must obey basic constraints in inertial force (i.e. flow rate), viscous force, gravity (i.e. buoyancy), and interfacial tension.[119] Our dispersed phase which contains the encapsulated catalyst and polymer is more viscous than our continuous phase which is water. Additionally, the viscosity of the dispersed phase will be changing over time as more polymerization occurs. Lastly, the interfacial tension between the two phases will be modulated utilizing amphiphilic molecules to encourage clean droplet formation in the dripping regime.

Several dimensionless numbers are useful in studying droplet generation and dynamics, **Table 2.1**. When choosing which dimensionless numbers are relevant to represent our four forces (i.e. viscosity, inertia, surface tension, and buoyancy), we must first take into account the scale of our system. In our device, the total flow rate within the device can vary from 16 µL/min to 240 µL/min and all channels for the dispersed phase are smaller than 1mm. Because our flow velocities are low and we are operating in micron-sized channels (i.e. the surface to volume ratio is high) the gravity and initial forces become insignificant.[120] Previous work has shown that gravity plays a negligible role during the formation of droplets with respect to capillary effects so the Bond number $\ll 1$.[121] Similarly, the Weber number < 1 as capillary forces also overcome inertial forces.[122] Therefore, we will not be considering the Bond and Weber numbers for our system. The dimensionless numbers that apply to our system will involve the viscosity and interfacial forces.

Table 2.1: Non-dimensionless numbers applicable to droplet-based microfluidic applications

Name	Symbol	Formula	Definition
Reynolds Number	Re	$Re = \dfrac{\rho v D}{\mu}$	Inertia/Viscous
Capillary Number	Ca	$Ca = \dfrac{\mu v}{\gamma}$	Viscous/Interfacial

Table 2.1: (cont.)

Viscosity Ratio	λ	$\lambda = \dfrac{\mu_d}{\mu_c}$	Dispersed Viscosity/Continuous Viscosity
Flow Rate Ratio	$\overline{\overline{Q}}$	$\overline{\overline{Q}} = \dfrac{Q_d}{Q_c}$	Dispersed Flow Rate/ Continuous Flow Rate
Bond	**Bo**	$Bo = \dfrac{\Delta \rho g D^2}{\gamma}$	Buoyancy/Interfacial
Weber Number	**We**	$We = \dfrac{\rho v^2 D}{\gamma}$	Inertial/Interfacial

The Reynolds number (Re), which represents inertia to viscous forces, takes into account density (ρ), velocity (v), the diameter of the channel (D), and viscosity (μ)of the phase of interest (either dispersed or continuous). Microfluidics is inherently characterized by a fluid flow that is laminar or has a low Re, typically between 10^{-6} and 10. In the laminar regime, there is no turbulence in the flowing fluids; therefore, any mixing occurs via diffusion rather than convection. We used this characteristic of laminar flow to our advantage. Since there is only diffusive mixing, we can ensure that our catalyst will primarily be in the center of our dispersed phase before droplet formation.

The droplet generation phenomenon is mainly controlled by surface tension and the viscous forces exerted by the liquid. The most fundamental dimensionless number for our system is the Capillary number, which is represented by the viscosity (μ), velocity (v), and the surface tension (γ), *Figure 2.2*. The capillary number evaluates the competition between the surface tension attempting to minimize the surface area of the droplet and the viscous stress acting to elongate the interface. Droplet breakoff occurs above a certain critical capillary number, which depends on both the device geometry and the relative viscosity between the continuous and dispersed phases. In

microfluidics, the capillary number to achieve droplet formation is typically within the range of 10^{-3} to 10. As the Ca increases the forces involved in droplet production change. For Ca $< 10^{-2}$ the droplets form a plug in the collection channel which causes a pressure buildup and leads to droplet formation. For Ca $> 10^{-2}$ the droplets do not fill the outer channel and the breakup is due to a balance of surface tension and shear forces acting on the dispersed phase.[78,123] As the Ca increases, through changing any combination of the parameters, the size of the droplet decreases.[124] Droplet formation in our microfluidic device requires precise control of each of the parameters in the capillary number. Velocity is easily controlled through the variance of the flow rate of both the dispersed and continuous phases. The viscosity, however, is a more complicated parameter to control since the viscosity of our dispersed phase will be changing as a function of the residence time and, correspondingly, the polymerization progress. Lastly, the surface tension between the dispersed and continuous phases must also remain low to allow the shear of droplets in flow.
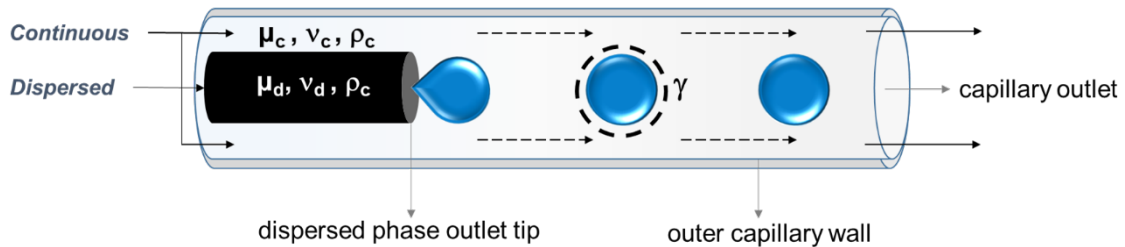

Figure 2.2: Depiction of a biphasic droplet-generation microfluidic device with the corresponding viscosity, velocity, and density of both the outer continuous phase and the inner dispersed phase

Velocity

The velocity ratio ($Q = \frac{Q_d}{Q_c}$) is the ratio of the dispersed flow rate and the continuous flow rate. As this ratio changes the flow regime we are operating in changes as well, *Figure 2.3*. The three flow regimes we transition between within the bounds of our Ca listed above are the slug,

dripping, and jetting regime. As we decrease Q we transition from the slug flow regime to the dripping regime and finally to the jetting regime. We have precise control over the flow rates of our system by employing syringe pumps as a means to supply both the dispersed and continuous phases. For our microfluidic system, we found that operating at a Q between 0.3 and 0.5 produces droplets in the dripping regime.

At larger Q the dispersed phase expands more into the main channel since it has less resistance from the continuous phase generating a slug. The slugs move through the glass capillary sliding alongside the walls which results in two disadvantages for our system. First, by sliding alongside the capillary there is mixing induced within the droplet in the form of vortexes.[125,126] The success of the catalyst encapsulation within the droplet relies on the catalyst being in the center of the droplet, which allows the catalyst more time to polymerize before water diffuses into the droplet and quenches the catalyst. Secondly, if the droplet is plugging the outer channel and moving alongside the walls the amphiphilic block copolymer (ABC) that we will be using the stabilize the droplet during flow and collection will be perturbed.

The dripping regime which is our regime of interest is a very narrow region compared to the slug and jetting regime. In the dripping regime, the droplet is completely surrounded by the continuous phase and does not interact with the outer capillary wall. As the continuous phase flow rate increases the droplet diameter decrease and the boundary layer between the droplet and the capillary wall increases. In the dripping regime, the droplet experiences two forces, the surface tension holding the droplet to the outlet tip and the viscous drag pulling it downstream. If the Q becomes too small (i.e. the continuous phase flow rate is large) the diameter of the droplet becomes smaller than the dispersed phase outlet tip we transition into the jetting regime.

The jetting regime is characterized by the dispersed phase being dragged out further from the dispersed phase outlet tip into the outer capillary tube before experiencing Rayleigh-Plateau instability and eventually forming droplets downstream. The jet diameter decreases with the distance downstream, which results in a droplet diameter small that the dispersed phase outlet tip. In this regime, the drop formation is driven by the viscous drag from the continuous phase. Droplets formed in the jetting regime are less desirable as they are less uniform because droplet breakup is erratic, and the jetting stream exposes more surface area to the aqueous phase before droplet formation, leading to faster quenching of the polymerization.[127]
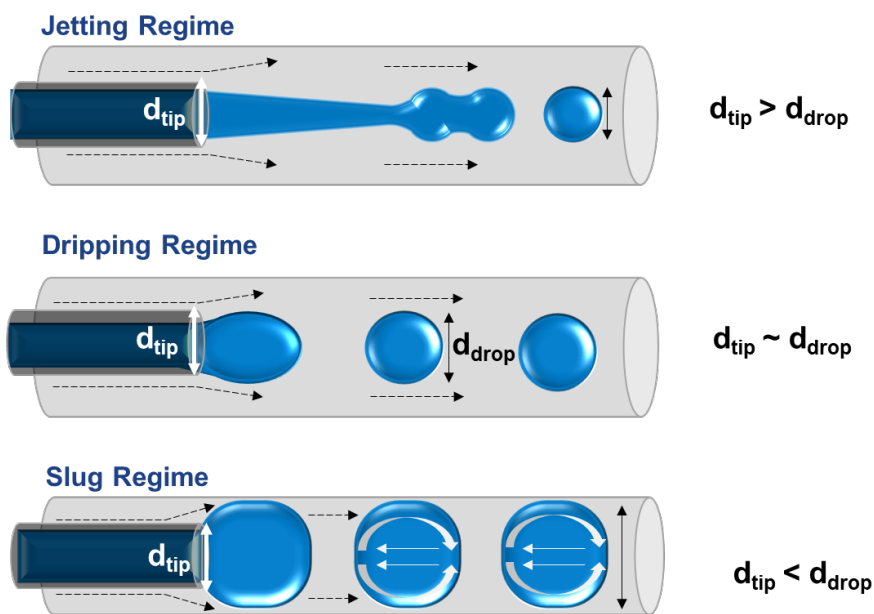

Figure 2.3: The three flow regimes of interest include the jetting regime where the droplets are produced downstream and the resulting diameter of the droplet is less than the outlet tip. The desired dripping regime, where the diameter of the resulting droplet is approximately the diameter of the dispersed phase outlet tip. The slug flow regime where the droplets fill the entire outer capillary tube before pinching off into droplets whose diameter is larger than the outlet tip.

Viscosity

The effect of viscosity on the capillary number is well understood for systems where the viscosity ratio between the two phases (i.e., $\lambda = \mu_{Dispersed}/\mu_{Continuous}$) is less than 1.[128] Traditionally in the microfluidic literature, the dispersed phase is a lower viscosity solution and the continuous phase is a higher viscosity solution. Having a viscosity ratio <1 is advantageous because, experimentally, it is harder to produce droplets with a λ>1. Our system operates at a λ>1 as our continuous phase is aqueous and our dispersed phase is a viscous polymer solution, so it was imperative that we understood the limitations of droplet production with a larger λ. Previous studies have shown that the viscous stress of the dispersed phase can impact droplet production since it is difficult for the continuous phase to fragment the dispersed phase.[129] This viscous stress makes the dripping-to-jetting transition very sharp, and the only way to remain in the dripping regime is to keep the flow rate ratio of the dispersed to continuous phases low, for our system Q < 0.5.

In our droplet-based microfluidic encapsulation system, the viscosity of the continuous phase is kept constant, whereas the dispersed phase is changing with residence time within the reactor. Since a polymerization is being performed within the reaction volume of the device (i.e. once the catalyst phase and monomer phase come in contact) we see the viscosity of the dispersed phase increase with increased time within the reaction volume. As fast dispersed phase flow rates the residence time (rt) within the reactor is short, and therefore the degree of polymerization (DP) is low resulting in a less viscous dispersed phase. If the rt within the reactor is long the DP is high resulting in a more viscous dispersed phase. Since we want to be able to operate at a wide range of residence times with corresponding viscosities we have to modulate the surface tension so it

dominates initially at the outlet tip holding the droplet there as it grows before the viscous stress pulls the droplet downstream.

Surface Tension

The surface tension of our dispersed phase will be increasing with the increasing molecular weight of the polymer; therefore, we began exploring hydrophobic solvents that decreased the surface tension of our solution, thus expanding the range of flow rates for droplet formation. Some hydrophobic solvents that we tried ranged from non-polar solvents (e.g. toluene, chloroform, dichloromethane) to bio-based and synthetic oils (e.g. soybean, corn, sesame, mineral oil). First, we had to analyze the compatibility of the different solvents with the ROP chemistry. It was important that the ROP kinetics were not negatively impacted because we need the ROP to compete with the catalyst quenching. We also had to test each solvent to determine the range of residence times (i.e. flow rates) in which we could obtain droplets in the dripping regime. Ultimately, the solvent needs to be 1) immiscible with the continuous phase, 2) compatible with the ROP chemistry, and 3) able to produce droplets over a wide range of rt with an aqueous continuous phase. The results from the solvent choice can be found in **Chapter 3**.

Another method for modulating the surface tension of the droplet is through the use of surfactants, amphiphilic molecules with a hydrophilic and hydrophobic portion. The use of surfactants in the dispersed and/or continuous phase in low concentrations of 1-5% wt% has been shown to aid in the stability of the droplets produced and reduce the instances of droplet coalescence. The surfactant molecules naturally orient at the interface between the two immiscible fluids to have the hydrophilic head and hydrophobic tail in contact with the appropriate fluid. The choice of surfactant is dependent on which phase you are introducing the surfactant and what

solvent/fluid is used for the dispersed and continuous phases. For example, when we add surfactant to organic fluids, we can use amphiphilic block copolymers synthesized in-house, Span 80, or Triton X-100. If we add surfactants to the aqueous phase, we can use Tergitol, Tween 20, Tween 80, or Polyvinyl alcohol. We can also add amphiphilic molecules to the dispersed phase if we use amphiphilic block copolymers (ABC). These polymeric materials act as surfactants and align at the immiscible interface stabilizing the droplet. The only constraint for choosing surfactants or ABC is to ensure that they are not detrimental to the ROP kinetics.

2.4 Amphiphilic Block Copolymer Shell

The amphiphilic block copolymer migrates to the interface between the two immiscible phases and forms a shell around the droplet. The concept of utilizing these amphiphilic shells was threefold. Firstly, the shell decreases the surface tension of the dispersed phase and breaks off into droplets when the viscosity of the droplet is high. Secondly, the shell decreases the affinity of the particles to coalesce during flow and collection. Thirdly, the shell will form a membrane around the particle, which will create a barrier between the reacting material and the aqueous phase, *Figure 2.4*. The rate of polymerization and degree of polymerization achieved inside the capsule will be a function of the rate of transport of water through the capsule shell. The chemistry of the shell can be tuned to optimize the mass transfer of water across the membrane via changing the block number, hydrophobicity, and/or crosslinking ability. The amphiphilic molecules, either in the form of block copolymers or surfactants, can be added to the continuous phase or the dispersed phase

We aimed to design a device that allows a quick and efficient way to probe the different block copolymers by comparing the maximum conversion attainable and identifying the optimum

chemical structure of the polymer. The ideal block copolymer for the ROP in water will ultimately form a selective barrier between the catalyst and the aqueous phase. Each block copolymer of interest can be easily implemented in the droplet ring-opening polymerization, and the kinetics of the ROP can be analyzed. The results from the rates of reactions and water transport will be combined into a powerful model, capable of predicting the achievable degree of polymerization based on ABC composition and properties, **Chapter 4**.
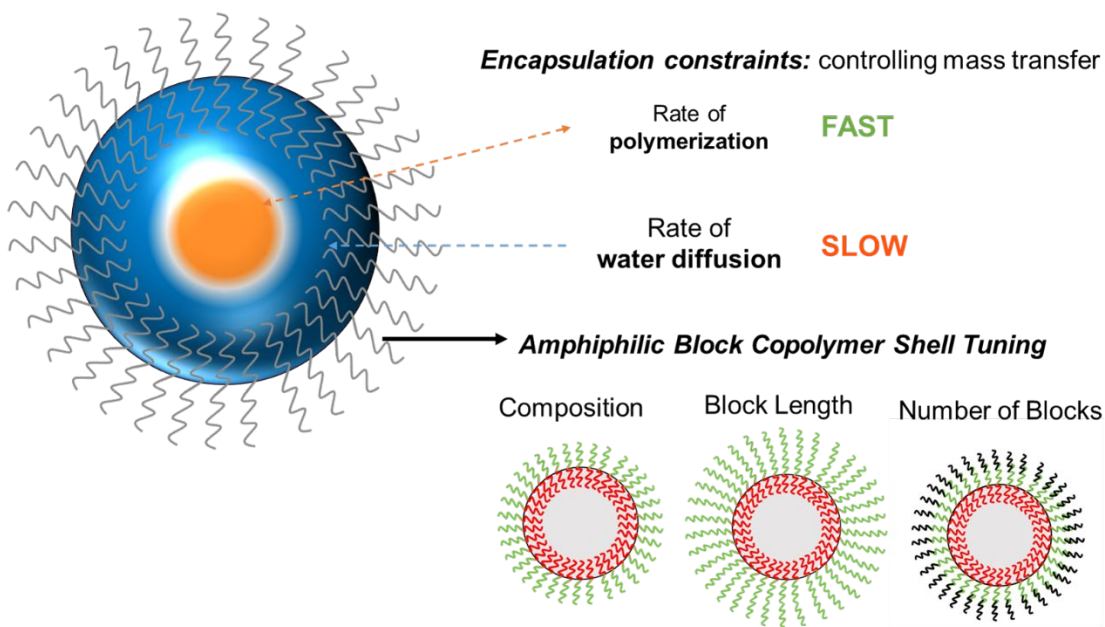

Figure 2.4: The amphiphilic molecule will form a shell around our particles which will help slow the rate of water diffusion into the droplet by aiding in the production of droplets at the outlet tip by decreasing the surface tension, acting as the first layer slowing water diffusion into the droplet, and preventing coalescence during flow and collection. The amphiphilic block copolymers can be tuned by changing the composition, block length, and the number of blocks.

2.5 Droplet Device Considerations

Device Materials

The material used for the device components and the fluids used for the droplet generation must be compatible for successful droplet formation. Most microfluidic systems are fabricated using poly(dimethyl) siloxane (PDMS). For our purposes, PDMS would not be a compatible

material as it would undergo swelling and deformation in the presence of our organic solvents, toluene, and tetrahydrofuran. Therefore, we explored the use of glass and organic solvent-resistant polymers like polytetrafluoroethylene (PTFE) and polyether ether ketone (PEEK). All three of these materials are compatible with our organic solvents and would withstand repeat use and cleaning over time.

The contact angle between the fluids and the droplet generating device surface. When our two immiscible fluids come in contact with a substrate either one fluid preferentially wets the wall and separates the other from the surface or both fluids partially wet the wall. Since our channels are on the micron scale the wetting conditions strongly influence the formation and transport of droplets in the microchannels. Ideally, we want the aqueous continuous phase to preferentially wet the surface of the channels to ensure stable flow regimes. Therefore, the collection channel wall needed to be hydrophilic to be suitable for making organic droplets in an aqueous phase (oil-in-water), which is how we chose glass as our device collection material.

Device Geometry

Device geometry is another parameter we explored extensively while designing different microfluidic devices. The three geometries we tested were coaxial flow, flow focusing, and co-flow, *Figure 2.5*. Methods for droplet generation can either be active or passive, where active methods utilize additional energy input to promote interfacial instabilities and passive methods generate droplets without external manipulation.[78] The droplet generation in all three geometries we designed and tested originates from fluid instabilities from the introduction of one immiscible fluid (i.e. our organic dispersed phase) into another (i.e. our aqueous continuous phase). Therefore,

we focused entirely on passive means for microfluidic droplet generation, depending on the competition of capillary, interfacial, viscous, and inertial forces.
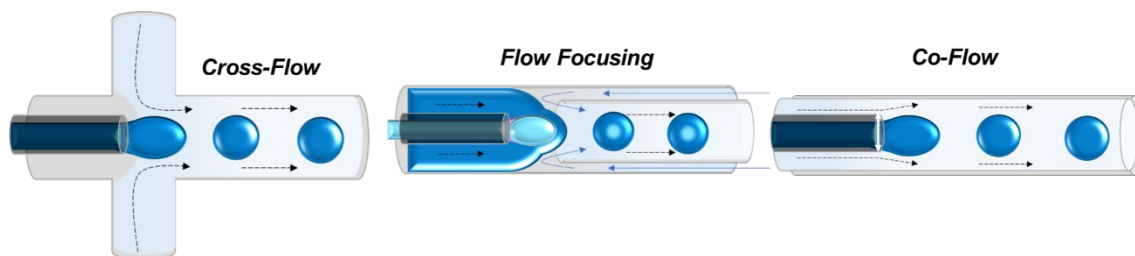

Figure 2.5: The three geometries that we designed and analyzed for droplet formation included a cross-flow, flow focusing, and co-flow configuration.

Our first attempt was a cross-flow configuration, *Figure 2.6*. In this geometry, the dispersed phase is supplied between two streams of the continuous phase cross-flow. In the first two generations of this device, *Figure 2.6.a/b*, the catalyst was separately supplied from the monomer before the co-flowed stream would be sheared off by the continuous phase. These devices experienced instantaneous quenching of the ROP catalyst. This informed our decision to focus on device designs where the catalyst would be supplied through a middle inlet and sheathed between two steams of monomer before being sheared off by two streams of the continuous phase, *Figure 2.6.c/d.*
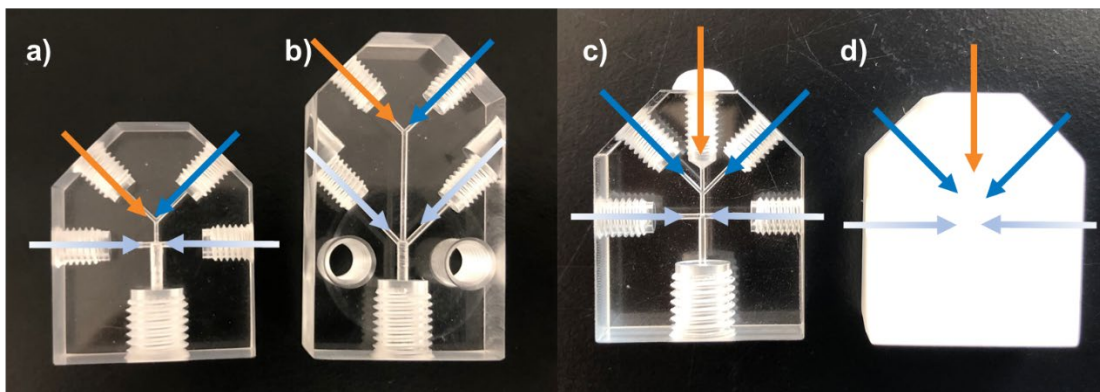
Cross-Flow Devices

Figure 2.6: a) First generation cross-flow device where the monomer and catalyst were supplied in tandem before being sheared off into droplets. b) the same configuration as a. however, this one allowed more mixing time between the catalyst and the monomer. c) Second generation cross-flow device where the catalyst is supplied in between two streams of monomer before droplet generation. d) the same configuration as c. however, this device was made with Teflon.

These devices were made with both plexiglass and Teflon. The plexiglass allowed us to visualize our droplet generation and determine flow rates amenable to droplet formation. However, this material is not resistant to our organic solvents and over time, became fouled and degraded. The Teflon device was more resilient with the organic solvents, but without seeing the droplet formation, we could not confirm whether we were forming droplets in the dripping or the jetting regime. We moved on from this geometry with the new constraint that we want to see the dispersed phase outlet tip to ensure that we can monitor droplet formation and flow regimes.

The next geometry we designed and tested was the flow-focusing configuration, where the dispersed and continuous phases are forced through a narrow region in the microfluidic device, *Figure 2.7*. For this configuration, we employed a double capillary design which is utilized heavily in the drug delivery literature.[130–132] This design if executed properly, employs symmetric shearing by the continuous phase on the dispersed phase.[133] The issue with this system in our opinion, was the lack of reproducibility. In order for the device to successfully make droplets, the capillaries

must be aligned perfectly as any deviation would drastically prevent the device's efficiency. We moved on from this geometry with the new constraint that we wanted to develop a device that was user-friendly, reproducible, and consistent.
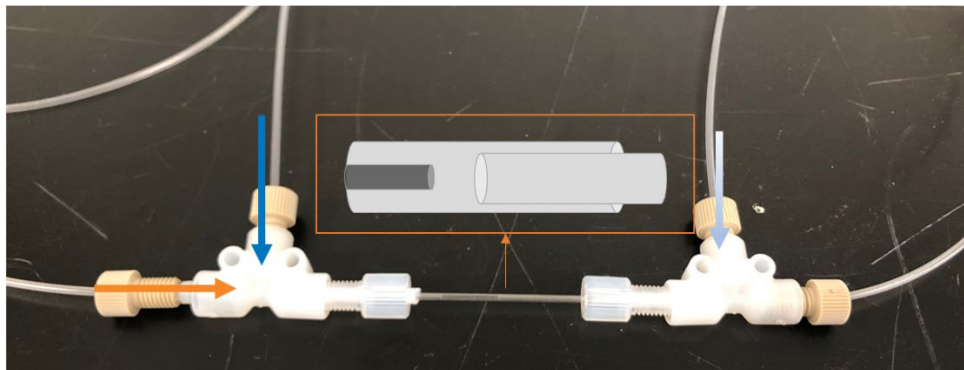
Flow Focusing Device

Figure 2.7: a) Double capillary flow-focusing device, where the monomer stream encapsulates the catalyst stream before shearing off into droplets via an immiscible aqueous phase that focuses the droplets into a secondary receiving capillary.

The final configuration that we found the most reproducible and fitting for our purpose was the co-flow configuration, where the dispersed and continuous phase flow in the same direction at the junction, *Figure 2.8*. For this geometry, we purchased all commercially available components that required no additional modifications. In addition to being commercially available, user-friendly, and reliable this geometry also resulted in the largest range of flow rates for droplet generation. Herein, we will focus on this device geometry for our droplet-based catalyst encapsulations.
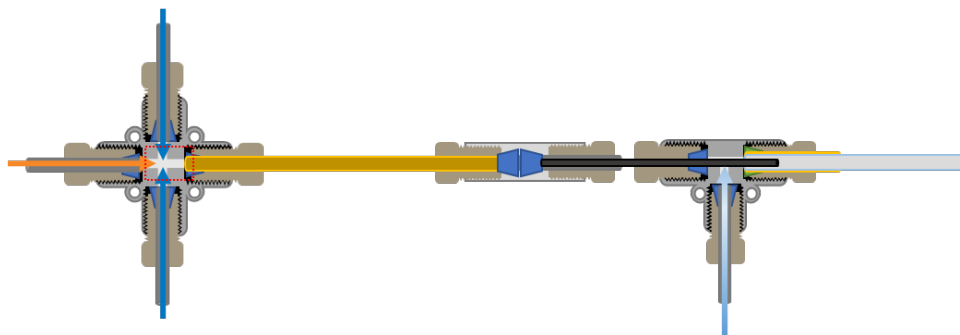
Co-Flow Device

Figure 2.8: a) Co-flow droplet generating microfluidic device where the catalyst is supplied between two monomer streams. This dispersed phase flows down the length of the reactor before coming in contact with the aqueous phase that shears the dispersed phase into droplets.

2.6 "Off-the-Shelf" Droplet-Based Microfluidic Device

Catalyst Encapsulation Design

To perform the ROP chemistry in aqueous dispersion, we apply the multiphase microfluidic device to generate an oil-in-water (O/W) emulsion using the aforementioned co-flow geometry reactor constructed with commercially available components. This "off-the-shelf" design, has a fixed reaction volume. Thus residence time is tuned by flow rate control.[134] The catalyst and monomer solutions must be supplied separately to prevent the polymerization from proceeding in the syringes. Therefore, the organic phase comprises two separate organic streams, which are supplied through a cross tee and travel through the small reaction volume before being dispersed in water. By supplying the catalyst through the middle inlet, we can further ensure that the monomer and hydrophobic solvent surround the catalyst before reaching the aqueous phase. The laminar flow of the fluid through our device ensures that the catalyst will remain primarily in the center of our dispersed phase before the droplet formation since any mixing occurs via diffusion rather than convection.

The size of the droplet plays an essential role in the extent of polymerization time once the droplets are formed. A smaller sized droplet would have a larger surface-area-to-volume ratio, leading to shorter diffusion distances, which would result in a faster quenching of the catalyst.[119] Therefore, we chose to focus on micron-sized droplets to provide more time for the polymerization to proceed after the droplet formation. The dispersed phase outlet tip sets a lower limit for droplet diameter as the tip shields the growing droplet from the sheer force of the continuous phase,[135] thus, we chose a large enough diameter to produce droplets with a minimum diameter of 300 μm. The dispersed phase is expelled into a glass capillary tube, where the continuous water phase is supplied through a secondary tee. The dispersed phase outlet tip must sit centered in the middle of the glass capillary, as this allows enough space for the water to flow through the gap around the metal tubing to shear off the droplets.

Advantages and Limitations

The power of this droplet-based microfluidic system is that any user would be able to build and operate the device since it is made from commercially available components and does not require prior technical training or knowledge. Additionally, because all of the materials were either PEEK, glass, or stainless steel, we could operate with organic solvents without risking the degradation of the materials. The system also allows changing residence times within the reactor and controlling flow regimes very easily through simple changes in flow rate via the three syringe pumps. The entirety of the setup does not take up much space on the benchtop and can be easily set up, taken down, and moved. Overall, the droplet generation efficiency is great, the device production cost is low, and the device is reusable.

Some limitations of this device, and other microfluidic devices, is that the small micron-sized channels are hard to clean. We found that small clogs could be removed, but larger blockages resulted in sections of tubing needing to be replaced. The outlet tip diameter limits the size of the droplets produced in the dripping regime. If the user wants to change droplet diameter, they have to change the hypodermic tubing responsible for droplet formation. This limit on the size of droplets attainable can be overcome by producing droplets in the jetting regime, which we do not recommend for water-sensitive ROPs, as it would result in faster catalyst quenching.

Recommended Cleaning Techniques

The channel sizes within the device are small (170-300μm) which means that they can frequently be clogged and blocked as the viscosity of the polymer solution increases with increasing residence time. To reduce blocked channels and prolong the lifetime of the device tubing, do not operate the device at extended residence times where the viscosity of the solution causes elevated backpressure. It is recommended to start at high flow rates (low residence times) and slowly decreases the flow rates (increase residence time). At the end of each run, flush the entire device with tetrahydrofuran or acetone, or any other solvent compatible with the dispersed phase. Flushing the device will remove any leftover material and prepare the device for the next trial. If blockages occur and flushing becomes impossible, the user can try placing the clogged portions in the ultrasound bath for 10-15 minutes and repeat flushing. However, if there are larger blockages or crosslinked polymer blockages, one can easily replace sections of the device tubing at a low cost.

2.7 Conclusions

In conclusion, we have investigated many different droplet-based microfluidic designs and the theory governing their droplet generation and droplet dynamics. We ultimately moved forward with a co-flow droplet-generating device made of commercially available components. The device separately supplies our water-sensitive catalyst in between two monomer streams. The monomer streams surround the catalyst before being exposed to the aqueous phase and becoming sheared off into droplets. The device produces a continuous flow of monodispersed droplets over a large range of flow rates.

CHAPTER 3: Ring-Opening Polymerization of Cyclic Esters in an Aqueous Dispersion [1]

3.1 Chapter Overview

Aqueous polymer dispersions are commodity materials produced on a multi-million-ton scale annually. Today none of these materials are biodegradable because the process by which they are made is not compatible with the synthesis of biodegradable polymers. Here we report an encapsulation strategy for protecting a water incompatible ring-opening polymerization (ROP) catalyst from the aqueous phase, yielding biodegradable polymer particles dispersed in water. The capsules containing the ROP catalyst and monomer are fabricated using a microfluidic device. Polymerization yields 300 μm sized particles comprised of biodegradable poly(δ-valerolactone) with molecular weights up to 19.5 kg mol^{-1}. The success of this approach relies on simultaneous precise control of the kinetics of polymerization, the rate of mass transfer rates, and fluid mechanics. Ultimately the methodology was applied to the synthesis of crosslinked polymer particles through the copolymerization of bis(ε-caprolactone-4-yl)propane and δ -valerolactone, producing crosslinked poly(poly(δ -valerolactone) with molecular weights reaching 65.3 kg mol^{-1}. Overall, this encapsulation technique opens the door for the synthesis of biodegradable polymer latex and processable, biodegradable elastomers.

3.2 Introduction

The quest for biodegradable polymers has gained momentum over the past decades, motivated by an alarming accumulation of plastics in landfills and oceans.[8,67] Despite the successful commercialization of many biodegradable thermoplastics targeted at substituting non-degradable polymer, to date no alternative to widely used synthetic and non-biodegradable

polymer latexes have been developed.[69,136–138] A polymer latex is characterized by polymer nanoparticles stabilized by amphiphilic emulsifiers dispersed in an aqueous phase. They account for 10% of the global annual polymer production and are traditionally synthesized through an emulsion polymerization process. [139–142] Polymer latex applications range from coatings,[143,144] adhesives,[145,146] and drug delivery carriers.[147–150] With such a vast range of products, the development of a technique to produce biodegradable polymer latexes would provide a unique opportunity to enhance the sustainability of the polymer industry.

Biodegradable polymers and polymer latexes both possess excellent tunability in fabrication, but they have remained autonomous of one another due to the incompatibility of the polymerization method used to synthesize biodegradable polymers with water.[5,151] Most biodegradable polymers are synthesized through a catalytic ring-opening polymerization (ROP) of aliphatic cyclic esters. The ester bond in the repeating unit makes the polymer susceptible to biological and hydrolytic degradation conferring its biodegradability.[152,153] In industry, the ROP is traditionally performed under moderately anhydrous conditions as water can both deactivate the catalyst and act as an initiator; thus excess water severely limits the attainable molecular weight.[154–156] In academia, despite the plethora of novel catalysts being developed, most new catalysts are presumed to be quickly and quantitatively deactivated by water, and thus are used under purely anhydrous conditions.[12] This water reactivity has thus far categorically prevented the implementation of ROP in an aqueous environment, which would be essential for emulsion polymerization.[68,157]

Miniemulsion polymerization has been successfully implemented for catalytic polymerizations using catalysts that are moderately compatible with water.[70,71,158] The anionic ROP of high ring strain epoxides has been successfully performed using this technique, however,

the high water content limits the molecular weight of the polymer produced (Mn $\leq$730 g mol^{-1}).[159] In the miniemulsion process, the catalyst and the monomer are combined with a hydrophobic solvent, and the mixture is dispersed into nanodroplets stabilized by a large amount of surfactant using high shear. The polymerization proceeds independently in each droplet to yield the desired nanoparticle dispersion. During the emulsification process, the catalyst/initiator is exposed to both water, which leads to deactivation, and to the monomer, which initiates polymerization.[72] Consequentially, the catalyst needs to be water-compatible and the polymerization needs to remain slow or completely stalled during the emulsification phase.[73,74] For the ROP of cyclic esters, these two requirements have not been met to date, making it incompatible with the miniemulsion process.[12] This limitation, as well as the vast potential for applications of biodegradable polymer latexes, motivated us to develop an alternative encapsulation strategy for performing the ROP in the presence of water.
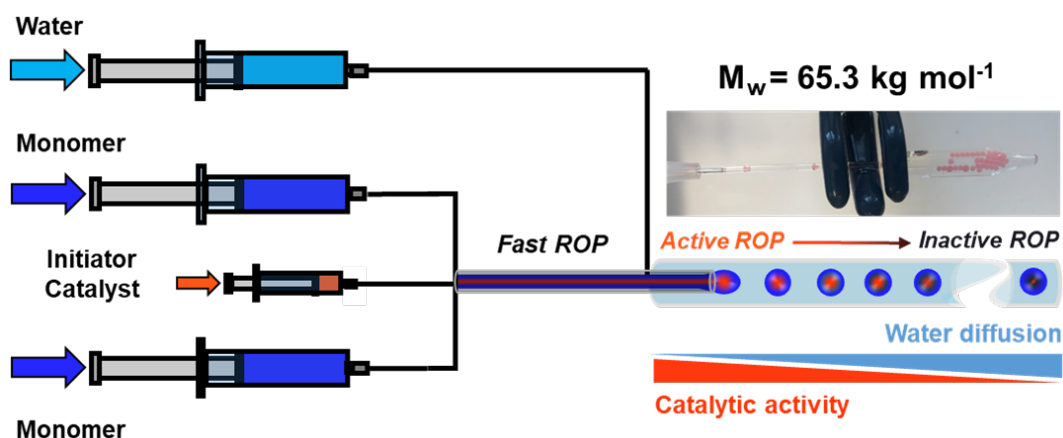

Figure 3.1: Droplet microfluidic encapsulation of water sensitive ring-opening polymerization catalyst. The combination of the fast polymerization and the controlled encapsulation of the catalyst allows the catalyst enough time to polymerize before water diffusion into the droplet can quench the reaction.

Our approach consists of utilizing a microfluidic encapsulation strategy where the dispersed phase, comprised of a monomer and a catalyst solution, is fed into a narrow tube to initiate polymerization, before meeting the immiscible continuous aqueous phase at a junction to form micrometer size droplets, *Figure 3.1*. The catalyst and monomer solutions are initially supplied from different syringes to prevent premature polymerization before entering the droplet-generating device. The polymerization starts once the catalyst and monomer solutions come in contact and will continue within the droplet until water diffuses throughout the droplet and completely deactivates the catalyst. By design, the catalyst is supplied between the monomer streams to retain the catalyst in the core of the droplets, which is thought to provide more time for the catalyst to remain active before water quenches the polymerization. Water diffusion into the droplet directly limits the polymerization time. Therefore, this approach requires a fast ROP for the polymerization to produce a high molecular weight polymer before water completely deactivates the catalyst.

This report outlines the engineering of a droplet based microfluidic device that facilitates encapsulation of the water sensitive catalyst, and allows, for the first time, ROP of synthetic biodegradable linear and partially crosslinked polymers in an aqueous dispersion. Our approach relies on the understanding of fluid mechanics, precise formulation of the polymerization solution, and control over ROP kinetics within the device and the subsequent droplets.

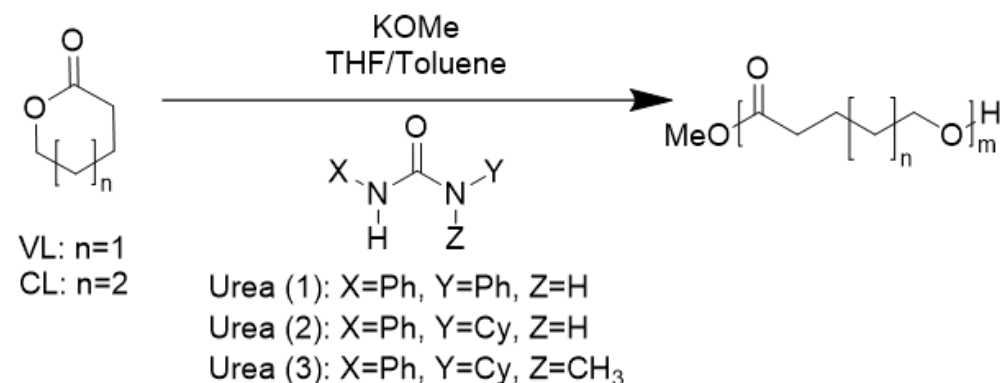## 3.3 Results and Discussion

ROP Chemistry Selection

The primary constraint for the success of the encapsulation approach is the selection of a catalyst system that provides a high rate of polymerization, as the time for the polymerization to

achieve completion before water diffuses throughout the droplet and deactivates the catalyst is finite. We opted to implement urea organocatalyzed ROP of cyclic esters, (**Scheme 3.1**) because this family of catalysts is known to exhibit fast kinetics and high selectivity.[24,160]

Scheme 3.1: Urea anion catalysts for the ring-opening polymerization of δ-valerolactone and ε-caprolactone.

VL: n=1
CL: n=2

Urea (1): X=Ph, Y=Ph, Z=H
Urea (2): X=Ph, Y=Cy, Z=H
Urea (3): X=Ph, Y=Cy, Z=CH$_3$

We opted to use δ-valerolactone (VL) and ε-caprolactone (CL) as our monomers for two reasons. First, they yield biodegradable polymers, and second, they are liquid at room temperature, which allows for the preparation of highly concentrated monomer droplets. At concentrations greater than 3 mol L^{-1}, a slight increase in the polymer dispersity and viscosity was observed in batch polymerizations. To avoid pressure build-up or even clogging in the small dimeter tubing due to the high viscosity of the neat solution, we chose to operate at a monomer concentration of 3 mol L^{-1} for all subsequent reactions in the flow system. Similarly, the catalyst/initiator solution was made as concentrated as possible; however, the solubility of the initiator, potassium methoxide (KOMe), is highly influenced by the ratio of the catalyst to the initiator. **Urea (1)** and **Urea (2)** could be solubilized with a ratio of initiator:catalyst:monomer of 1:3:200, while **Urea (3)** needed a 1:4:200 ratio. The high solubility of the catalyst and initiator is preferred in order to minimize

the amount of organic solvent as it remains in the final product. Under this concentration, we confirmed that **Urea (1)** and **Urea (2)** exhibit fast rates of polymerizations for VL, with complete conversion in less than 10 seconds in batch experiments, ***Figure Appendix A.1***. **Urea (2)** was identified as a highly active catalyst for CL polymerization and VL/CL copolymerizations.[50,161] We will utilize this reactivity for synthesizing biodegradable elastomeric particles, *vide infra*. **Urea (3)** suffered from a few disadvantages, including slower polymerization kinetics for both monomers and a lower solubility compared to the other catalysts. ***Appendix A. Table A.1*** summarizes the batch polymerization results. Once we identified **Urea (1)** or **Urea (2)** as potential catalysts for our system, we proceeded to design the microfluidic device.

Device Design

To perform the ROP in droplets dispersed in water, we implemented a microfluidic device that generates an oil-in-water (O/W) emulsion using a co-flow geometry reactor constructed with commercially available components, ***Figure 3.2a***.[6,75–77] By exploiting the unparalleled control over droplet size and encapsulation efficiency intrinsic to droplet-based microfluidics,[78–84] we hypothesized that we could protect the ROP catalyst from water, thus temporarily sustaining catalyst activity in the presence of water. The organic phase is comprised of two organic streams, the catalyst solution and the monomer solution that merge at a cross tee into a tube, which in turn is being dispersed in water. The choice of the cross tee, with two monomer streams surrounding the catalyst stream, at the inlet is deliberate, as it generates the first level of protection of the catalytic material. The inherent laminar flow of the fluid in the small dimeter, short channel ensures that the catalyst remains primarily in the center of our organic phase before droplet formation when a sheath flow of water is introduced since mixing in the tube occurs only via diffusion, ***Figure***

3.3b. The diameter of the tubing after the cross tee plays an important role in the molecular weight and dispersity of the polymer produced.[65,103,162] Upon reducing the inner diameter of the tubing from 304.8 µm to 177.8 µm, the diffusion length decreases, which increases the homogeneity of the polymerization solution. In turn, this increase in homogeneity results in an increase in monomer conversion and molecular weight, and a decrease in dispersity, ***Appendix A. Figure A.2.*** Therefore, the final device design utilizes the smallest ID tubing (177.8 µm) for the organic phase to ensure control over the monomer conversion, molecular weight, and dispersity of the polymer generated. The organic phase expels in the center of a glass capillary tube, in which the continuous water phase is supplied through a secondary tee and shears the organic phase into droplets. ***Appendix A. Figure A.3***, provides a more detailed description.

The surface-area-to-volume ratio of the droplet is presumed to greatly impact the polymerization time. A smaller sized droplet has a shorter diffusion path to the core of the particle, which would result in a faster quenching of the catalyst.[119] The organic phase outlet tip sets a lower limit for droplet diameter as the tip shields the growing droplet from the shear force of the continuous phase.[135] Thus, we chose a sufficiently large diameter to produce 300 µm droplets. This microfluidic design comprised of "off-the-shelf" parts has a fixed reaction volume; thus the residence time (rt) can only be tuned by varying the flow rate.[134]
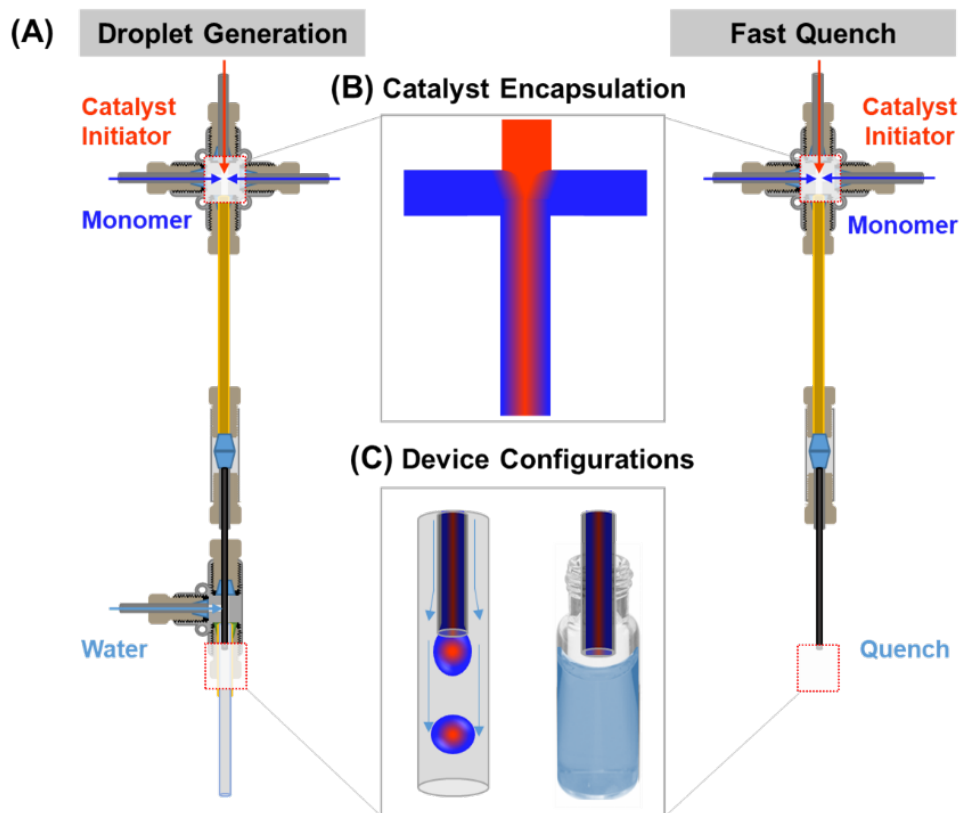
Figure 3.2: (A) Droplet-generating microfluidic device made from commercially available components. (B) Catalyst encapsulation within two streams of monomer and organic solvent. (C) Droplet (left) and fast quench (right) configurations of the microfluidic device

To demonstrate that the polymerization proceeds in the aqueous phase after droplet formation, we must precisely determine the monomer conversion at the end of the organic phase outlet tip. Therefore, we ensured that we could operate our device in a second 'fast quench' configuration; instantaneously quenching the polymerization in a solution of acetic acid and THF, at the tip of the organic phase outlet while still being able to vary the polymerization time, ***Figure 3.2c***. After establishing the design of the microfluidic device, we then identified the appropriate formulation and flow rates to achieve excellent control over the size, shape, and homogeneity of the droplets and particles formed.[119]

Droplet Formulation and Flow Rates

Three types of forces influence droplet generation in our system: viscous force, capillary force, and the dominating interfacial force. During droplet generation, the interface deforms significantly due to interfacial tension between the two phases, which results in necking, i.e. the interface fragmenting spontaneously and decaying into disconnected droplets.[163] To determine droplet dynamics, such as fission or droplet break off, we leveraged the non-dimensionless capillary number (*Ca*), defined as $Ca = \mu v/\gamma$ (where μ is the viscosity of the phase of interest, v is the velocity of the phase of interest, and γ is the interfacial tension between the two phases), ***Figure 3.3***. Droplet formation requires precise control of each of the parameters in the capillary number, especially the interfacial tension.[124] The interfacial tension of our dispersed phase increases with increasing monomer consumption. At low conversion, the interface between the organic and aqueous phase is miscible, and the surface tension is low, both of which prevent droplet formation. Therefore, we explored hydrophobic solvents that improve the immiscibility of the two phases and expand the range of flow rates for droplet formation. The standard polymerization conditions used to identify a compatible solvent were a 1:3:200 ratio of [initiator]:[catalyst]:[monomer], with a VL monomer concentration of 3 mol L^{-1}. A series of batch polymerizations at room temperature identified toluene as a promising hydrophobic solvent, as it exhibited the fastest rate of living polymerization (full conversion within 10 seconds) and produced the highest molecular weight polymer (24 kg mol^{-1}) among all solvents tested, ***Appendix A. Figure A.4***.
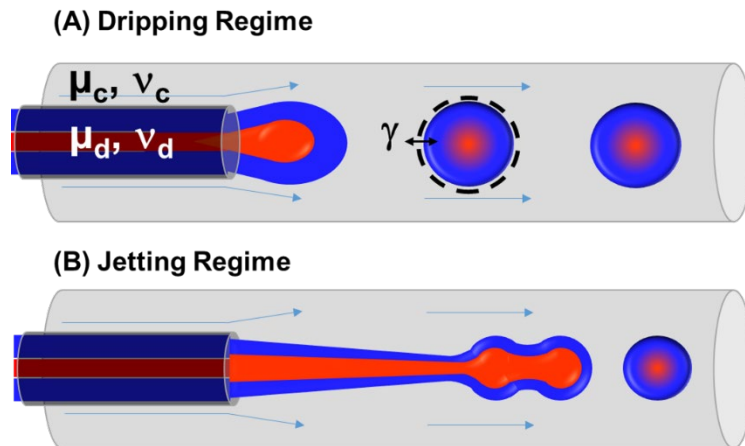
Figure 3.3: Visual representation of the capillary number parameters and illustration of the desired dripping regime (A) and the undesirable jetting regime (B).

The two other parameters that affect the Ca are velocity and viscosity. Flow velocity is easily controlled in our system by varying the flow rate of both the dispersed and continuous phases. Reliable droplet generation at the organic phase outlet tip with the chosen formulations, the combined flow rate of the two organic phases could not exceed 140 µL/min, which corresponds to a lower limit for the residence time (rt) of 5s. The viscosity is a more complicated parameter to control, since the viscosity of our dispersed phase is changing as a function of the rt. As the polymerization progresses the viscosity ratio between our two phases (*i.e.*, $\lambda=\mu_{dispersed}/\mu_{continuous}$) is greater than 1. Also, prior work has shown that the viscous stress of the dispersed phase can impact droplet production since it is difficult for the continuous phase to fragment the dispersed phase.[128,129] This viscous stress makes the dripping-to-jetting transition very sharp, and the only way to remain in the dripping regime is to keep the flow rate ratio of the dispersed to continuous phases (*i.e.*, $Q=Q_{dispersed}/Q_{continuous}$) low, particularly below 0.5 for our device geometry.[164,165] After careful selection of flow rates and formulation, we were able to produce uniform droplets in flow

over a broad range of residence times (rt=5-21s). We used these flow rates and the formulation to perform the ROP in the microfluidic device.

ROP in Fast Quench Configuration

Before determining how much, if any, polymerization occurred in the dispersed droplet, we precisely determined the conversion at the end of the organic phase outlet tip. To do so, we operated the device in the 'Fast Quench' configuration, which allowed us to build a rt versus conversion ladder, *Figure 3.4*.
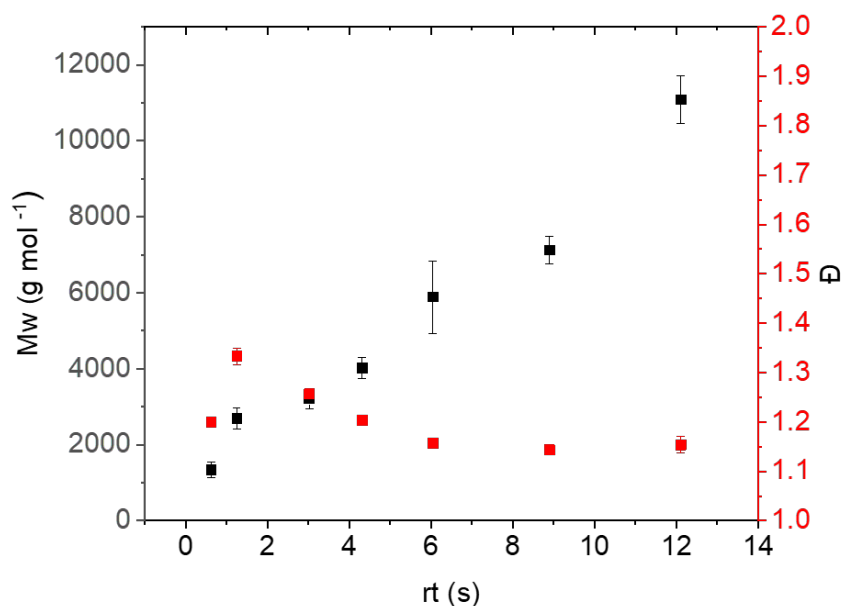

Figure 3.4: Residence time ladder using the microfluidic device in the fast quench configuration with toluene as the hydrophobic solvent. Reaction conditions: [KOMe]:[urea]:[monomer] = 1:3:200 and [monomer]0 = 3 M in THF at room temperature. Mw and Đ determined by PS calibrated GPC in THF.

The molecular weight increases with rt, reaching 10 kg/mol and a conversion of 50% for a rt of 12 seconds. The process was stable as illustrated by the constant conversion achieved for

different flow rates over hundreds of residence times, ***Appendix A. Figure A.5***. Compared to the batch polymerization, which reaches 100% conversion after 5s, polymerization in the flow device is significantly slower. Additionally, the molecular weight increases linearly with rt, which differs from batch experiments, ***Appendix A. Figure A.1***. Both observations are indicative of the inhomogeneity of the reaction mixture in the tubular reactor. In our flow device, the monomer and catalyst streams are relying exclusively on diffusion to mix. The heterogeneous reaction is diffusion controlled, as the catalyst and initiator solution in the center of the stream is poorly soluble in the surrounding toluene and monomer. The poor solubility further slows down the homogenization of the solutions and thus the polymerization. While this difference in solubility and slow diffusion hampers polymerization, this difference aids in isolating the catalyst to the center of the droplets, thus delaying quenching by water.

ROP in Droplet Configuration

Using the same formulation and flow rates as in the fast quench configuration, we performed the ROP in the droplet configuration. By design, we want to keep the monomer conversion low within the microfluidic device to maintain a low enough viscosity of the polymer solution to allow flow through the device without clogging, therefore we aimed for a rt less than 30 seconds. While continuing to keep the flow rate ratio less than 0.2, flow rates enabling the formation of the droplets were extremely small. The total dispersed phase flow rate had to stay below 100 μL/min (or a rt greater than 10s) to obtain consistent droplet formation. At dispersed flow rates greater than 100 μL/min, the dispersed phase shifts into a jetting regime near the hypodermic needle tip before experiencing Rayleigh-Plateau instability and eventually forming droplets downstream, ***Figure 3.3b***.[124] The molecular weight of the polymer obtained in this jetting

regime was similar to the one obtained in the fast quench experiment at identical flow rates, **_Table 3.1_**. We attributed this negative result to the jetting regime exposing more surface area to the aqueous phase before droplet formation, leading to faster quenching of the polymerization.

Table 3.1. Comparison of droplet reactor polymerization performance

Entry	Configuration	Water	Time (s)	X (%)^a	$M_{n, theor}$ (g mol^{-1})	$M_w{}^b$ (g mol^{-1})	Đ^b
1	**Batch**	-	10	90	18,000	20,700	1.2
2	**Batch**	+ 100 eq	120	0	0	0	-
3	**Fast quench**	No	10	26	5,200	7,700	1.3
4	**Droplet** *jetting to dripping regime*	Yes	10	27	5,400	7,900	1.3
5^c	**Droplet** *dripping regime with surfactant*	Yes	10	55	11,000	13,800	1.6
6^d	**Droplet** *dripping regime with crosslinker*	Yes	10	N/A	N/A	45,200	2.4

Reaction conditions: [KOMe]:[urea]:[monomer] = 1:3:200 and [monomer]0 = 3 M in THF at room temperature. All batch reactions were performed under anhydrous conditions and quenched with benzoic acid. *a.* Conversion determined by 1H NMR. *b.* Mw and PDI were determined by PS calibrated GPC in THF. *c.* Tergitol 1% was added to the continuous water phase. *d.* BCP crosslinker 0.5% added to the monomer streams.

As mentioned earlier, the flow regime is directly related to the capillary number. The flow rates and viscosity are mostly set by the polymerization rate; therefore, we focused our attention on the difference in interfacial tension between the two streams. We hypothesized that we could extend the flow rates that produced the desired dripping regime by adding a surfactant in the aqueous phase. Indeed, in the presence of 1% of Tergitol in the aqueous phase, the droplet break-

off at the hypodermic needle tip was sharp and consistent across a large set of residence times (5-21 seconds), Video S1. In the presence of surfactant, the polymer formed in the droplet reached a molecular weight and conversion double that of the fast quench set-up. The clear difference in molecular weight of the polymer formed between the droplet regime and the fast quench demonstrates that polymerization proceeds in the droplet (Table 1, entry 5).

Interestingly, the dispersity of the polymer obtained in the droplet configuration is broader than in any other set-up with an asymmetrical distribution skewed towards lower molecular weight, *Appendix A. Figure A.6*. This asymmetrical distribution is consistent with the absence of chain transfer and the slow quenching of the polymerization caused by the diffusion of water, further validating that the polymerization proceeded in the droplet. We confirmed this result by performing a systematic study where the molecular weight of the polymer synthesized at several residence times was compared between the fast quench and droplet configuration. At each tested rt, the droplet encapsulation technique produced higher molecular weight polymers compared to fast quench, *Figure 3.5*. This higher molecular weight demonstrates, for the first time, successful ring-opening polymerization of biodegradable cyclic esters in an aqueous dispersion.
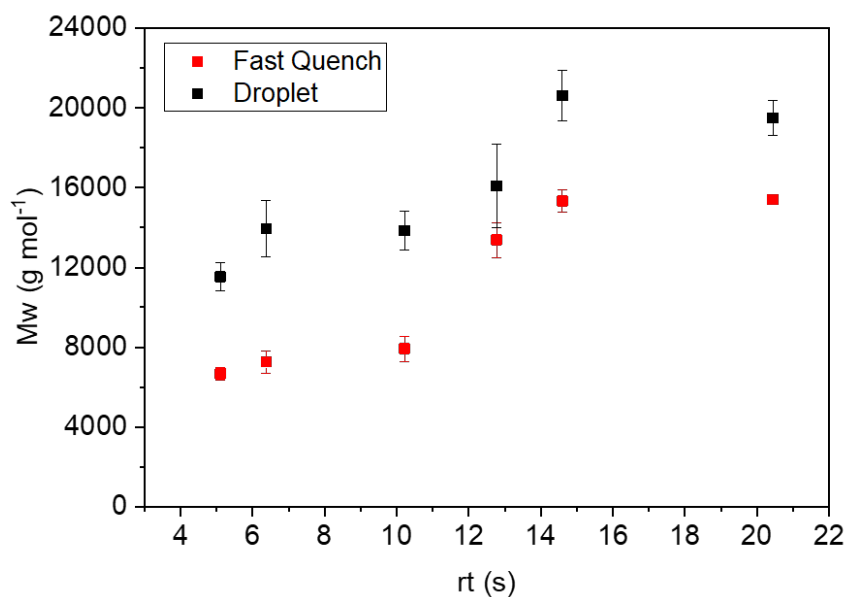
Figure 3.5: Comparison between the molecular weight of polymer produced using the fast quench and droplet generation configuration Reaction conditions: [KOMe]:[urea]:[monomer] = 1:3:200 and [monomer]0 = 3 M in THF at room temperature. Mw determined by PS calibrated GPC in THF. Fast quench configuration: quenching solution is acetic acid. Droplet generation configuration: Tergitol 1% added to the continuous water phase.

To demonstrate the benefit of performing a ROP in dispersion, we aimed to synthesize biodegradable elastomer particles by introducing a crosslinking monomer within the dispersed phase. We chose bis(e-caprolactone-4-yl)propane (BCP), because this crosslinker is compatible with the urea organocatalyzed ROP.[92,166] We maintained the polymerization conditions used above, but the catalyst was switched from **Urea 1** to **Urea 2** to allow for the copolymerization of the VL monomer with the CL-based crosslinker. Slight modifications to the device were made to prevent increased pressure and potential clogging from the higher viscosity of the crosslinked polymer solution, see *Appendix A. Figure A.8* for more details. The addition of a 0.5% loading of BCP led to a dramatic increase in molecular weight to 45.2 kg mol^{-1} in 10 seconds, **Table 1 entry**

6. The dispersity of the resulting polymer simultaneously increased to 2.4, consistent with the presence of crosslinking. When comparing the fast quench to droplet configuration for a range of rt between 5-13 seconds, the polymer obtained from the droplet polymerizations showed higher molecular weight for every flow rate tested, ***Appendix A. Figure A.10.*** After increasing the loading of the BCP to 1% we produced crosslinked particles with a molecular weight of 65.3 kg mol^{-1} and a dispersity of 2.6, ***Appendix A. Figure A.9***. The crosslinked polymer droplets still contained the hydrophobic solvent, toluene, and therefore were not robust solid particles. The addition of methanol to the collection vessel allowed the toluene to diffuse out of the droplets into the aqueous phase, in turn, creating solid particles, ***Video S2***. Through the introduction of the crosslinker BCP, we were able to expand the use of the encapsulation technique to produce crosslinked biodegradable materials in flow.

3.4 Conclusions

With the development of this encapsulation technique for water-sensitive ring-opening polymerization catalysts, we have demonstrated, for the first time, ROP in an aqueous dispersion, as well as the generation of crosslinked biodegradable elastomer droplets in flow. Through device design and understanding of fluid mechanics, we were able to encapsulate the water-sensitive urea organocatalysts in between monomer and hydrophobic solvent. The heterogeneous polymerization protected the urea catalyst from the aqueous phase, allowing polymerization to proceed while in the aqueous phase. The droplet ROP encapsulation was able to produce a maximum molecular weight of 20.6 kg mol^{-1} compared to the fast quench configuration maximum of 15.3 kg mol^{-1}. This encapsulation technique offers a wide variety of tunability of the polymer particles produced. To illustrate this, we introduced a crosslinking monomer into the formulation to produce

biodegradable elastomer particles. The molecular weight of the resulting elastomer droplets reached a maximum of 65.3 kg mol^{-1} with a dispersity of 2.6, confirming the that crosslinking had occurred. These particles can then be isolated and processed similarly to non-biodegradable coagulated latex (*e.g.*, styrene butadiene rubber and natural rubber) offering a sustainable alternative to the accumulation of non-biodegradable thermoset based objects in landfills. Further work into the functionalization of these particles for more advanced applications could further a diverse field of research, including coatings, drug delivery, and biomedical applications.

CHAPTER 4: Design Rules For Performing Water-Sensitive Polymerizations in an

Aqueous Dispersion [2]

4.1 Chapter Overview

The water sensitivity of ring-opening polymerizations (ROP) prevents any polymerization technique using water as a solvent which ultimately sets a limit on the polymeric material accessible. We implement a droplet microfluidic encapsulation strategy to create polyester and polyether particles dispersed in water. In this work, we systematically investigated the process and formulation parameters that govern the stability of the micro-droplets during generation, flow, and collection. More specifically, we tune droplet viscosity, surface tension, and hydrophobicity through the addition of amphiphilic block copolymers (ABC) and hydrophobes to further shield the ROP catalyst in the aqueous dispersion. The increased catalyst stability ultimately results in higher monomer conversion and higher molecular weight polymer. We subsequently show that by changing the ABC composition, we can further tune the ROP reaction time. Finally, we applied the encapsulation technique and formulation optimization to perform another water-sensitive ROP in an aqueous dispersion. Utilizing our design rules to tune the viscosity and surface tension of the droplets, we successfully synthesized polyether particles dispersed in water. Overall, we demonstrate the power and versatility of the encapsulation methodology and establish the fundamental guiding principles to encapsulate water-sensitive polymerization catalysts to yield spherical polymer particles dispersed in water.

4.2 Introduction

The process used to produce a polymer is known to impact the final properties of the material. For example, polystyrenes synthesized via solution polymerization versus suspension

polymerization have different material properties and thus are used for different applications (e.g., expanded polystyrene and high impact polystyrene).[167–169] Suspension polymerization is a process that uses mechanical agitation to generate monomer droplets suspended in a nonsolvent. The polymerization occurs within the monomer droplets, and the liquid phase outside of the droplets provides temperature and viscosity control allowing the polymerization to reach high molecular weight. Water is a very common continuous phase for suspension polymerizations as it is economical, environmentally friendly, and has extremely low solubility in most synthetic polymers.[170,171] Aqueous suspension polymerization, however, is incompatible with water-sensitive chemistries like the ring-opening polymerization (ROP) of cyclic monomers (e.g., ester and ether), with the exception of ring-opening metathesis polymerization (ROMP).[12,18,160,172,173] In previous work, we encapsulated water-sensitive ROP catalysts via droplet-based microfluidics, which temporarily shielded the catalyst and allowed polymerization to proceed in an aqueous dispersion.[127]

The microfluidic encapsulation strategy separately supplies a catalyst solution and a monomer solution in a hydrophobic solvent, which are fed into a narrow tube where the polymerization starts before meeting the immiscible continuous aqueous phase at a co-flowing junction to form micrometer-sized droplets, *Figure 4.1a*. By supplying the catalyst solution between two monomer streams, we ensure that the hydrophobic solvent and monomer surround the catalyst to protect the catalyst during droplet formation. The device can operate in both a droplet generating orientation and a 'fast quench' orientation, *Appendix B. Figure B.1*. The fast quench configuration allows us to precisely determine the reaction extent at the end of the hypodermic tubing outlet tip responsible for droplet generation for each flowrate before droplet formation. This technique allows us to access particles that could not be directly synthesized using

any other polymerization technique, specifically we will show production of spherical crosslinked polyester[127] and polyether particles in flow.[174]

To further expand this methodology to other water-sensitive ROP chemistries, we sought to understand the parameters enabling control of the rate of water diffusion. A slower rate of water diffusion would equate directly with a longer polymerization time and thus higher monomer conversion and polymer molecular weight. From our previous studies, we revealed that the addition of a nonionic surfactant to the aqueous phase led to both increased consistency in the droplet formation and minimized coalescence of the droplets during collection. Both observations appeared vital to the success of the methodology as any perturbation of the droplets during generation or collection would decrease the amount of time the catalyst has to polymerize before water diffusion into the droplet resulting in catalyst deactivation. Herein, we focus on probing and altering the two most important droplet generating parameters (i.e., the viscous and interfacial forces). By changing the viscous and interfacial forces through the formulation of the organic phase, we hypothesized that we would slow the diffusion of water into the droplet and, therefore, extend the catalyst's lifetime in the aqueous dispersion. The encapsulation methodology lets us easily tune droplet viscosity, surface tension, and hydrophobicity by adding amphiphilic block copolymers (ABC) and hydrophobes within the polymerization solution, **_Figure 4.1b_**. We will explore the organocatalyzed ROP of δ-valerolactone with urea anion catalyst to form microparticles. The design rules we develop show how changing the ABC loading and composition can change the water-sensitive ROP catalysts' polymerization activity in an aqueous phase. Finally, we expand the encapsulation methodology to include another water-sensitive ROP system to demonstrate the versatility of this methodology. We will show the ROP of propylene

oxide catalyzed by a frustrated Lewis pair (phosphazene + organoboranes) with and without crosslinker to form polyether microparticles.
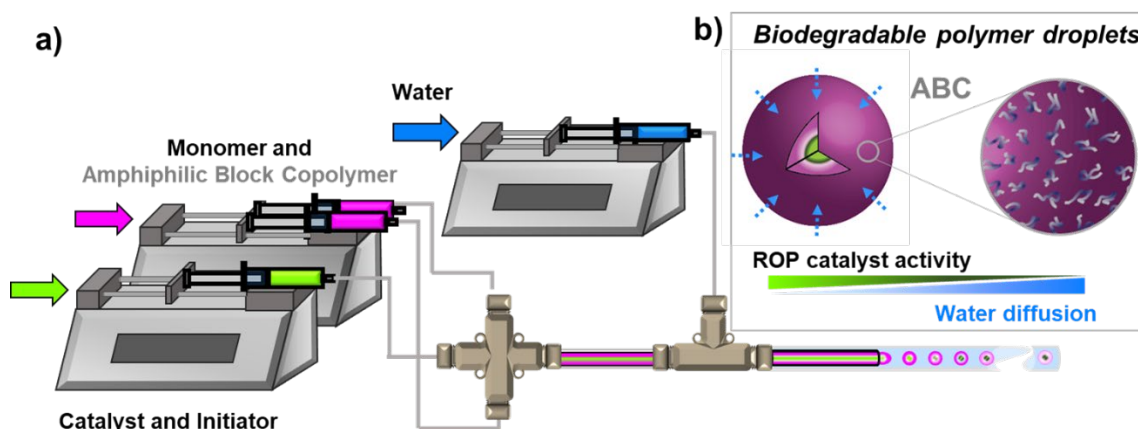

Figure 4.1: a) Schematic of the droplet-based microfluidic device, where the monomer and catalyst streams are separately supplied until they reach the cross-tee. The ROP is initiated within the reactor volume until coming in contact with the immiscible water phase and shearing off into droplets. b) After droplet generation, water begins to diffuse into the droplet microreactor, consequently quenching the ROP catalyst. As more water diffuses into the droplet, catalyst activity decreases. The amphiphilicity of the ABC added in the monomer phase allows its migration to the droplet interface, stabilizing the droplet.

4.3 Results and Discussion

Formulation and Fluid Dynamics

The droplet-based microfluidic device we implement is a co-flow geometry reactor constructed with all commercially available components and generates an oil-in-water (O/W) emulsion of 300μm sized droplets.[127] ***Appendix B. Figure B.2*** provides a detailed description of the device. The choice of microfluidics as the encapsulation method allows great control over encapsulation efficiency and homogeneity in droplet size. The droplet formation is influenced by four forces, including viscous, interfacial tension, inertia, and buoyancy. Because flow velocities are relatively low (uL/min-mL/min) and the surface to volume ratio is high for micron-sized

droplets, gravity and inertia forces become insignificant.[120] Thus, we are left with viscous and interfacial tension as the two main forces that influence droplet dynamics.[175] The viscous stresses at the tip of the needle act to elongate the interface before droplet formation, whereas the surface tension attempts to minimize the surface area. These two forces are best expressed by the Capillary number $Ca = \frac{\mu U}{\gamma}$ (viscous/interfacial), where μ is viscosity, U is flow velocity, and γ is interfacial tension.[176]

To control droplet generation, breakup, coalescence, and mixing, we can tune each of the parameters in the Capillary number individually to see its effect on polymerization progress in the aqueous phase. Firstly, we looked at velocity (U), which is the most straightforward parameter to control via the flow rates (Q). For consistent catalyst encapsulation within microdroplets, we must operate in a dripping regime, where the droplet pinches off near the organic phase outlet tip before the droplet fills the cross-section of the outer capillary channel. The organic phase intrudes into the outer capillary, where the aqueous phase is continuously flowing. The droplet begins to form under the competition of interfacial tension, drag force, and momentum force. As the droplet size increases, the flow of the aqueous phase is obstructed and the drag force induced by the outer phase increases, which elongates the droplet and eventually leads to droplet break-off. The point at which the droplet breaks off is dependent on the flow rate ratio (*i.e.*, $Q=Q_{dispersed}/Q_{continuous}$). The use of syringe pumps allows precise control over the flow rates, which is paramount because if the flow rate of the continuous phase is too high (*Q<<1*) droplet forms in the jetting regime. Droplets formed in the jetting regime are less desirable as they are less uniform because droplet breakup is erratic, and the jetting stream exposes more surface area to the aqueous phase before droplet formation,[177] leading to faster quenching of the polymerization, ***Appendix B. Figure B.3a.*** On the other hand, when the continuous phase flow rate is too low (Q>1), the flow regime shifts to the

slug regime, where the droplet fills the width of the outer capillary channel. The interaction between the capillary tube wall and droplet perturbs the interface. This perturbation induces mixing and, therefore, would increase the diffusion of water into the droplet, *Appendix B. Figure B.3b*.[178–180] For this geometry to operate in the dripping regime, we keep the flow rate ratio between 0.3 and 0.5.

Next, we look at optimizing the interfacial tension (γ). In the dripping regime, the shear force acts against the interfacial force. The addition of a surfactant, which contains hydrophobic and hydrophilic portions, lowers the surface tension at the interface between the two immiscible phases.[181,182] Thus, during passive droplet formation, surfactants are transported to the interface, where they stabilize the droplets against coalescence.[183] Previously, we found that a 1 wt% Tergitol loading to the aqueous phase was sufficient to improve droplet formation and prevent coalescence during flow and collection. However, we found that when an insufficient amount of surfactant was added to the system, we only produced droplets in a small area of flow rates, and most process conditions were producing droplets in the jetting regime. Alternatively, when an excess of surfactant was added, the droplets would break apart into smaller droplets during flow and coalesce during collection. Thus, relying solely on the addition of surfactant to the aqueous phase is insufficient to improve droplet formation without detrimental changes to the flow regime.

Lastly, we looked at the role of viscosity. We hypothesized that if we increased the viscosity of the droplet, we could increase the stability of the droplet during collection. The viscosity of the organic phase has a positive correlation to the extent of the ROP. As the residence time within the reactor volume increases, the polymerization conversion and the resulting continuous phase viscosity increase concurrently. As the mass concentration of polymer in the droplet increases, there is an increase in the fluid viscosity and shear resistance. If we change the

viscosity of the solution through the change of formulation, we will also change the droplet generation dynamics.[184] Therefore, the force required for droplet break-off increases. With this in mind, we looked towards changing the formulation of the organic phase through both the interfacial tension and viscosity. Ultimately, we opted to add an amphiphilic block copolymer to the dispersed phase, which would both increase the viscosity of the organic phase and alter the surface tension between the two phases leading to clean and consistent droplet formation, *Figure 4.2*.
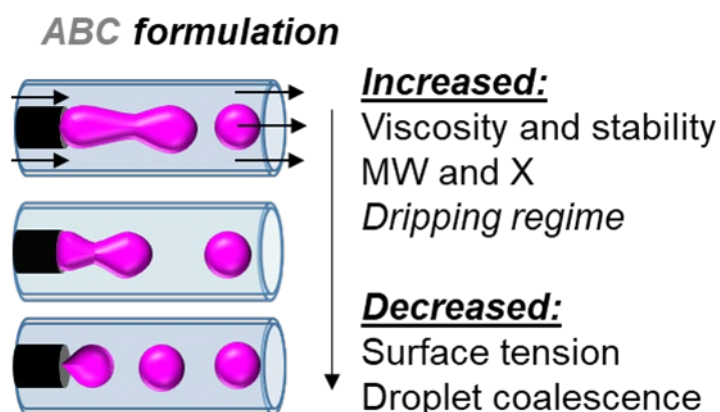

Figure 4.2: Through formulation and fluid mechanic optimization, droplet formation shifts from the undesirable jetting regime to the desirable dripping regime.

Urea Anion ROP Chemistry and Amphiphilic Block Copolymers

We focus the encapsulation methodology on urea anion catalysts which perform the ring-opening polymerization (ROP) of cyclic esters to yield biodegradable polymers, *Scheme 4.1a.*[12,30,160] The extreme water sensitivity of this polymerization allows us to easily see how the changes in the parameters affect the stability of the catalyst within the micro-droplets. Additionally, this catalytic system has been shown to exhibit fast kinetics (full conversion X >

90% in t<10 s) for several cyclic esters.[47,50,161] The success of the methodology relies on the high rate of polymerization to compete with the rate of water diffusion into the droplets. The faster the polymerization is, the better the chance of seeing polymerization progress before complete catalyst quenching via water diffusion. The choice of δ-valerolactone as the monomer is deliberate as it is a liquid monomer, which affords operation at high monomer concentrations with less solvent.

Scheme 4.1: a) The urea anion catalyst ring-opening polymerization of δ-valerolactone with the addition of amphiphilic block copolymers. b) Synthetic scheme for organocatalytic ROP of block copolymers poly(ethylene glycol)- poly(valerolactone) (PEG-PVL) and poly(ethylene glycol)-poly(caprolactone) (PEG-PCL). Structure of purchased Pluronic (PEG-PPG-PEG).
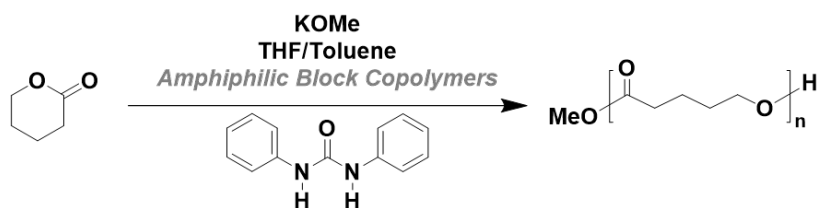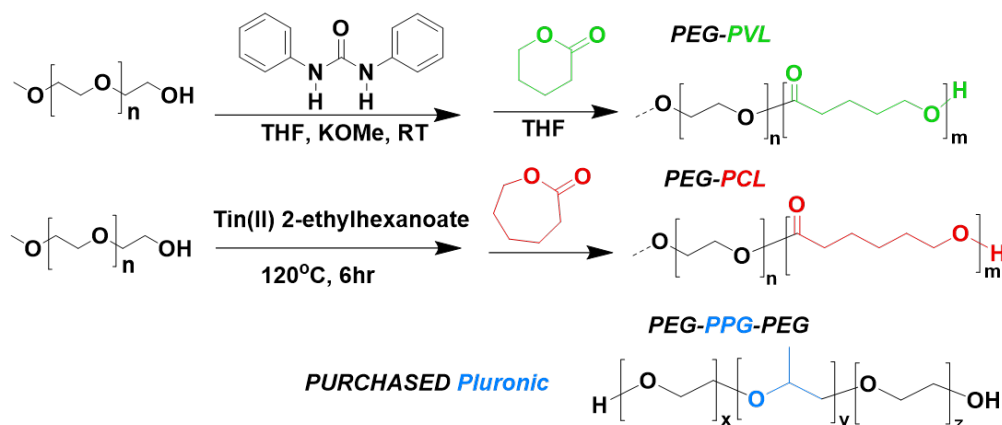
We synthesized two ABCs with different polyester blocks, including poly(ethylene glycol)-poly(caprolactone) (PEG-PCL)[185] and poly(ethylene glycol)- poly(valerolactone) (PEG-PVL)[186], and purchased a Pluronic (PEG-PPG-PEG), *Scheme 4.1b*. A table listing the ABC

molecular weights and block lengths can be found in ***Appendix B. Table B.1***. Before transferring the chemistry to the microfluidic device, we first tested the compatibility and impact of the ABCs on the urea anion catalyzed polymerization of δ-valerolactone. We found that even at an excess loading of 2 wt%, there was little to no effect on the polymerization kinetics in batch for PEG-PVL, PEG-PCL, and the Pluronic ***Appendix B. Figure B.5***.

Amphiphilic Block Polymer Loading Impact on Catalytic Activity

We chose the Pluronic (14 kg mol^{-1}) to build the ABC loading ladder and identify the optimal ABC loading to the monomer solution. The optimal loading of Pluronic would produce a large range of residence times in the droplet regime without clogging the device. If the viscosity increases too much due to the progress of the ROP and the addition of the Pluronic within the solution, it can lead to significant pressure build-up within the smallest internal diameter in the device and result in clogging or stalling of the pumps. By placing the Pluronic in the monomer phase, the amphiphilic molecule is added at the outer shell of the organic droplet and thus closer to the interface organic/water interphase, where it decreases the droplet's surface tension. At a loading below 0.25 wt% of Pluronic in the dispersed phase, we could not produce droplets in the dripping regime. At loadings higher than 1 wt%, the device would experience clogging at the longer residence times. Therefore, we focused the loadings in between those bounds. To measure the success of the ROP protection from the aqueous phase, we compared the monomer conversion (using gas chromatography, GC) and the polymer molecular weight (using gel permeation chromatography, GPC) obtained from both the fast quench and droplet samples.[187] Using a GC to determine the conversion of the monomer in the biphasic mixture was not trivial as we had to ensure that the biphasic aliquots were homogeneously dissolved in the GC solvent. We use THF

as the main solvent and decane as the internal standard. A detailed description of the polymer product analysis can be found in *Appendix B*.

First, we confirmed that the addition of the Pluronic has no adverse effect on the ROP in flow. To do this, we operated the device in the 'fast quench' configuration and compared the different loadings to a control with no Pluronic in the solution, ***Figure 4.3a,c.*** Both the polymer's molecular weight (GPC) and monomer's conversion (GC) data agreed that the addition of the Pluronic did not slow down the polymerization, as similar molecular weight polymers and conversion were obtained within the device at each residence time for all the loadings.
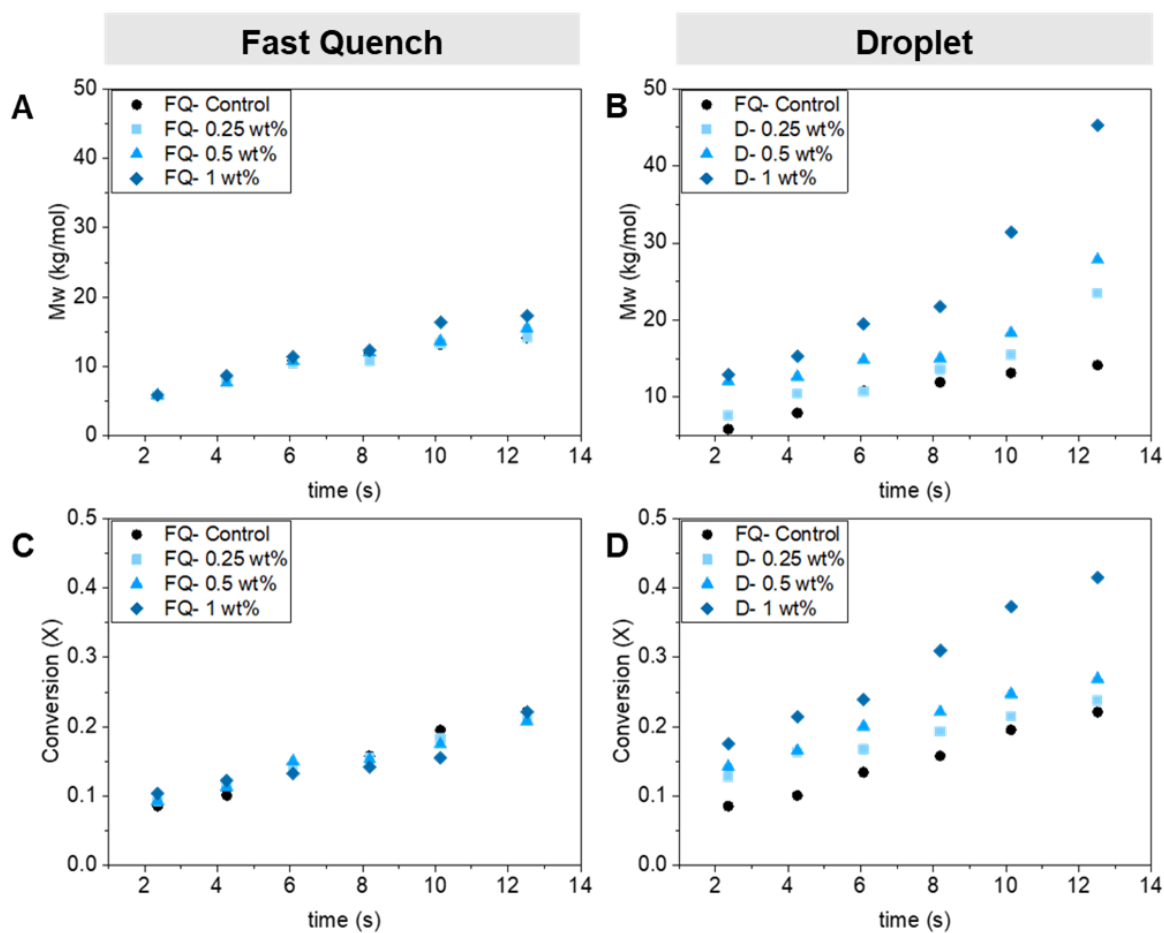

Figure 4.3: Figure showing the effects of Pluronic loading (0.25 wt%-1 wt%). a) GPC data

Figure 4.3: (cont.) for the Pluronic loadings during fast quench into acetic acid. b) GPC data for Pluronic loadings during droplet formation, using water as the continuous phase. c) GC data for Pluronic loadings during the fast quench, using decane as an internal standard. d) GC data for Pluronic loadings during droplet formation, using decane as an internal standard.

Next, we operated the device in the droplet generating configuration at each of the Pluronic loadings. We observed a positive correlation between the molecular weight and conversion attainable at each residence time with the increase in Pluronic loading from 0.25 wt% to 1 wt%, *Figure 4.3b,d*. For example, at the longest residence time ~12.5s, the conversion attainable with an ABC loading of 0 compared to 1wt% leads to an increase from 22% to 42%, respectively. The maximum molecular weight attainable was tripled with the addition of the 1 wt% loading compared to the 0 wt% control (14.6 kg mol^{-1} to 45.3 kg mol^{-1}). These results confirmed that we temporarily shielded the water-sensitive ROP catalyst from the aqueous phase by tuning the Pluronic loading to the organic phase allowing the ROP to proceed while in the aqueous dispersion.

Amphiphilic Block Copolymer Composition Impact on Catalytic Activity

After demonstrating that the loading of the Pluronic in the organic phase played a role in catalyst protection, we investigated whether the ABC chemical composition also affects the final molecular weight and conversion attainable in the droplet. First, we confirmed that neither the PEG-PVL nor PEG-PCL adversely affected the ROP kinetics in the 'fast quench' configuration at the optimal 1 wt% loading found previously, *Figure 4.4a,c.* Similarly, as residence time increases, there is a steady increase in molecular weight (GPC) and conversion (GC) for all the ABC implemented in the flow device. Therefore, we concluded that the composition of these three ABCs did not negatively affect the ROP kinetics while in the device.
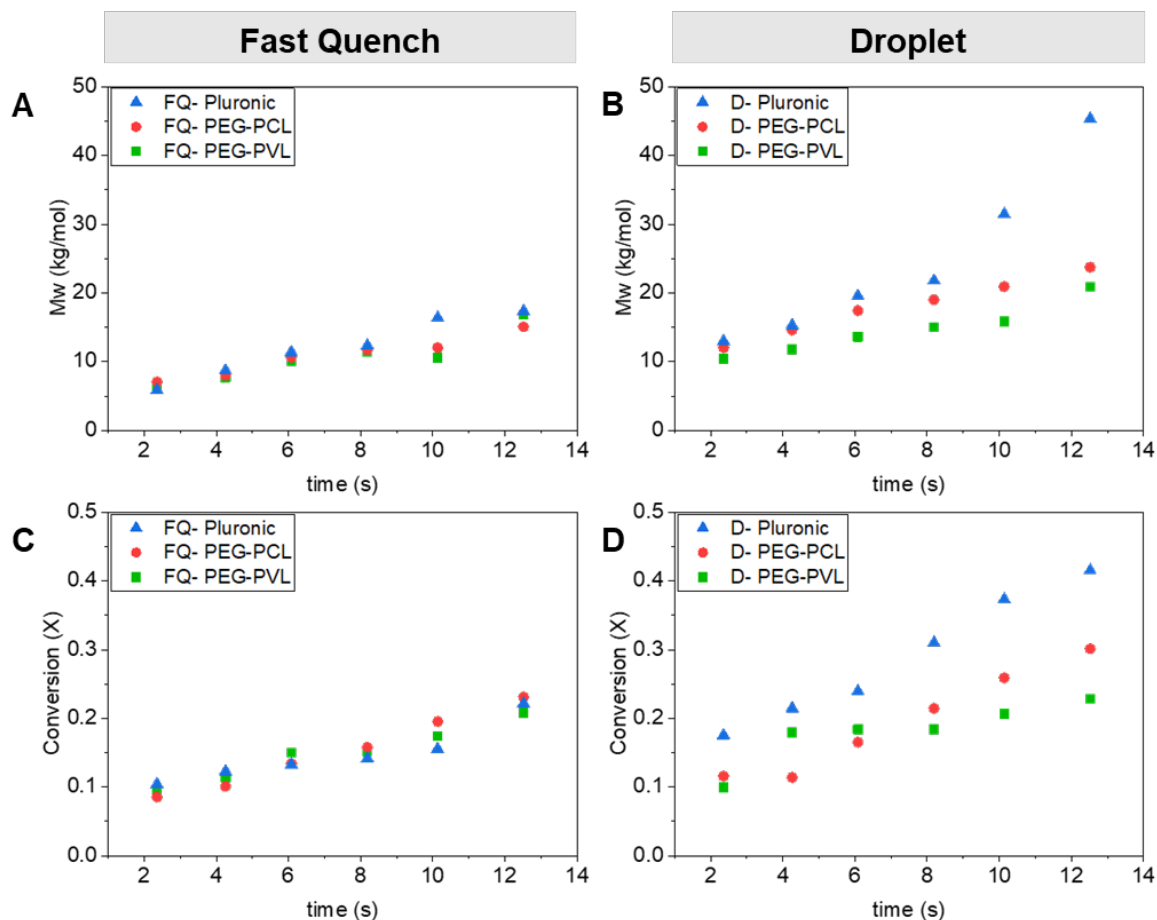
Figure 4.4: Figure showing the effects of ABC composition, comparing PEG-PVL, PEG-PCL, and Pluronic at 1 wt% loading. a) GPC data for the different ABC compositions during fast quench into acetic acid. b) GPC data for the different ABC compositions during droplet formation, using water as the continuous phase. c) GC data for the different ABC compositions during the fast quench, using decane as an internal standard. d) GC data for the different ABC compositions during droplet formation, using decane as an internal standard.

Next, we compared the impact of the three different ABC compositions on the ROP within the droplets. We observed a difference in the conversion and the ultimate polyester molecular weight between the three ABCs, *Figure 4.4b,d*. The Pluronic outperforms the two di-blocks, while PEG-PCL seems to perform slightly better than PEG-PVL at higher residence times. We

tentatively attributed this difference in performance to the difference in the hydrophilic-lipophilic balance values (HLB) between the ABCs used, **Table 4.1**.

Table 4.1: Composition comparison between amphiphilic block copolymers

Composition	Mw[a]	Hydrophobic/ Hydrophilic repeating unit	HLB
Pluronic[a]	14600	0.16	16.5
PEG-PCL	13300	0.71	7.08
PEG-PVL	6500	0.74	6.12

(a) Mw was determined by GPC in THF at 40°C versus polystyrene standards. *a)* Pluronic purchased from Sigma Aldrich. PEG-PCL and PEG-PVL synthesized

We conjecture that the larger amount of hydrophilic repeating units of the Pluronic increases the amount of hydrophilic units that migrate to the aqueous/droplet interface. The amphiphilicity of the ABC can lower the surface tension of the droplets during droplet generation and flow, which would lead to higher droplet stability and increased catalyst protection. The HLB for non-ionic surfactants takes into account the molecular weight of the hydrophilic portion of the molecule (M_h) and the molecular weight of the whole molecule (M), $HLB = 20 \times \frac{M_h}{M}$. As you increase the HLB of the ABC from 0 to 18 you shift from a hydrophobic/oil-soluble molecule (HLB~0-6) to a water-dispersible molecule (HLB~6-9) and finally to a hydrophilic/water-soluble molecule (HLB~8-18).[188–190] The PEG-PVL, PEG-PCL, and Pluronic, therefore, fall into the oil-soluble, water-dispersible, and water-soluble categories, respectively. The Pluronic, which

performs the best, has an HLB consistent with surfactants utilized as oil/water emulsifying agents. Since we are generating an oil/water dispersion, it is consistent that the micro-droplets and subsequent dispersion are most stable with the Pluronic as the ABC versus the other two compositions. As mentioned previously, the stability of the droplet during generation, flow, and collection is paramount to the success of the process. Any perturbation of the droplet throughout its formation could increase the rate of transport of water into the droplet and lead to faster catalyst quenching. Overall, these experiments revealed that the composition of the ABC impacts the catalyst protection efficiency, which affects the catalyst activity within the droplet before quenching.

Addition of Hydrophobes to Micro-Droplet Formulation

After seeing the dramatic increase in ROP stability that the Pluronic ABC gave to the ROP chemistry, we wanted to investigate whether adding a superhydrophobe to the dispersed phase formulation increased the conversion in the micro-droplets. The rationale behind adding a superhydrophobic agent to the reaction mixture was that it would further prohibit the diffusion of water into the micro-droplet and extend the reaction time before catalyst quenching. We probed a series of superhydrophobic solvents (hexane, silicon oil, and hexadecane) that were miscible with the starting reaction solution to determine which did not negatively affect the ROP kinetics. Ultimately, we chose hexadecane as our superhydrophobic agent because we found that the organic solution was transparent and homogenous, and the ROP reached high molecular weight and conversion in under 30 seconds in batch. The addition of hexadecane in batch was shown to not affect the ROP kinetics at 0.4M, ***Appendix B. Figure B.7.***

However, once we added the hexadecane into the flow reactor with the same reactant concentrations as in previous experiments, we observed a deviation from the stable increase in molecular weight and conversion in the fast quench with the addition of 1 wt% Pluronic, *Figure 4.5a,c*. The significant decrease in rate in the fast quench set-up was further observed in the droplet configuration with and without the addition of Pluronic to the trials containing the hydrophobe, *Figure 4.5b,d*. During droplet formation, we noticed that there were precipitants already forming inside of the droplet as the solution was exiting the outlet tip. We postulate that both the Pluronic and polymer resulting from the ROP have poor solubility within the hexadecane and therefore are crashing out of the solution.
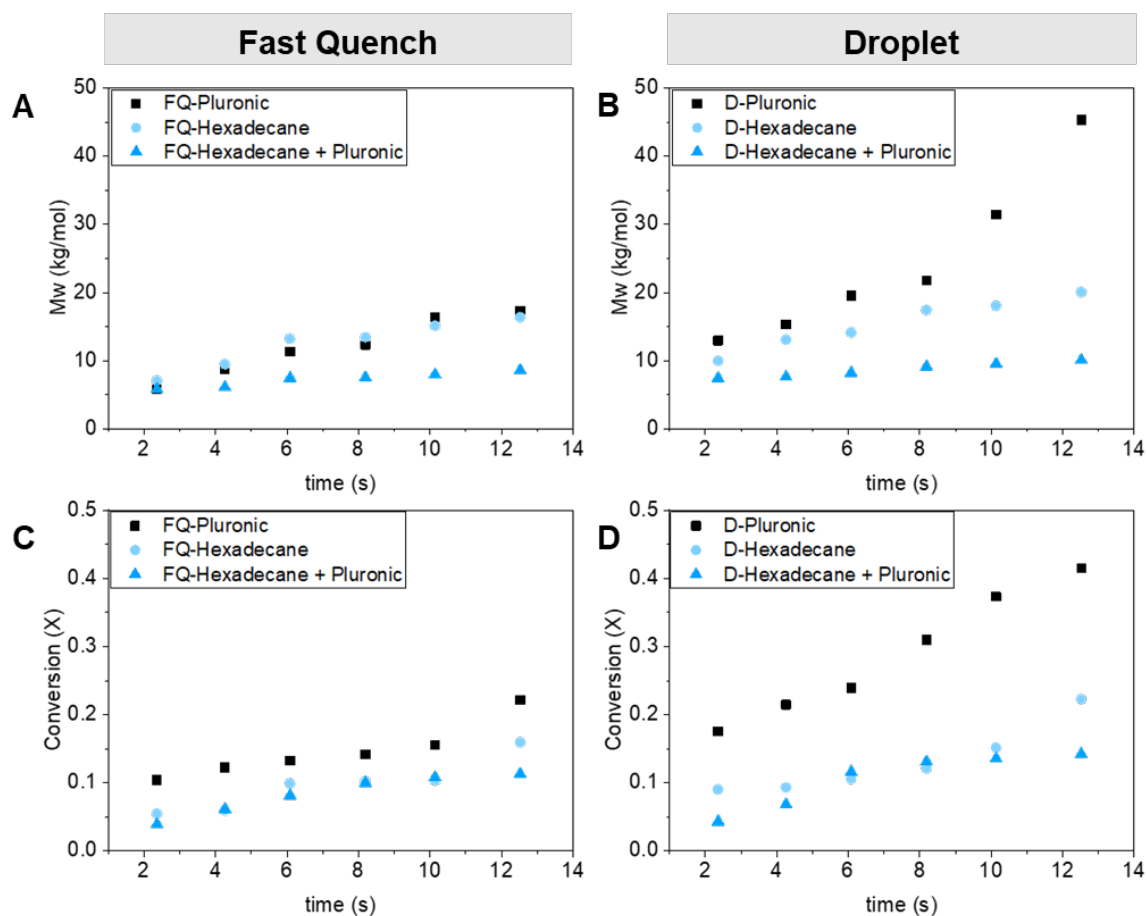
Figure 4.5: Figure showing the effects of superhydrophobic hexadecane addition at 0.4M with and without 1 wt% loading of Pluronic. a) GPC data for the addition of hexadecane with and without Pluronic during fast quench into acetic acid. b) GPC data for the addition of hexadecane with and without Pluronic during droplet formation, using water as the continuous phase. c) GC data for the addition of hexadecane with and without Pluronic during the fast quench, using decane as an internal standard. d) GC data for the addition of hexadecane with and without Pluronic during droplet formation, using decane as an internal standard.

Even though decreasing the polarity of the organic phase through the addition of the hydrophobe proved to be unsuccessful in this case, it highlighted an important constraint for this methodology. Specifically, we learned that we must ensure that the reactants, ABC, and the polymer product are soluble within the hydrophobe chosen. Further investigation into other

superhydrophobes in the system is needed to assess whether or not they have the potential to decrease water diffusion into the micro-droplets for enhanced catalyst protection efficiency from the aqueous phase.

Encapsulation of ROP Epoxide Catalysts

To demonstrate the robustness of the design rules, we aimed to expand polymerization techniques in a different water-sensitive catalyst system.[159] Specifically, we applied the micro-droplet encapsulation methodology to the ROP of epoxide catalyzed by a frustrated Lewis pair (phosphazene + organoboranes).[191–194] We performed the ROP of propylene oxide (PO) with octanol as the initiator, phosphazene base (P$_2$-t-Bu) and triethyl borane (Et$_3$B) as co-catalysts, *Scheme 4.2.* We opted for this polymerization chemistry as we hypothesized that it could yield high molecular weight polymers within seconds.

Scheme 4.2: a) The ring-opening polymerization of propylene oxide via phosphazene base (P$_2$-t-Bu) and triethyl borane.
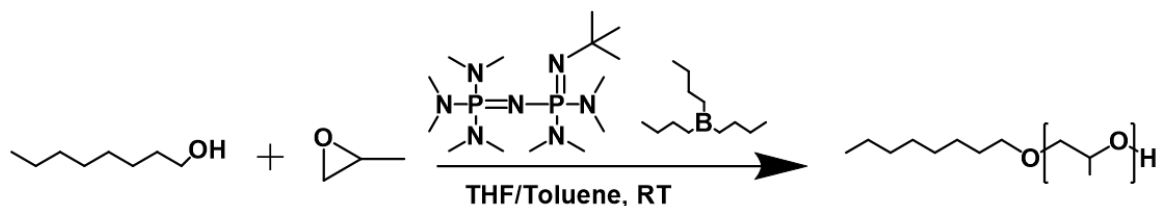
We first attempted to identify the loading of the catalysts and concentration of the PO to achieve fast kinetics in batch. However, the high rate of polymerization targeted also equated with a highly exothermic reaction due to the high heat of polymerization of epoxides.[195] Therefore, we utilized the microfluidic flow system to safely assess different catalyst loadings and monomer concentrations as the long microfluidic reactor could absorb the heat released by the

polymerization. Additionally, we immediately quenched the solution as it exits the outlet tip in the fast quench configuration and through the water diffusion into the micro-droplets. To further enhance the safety of the experiment, we slightly modified the microfluidic flow system to prevent any possible backflow of the catalyst solution into the monomer reservoir, ***Appendix B. Figure B.8***. More information on the modifications can be found in the ***Appendix B***. This set-up led us to safely identify a formulation that delivers the fast kinetics necessary to compete with water diffusion during droplet formation. The final formulation utilized a monomer loading of 4M and an initiator:base:borane:monomer ratio of 1:3:16:100.
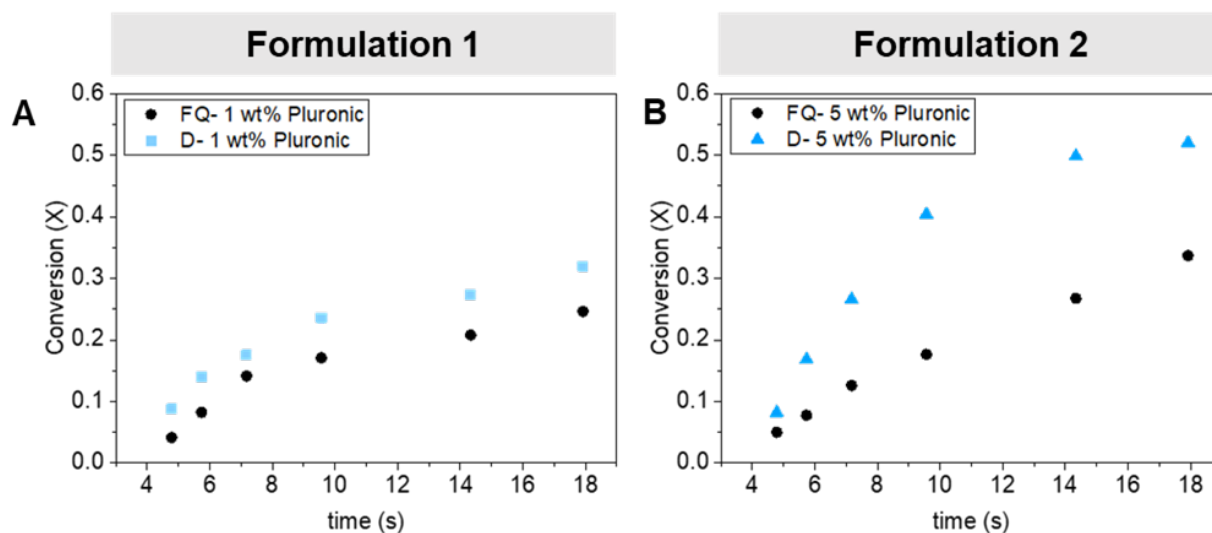

Figure 4.6: A) Fast quench (FQ) vs droplet (D) conversion for the ROP of PO with 1 wt% Pluronic B) FQ vs D conversion for the ROP of PO with 5 wt% Pluronic

We then verified that there are no negative effects on the reaction kinetics with the addition of the pluronic to the formulation ***Figure 4.6a***. Next, we performed the polymerization in the droplet configuration, and we saw a similar increase in the extent of the reaction for each of the residence times compared to the fast quench results, for example at rt = 9.5s the conversion in fast

quench compared to droplet was 17.1% to 23.5%, respectively. This slight increase in conversion was indicative that the droplets were providing some catalyst protection; however, we aimed to further increase the extent of reaction happening within the dispersion to validate that polymerization does continue in the aqueous phase. Based on the design principles we developed, we postulated that an increase in viscosity or an increase in ABC loading would enhance the stability of the droplet, which would lead to a greater extent of reaction in the dispersion. The first formulation modification intended to increase the viscosity of the polymer attained after droplet formation by adding a crosslinker, 1,4-Butanediol diglycidyl ether. With the addition of 1wt% crosslinker, we saw a rapid increase in viscosity after the 10s residence timepoint, which resulted in clogging within the device. Therefore, we operated between 2-10s to avoid clogging when adding the crosslinker. With the addition of the crosslinker, we saw an increase in conversion at rt = 9.5s from 26% in the fast quench to 41% during droplet generation, ***Appendix B. Figure B.9***. By introducing the crosslinking molecule, we increased the maximum conversion and molecular weight attainable in the dispersion.

The second formulation modification is intended to increase both the viscosity and decrease surface tension by increasing the ABC loading from 1 to 5 wt%. This formulation showed the largest catalyst stability enhancement in the dispersion illustrated by an increase in conversion from 17.6% to 40.3% at rt=9.5s, **Figure 4.6b**. Both these experiments further demonstrated the validity and robustness of the developed design rules. Through simple formulation optimization, we altered the viscosity and surface tension of the organic phase, which directly lead to an increase in catalyst stability and subsequently increased reaction extent. From our deep understanding of the role that viscosity and surface tension play on the stability of the droplet during generation, flow, and collection, we were able to temporarily shield a new water-sensitive catalyst and

promote, for the first time, the ROP of PO in an aqueous dispersion. Additionally, we confirmed that the micro-droplet encapsulation methodology can be applied to other water-sensitive catalytic systems, which can increase catalytic activity within an aqueous dispersion.

4.4 Conclusions

In conclusion, we have implemented a droplet encapsulation strategy on two water-sensitive ring-opening polymerizations to successfully polymerize 300μm size polyester and polyether particles in an aqueous dispersion. The encapsulation resulted in increased catalytic activity over our previous results owing to a systematic study probing the two most important droplet parameters, the viscous and interfacial forces. We assessed the addition of three amphiphilic block copolymers (PEG-PVL, PEG-PCL, and Pluronic) and a hydrophobe (hexadecane) and their effectiveness in improving particle formation and control leading to enhanced catalyst protection from the aqueous phase. We established that an increase in the loading of a Pluronic ABC resulted in an increase in catalytic activity. The 1 wt% Pluronic loading led to the highest molecular weight (45.3 kg mol^{-1}) and conversion (X=42%) compared to the 0 wt% loading (Mw= 14.6 kg mol^{-1} X=22%). Next, we showed that the composition of the ABC affects the catalyst protection efficiency. As the hydrophobic to hydrophilic repeat unit ratio increases, there are fewer hydrophilic units capable of assembling at the droplet interface, which would prevent the decrease in surface tension and therefore decrease droplet stability. Similarly, as the hydrophilic-lipophilic balance value increased we saw an increase in consistent droplet formation and stability during collection. The Pluronic which had the most hydrophilic repeating units and the largest hydrophilic-lipophilic balance was shown to best stabilize the oil/water micro-droplets in the aqueous dispersion leading to the highest monomer conversion. Next, we

investigated whether adding a superhydrophobe, hexadecane, would decrease or slow water diffusion into the micro-droplets. However, we found that the ABC and resulting polymer from the ROP would precipitate out of the solvent at the detriment to the catalytic activity.

Finally, we highlighted the versatility of the micro-droplet encapsulation methodology by expanding to another water-sensitive polymerization. Specifically, we performed the ROP of propylene oxide via an organic Lewis-Pair catalyst system. Through our deep understanding of the role that viscosity and surface tension play on droplet dynamics, we optimized the formulation to achieve a monomer conversion 20% higher within the microdroplets than in the fast quench. These results highlight that the off-the-shelf droplet-based microfluidic device and encapsulation methodology have the potential to be compatible with any fast water-sensitive polymerization.

CHAPTER 5: Expanding Biodegradable Elastomer Particles To Controlled Drug Delivery

5.1 Chapter Overview

Controlled drug delivery offers many advantages over conventional dosage forms, including improved convenience, reduced toxicity, and improved efficacy. The use of polymers for drug delivery systems comes with many advantages due to their tunability and wide range of physical, chemical, and mechanical properties. Herein, I will introduce controlled drug delivery and the benefits of utilizing polymer-based delivery systems. Then I will focus on synthetic biodegradable polymers, specifically polyesters, and their drug release kinetics and degradation mechanisms (i.e. surface or bulk degradation). Next, I will introduce our methodology for expanding the applications of our crosslinked biodegradable elastomers to tune the drug release profiles. Three polymer-based particles are proposed to show the effect of dispersed drug release, tethered drug release, and crosslinked/tethered drug release. The preliminary results show that the drug release kinetics can be improved by tethering and encapsulating the drug within our biodegradable elastomer droplets.

5.2 Introduction Controlled Drug Delivery and Biodegradable Polymers

Controlled drug release systems have improved modern treatments by reducing the number of drug administrations, eliminating the need for specialized drug administration, and increasing therapeutic activity compared to the intensity of side effects.[196–198] A large number of current drugs benefit from controlled release, including antiinflammatories, immunosuppressants, steroids, hormones, anesthetics, vaccines, antibodies, and chemotherapeutics.[199–202] The use of polymers-based drug delivery systems has proliferated since synthetic polymers can be synthesized with various physicochemical properties.[203,204] Molecular weight, composition, (e.g. hydrophobicity

and surface charge), crystallinity, and biodegradability are critical physicochemical properties of polymers utilized for controlled drug delivery.[205,206] Classifying this wide range of polymers is difficult because of the diversity of polymers available, but two broad classifications are 1) whether the polymer is non-biodegradable or biodegradable, and 2) whether the polymer is natural or synthetic,[3] *Figure 5.1*.
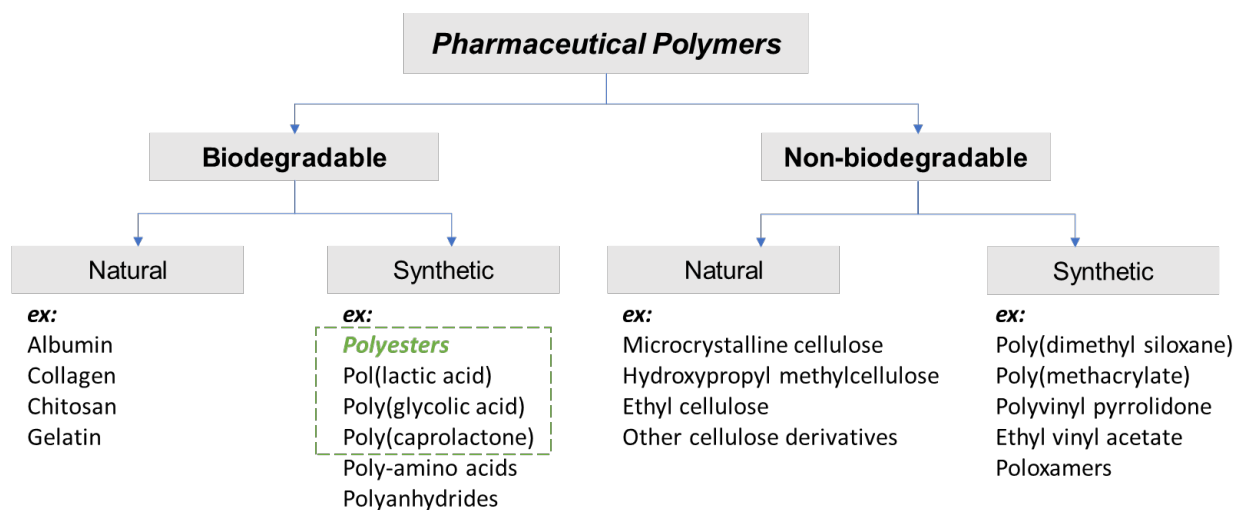

Figure 5.1: Classification of pharmaceutical polymers can be broadly categorized as biodegradable versus non-biodegradable, then subsequently categorized as natural or synthetic polymers. The synthetic biodegradable polyesters of interest are highlighted in green.

Polymers are selected on the basis of the drug formulation as well as the delivery mechanism (i.e. intravenous, topical, enteral, or parenteral).[207,208] The use of synthetic polymers comes with many advantages over naturally occurring polymers, including a wide range of physical, mechanical, and chemical properties that can be reproducibly modified as needed per application.[209–211] Similarly, biodegradable polymers offer many advantages over nonbiodegradable polymers. Most importantly, biodegradable polymers are naturally eliminated from the body through degradation, which eliminates the need for subsequent surgical removal of

the device or accumulation of the formulation within the body. Biodegradable polyesters were among the first synthetic biodegradable polymers to be successfully applied in medicine as resorbable sutures, drug delivery matrixes, pharmaceutical applications, tissue engineering matrices, and surgical implants.[212–216]

The most commonly used synthetic biodegradable polymers belong to the polyester family, whose synthesis was discussed in depth in **Chapter 1**. Poly(lactic acid) (PLA), poly(glycolic acid) (PGA), poly(lactic-co-glycolic acid) (PLGA), poly(valerolactone) (PVL), and poly(caprolactone) (PCL) are some of the most widely utilized synthetic polymers in drug delivery,[217,218] *Scheme 5.1.* These synthetic biodegradable polymers have been widely investigated due to their diversity, tunability, biocompatibility, and mechanical strength, which makes them successful drug delivery materials for biomedical applications because they have the potential to protect an active drug component from degradation while allowing a sustained release of the drug over time..[219,220] Polyesters undergo hydrolytic bond cleavage to form water-soluble degradation products that can dissolve in an aqueous environment, resulting in polymer erosion into body-friendly degradation byproducts.[221] The degradation period for these polymers ranges from one month to multiple years. The degradation rate can be impacted by both environmental conditions (i.e. temperature and pH) and the polymer's characteristics (i.e. chemical composition, molecular weight of the polymer, and crosslinking density (if any)).[222]

Scheme 5.1: A few of the most widely used polyesters utilized in drug delivery, their monomers, and their degradation products, including poly(lactic acid) (PLA), poly(glycolic acid) (PGA), poly(lactic-co-glycolic acid) (PLGA), poly(valerolactone), and poly(caprolactone) (PCL).

Scheme 5.1: (cont.)
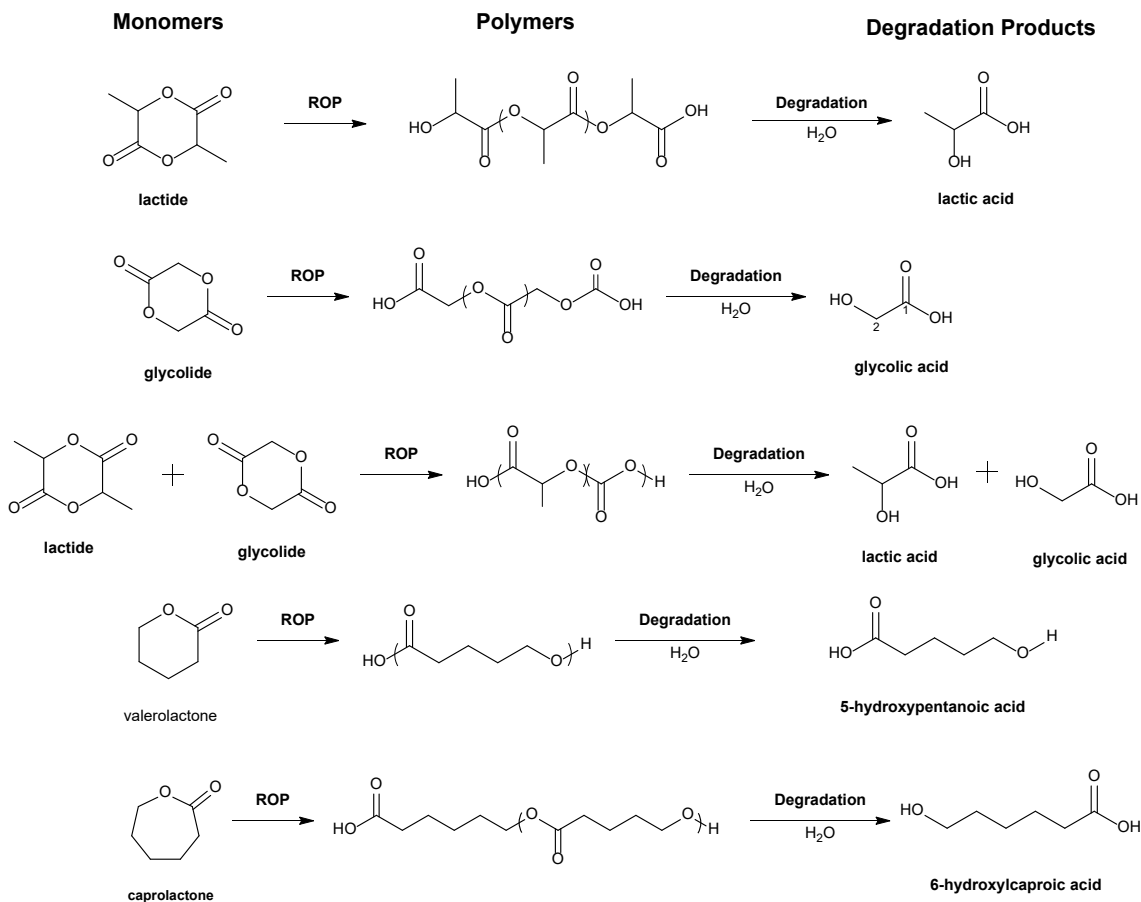
The main objective of controlled release delivery systems is to release therapeutics at the desired anatomical site and to maintain the drug concentration within a therapeutic window for the desired duration. The therapeutic window is bounded by two concentrations, the maximum safe concentration (MSC), where any concentration of the drug above this level starts showing toxicity, and the minimum effective concentration (MEC), where any concentration of the drug below this level shows no therapeutic effect..[223] Maintaining the drug concentration at any instance between the MSC and MEC is critical for the safety and efficacy of the therapeutic. Understanding and controlling drug release profiles is vital for proper dosage and sustained release within the

therapeutic window. Many profiles exist including sudden and delayed burst release, oscillating release, sustained first-order release, and zero-order release, ***Figure 5.2.***
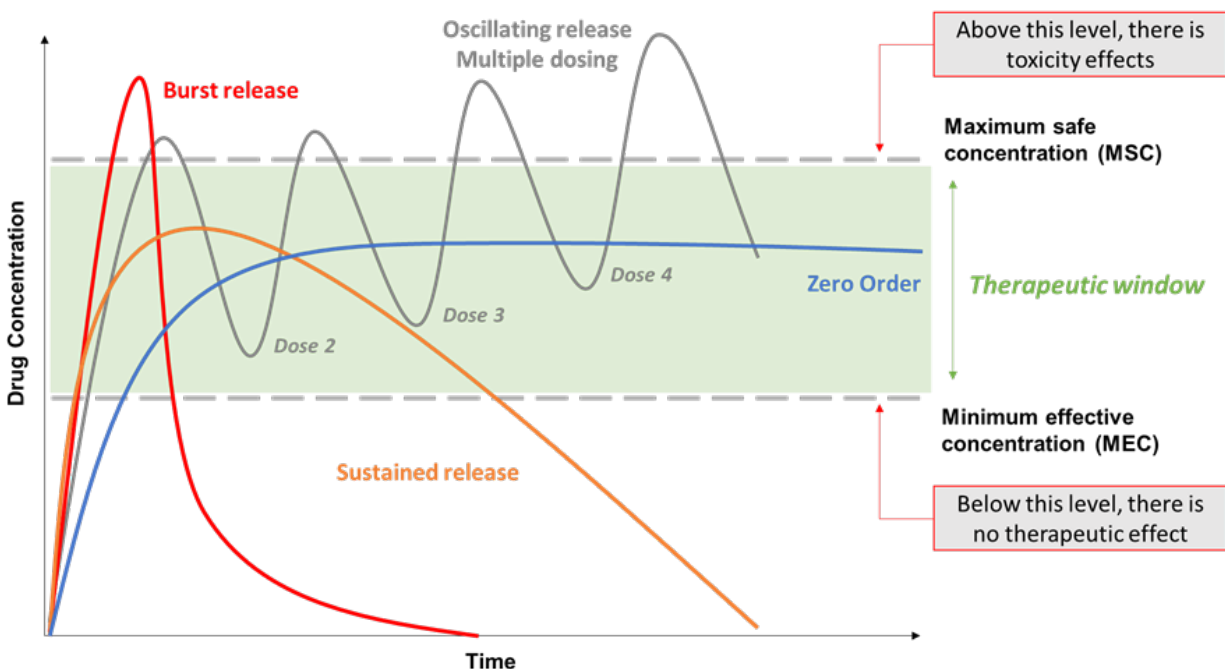

Figure 5.2: Drug delivery is effective without displaying toxicity between the therapeutic window, which ranges between the maximum safety concentration (MSC) and the minimum effective concentration (MEC) is shown in green. Drug release concentration profiles can either be oscillating (due to multiple dosing), burst release, sustained release, or the desired zero-order release.

Oscillating release kinetics result from multiple dosing from traditional non-controlled release systems. In an oscillating release, each dose results in a burst release, eventually compounding within the body to exceed the MSC. Burst release kinetics are undesirable as most of the drug is released over a short period of time usually above the MSC, and over time drug release continues below the MEC.[224] Sustained first-order release kinetics improve pharmacokinetics; however, there is an initial period of rapid release followed by a first-order release.[225] This shortens the amount of release time before the concentration of the drug falls below the MEC. Zero-order release systems are the most optimal as they overcome the issues facing the

previous release systems by releasing the drug at a constant rate.[226] Drug release profiles can be controlled through tuning the polymer composition and physical properties and through the mechanisms of release.

Various mechanisms exist to release the drug from synthetic biodegradable polymer systems, including diffusion-controlled release, solvent-controlled release, stimuli-controlled release, and polymer-degradation release,[227] *Figure 5.3*. The diffusion-controlled release has the drug dissolved or dispersed in a core surrounded by a polymeric membrane, and a concentration gradient across the membrane drives the drug diffusion.[228–231] Diffusion-controlled release usually results in a high initial release, called a burst release. The solvent-controlled release has water uptake from outside the carrier to the drug-loaded core, and release can either be considered an osmosis-controlled release or swelling-controlled release.[232–236] Solvent-controlled release profiles can be tuned depending on the diffusion rate of water through the polymeric carrier, initial drug distribution, and polymer composition. Stimuli-controlled release relies on internal or external stimuli (i.e. pH, temperature, electric field, magnetic fields, UV, ultrasound, ionic strength, etc.) to release drug cargo from polymeric systems.[237–240] Stimuli-controlled release usually results in burst release of the drug directly following the stimuli. Degradation-controlled release utilizes matrices made of biodegradable polymers (e.g. PLA, PLGA, PCL), which undergo degradation resulting in the release of drug cargo.[241–243] The rate of degradation of the polymers can be modulated via polymer composition, molecular weight, crystallinity, and crosslinking density.[244] By tunning these parameters, bulk or surface degradation can be achieved, which allows drug release kinetics to be modified.[245] Degradation-controlled polymers have the potential to achieve zero-order release kinetics to prolong drug concentrations within the therapeutic window.
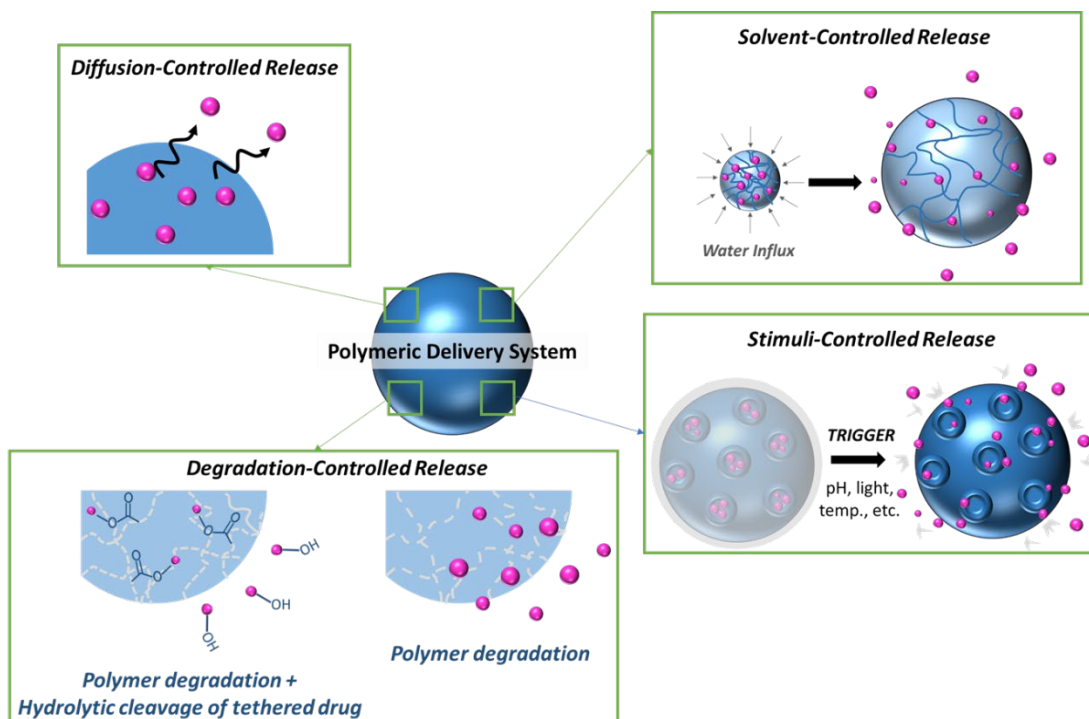
Figure 5.3: Various mechanisms for drug release from polymeric delivery systems including diffusion-controlled release, solvent-controlled release, stimuli-controlled release, and degradation-controlled release.

5.3 Surface versus Bulk Erosion

Degrading polymeric drug delivery systems occurs via surface or bulk erosion, *Figure 5.4*. In surface erosion, the polymer degrades from the exterior surface. Over time, the polymeric system decreases in surface area (i.e. mass) linearly, but the inside of the material does not degrade until the surrounding material has been degraded. This means that the strength and the molecular weight are very slightly impacted over time. In bulk erosion, degradation occurs throughout the entirety of the polymer volume equally. The surface and the inside of the material are degrading simultaneously, which leads to a dramatic decrease in the molecular weight and strength of the overall material. The polymer's erosion mechanism depends on the polymer matrix dimensions, the diffusivity of water into the matrix, and the degradation rates of the polymer's functional

groups.[246] It is important to note that surface and bulk erosion are not mutually exclusive, as many polymeric systems undergo a combination of the two or switch depending on the erosion conditions and the geometry.[247] Therefore, both erosion mechanisms can be thought of as a spectrum.
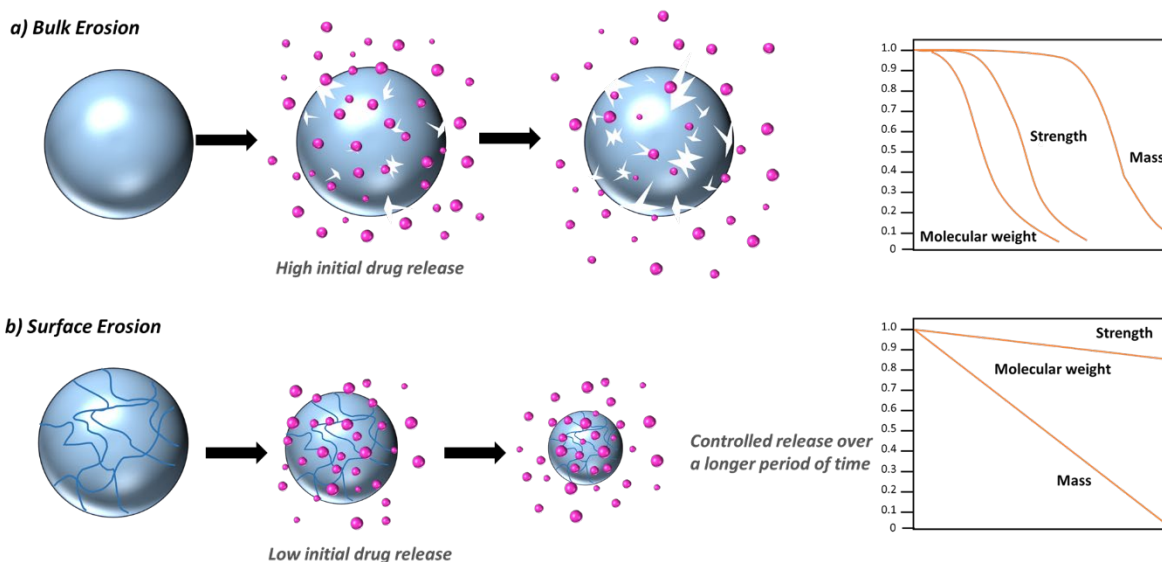

Figure 5.4: Erosion of polymeric delivery systems a)Bulk erosion results in material loss from the entire polymer volume releasing drugs quickly and then decreasing over time. The molecular weight and strength of the material are decreased over a short period of time. b) Surface erosion results in material loss from the exterior surface of the delivery system. This allows a sustained drug release over time and retains the molecular weight and strength of the material.

Bulk erosion results in material loss from the entire polymer volume and an erosion rate dependent on the total amount of material.[248] The erosion rate generally decreases as the polymer material is depleted. This decrease in release rates also provides less protection for the drug from body fluids, which results in drug degradation.[249] The length of time a bulk eroding polymer stays intact can be altered through chemical compositional changes, but not by the material size or shape since water penetrates and degrades the material's interior faster than the surface.[250] For ideal

surface erosion, the material is lost from the polymer matrix exterior surface, which results in an erosion rate that is directly proportional to the external surface area.[251] The length of time the polymer stays intact can be altered through material size and shape, and chemical properties. Surface erosion is easier to control than bulk erosion, so it is preferred in drug delivery. The constant and easily controllable degradation allows fine control of the drug release and can protect the drug from *in vivo* degradation.[249]

5.4 Biodegradable Elastomer Particle Methodology

In **Chapter 3,** we showed the successful generation of biodegradable elastomers via a synthesis of crosslinked polymer particles through the copolymerization of bis(ε-caprolactone-4-yl)propane and δ-valerolactone, ***Figure 5.5.*** Our motives for adding the crosslinker, at the time, were simply to produce higher molecular weight particles with improved integrity during collection. The crosslinker provides an easy way to drastically increase the molecular weight of the polymer without having to significantly change the composition of the solutions we are using in the flow device. By introducing a crosslinker, we produced 300 μm sized particles with molecular weights of 65.3 kg mol^{-1}.[127] However, upon further investigation, we found that this crosslinking chemistry was not conducted in spherical particles in continuous flow. Our droplet-based microfluidic system and deep understanding of the parameters surrounding the ring-opening polymerization (ROP) in an aqueous dispersion allowed us to produce novel spherical biodegradable elastomers.
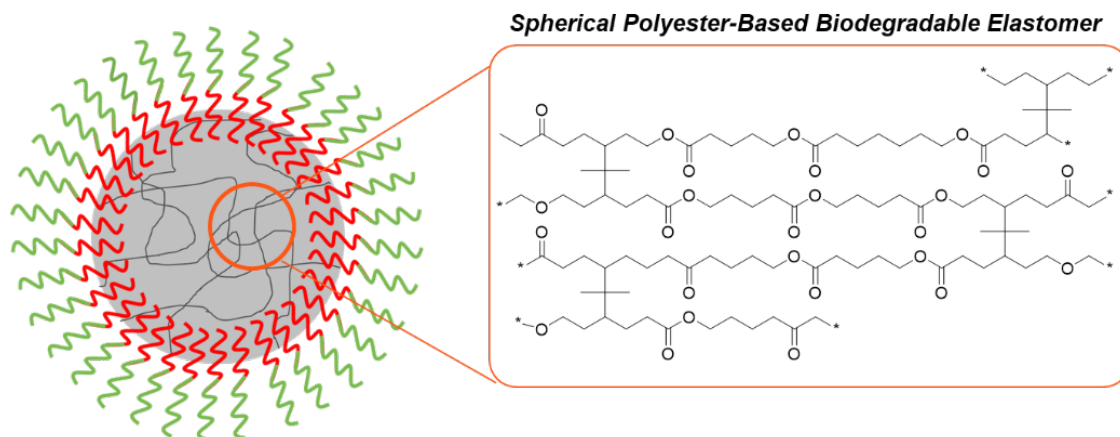
Figure 5.5: Spherical polyester-based biodegradable elastomer particles made via a droplet-based microfluidic device.

Crosslinking of polyesters with bis(ε-caprolactone-4-yl)propane (BCP) has been used to generate biodegradable elastomers, with various applications in the biomedical field, including tissue engineering and controlled drug delivery.[92,252–254] When BCP is utilized as a cross-linking agent, a polymer network is formed, where tetra-functional cross-links are incorporated into the growing polymer chain. By changing the loading of BCP, one can easily control the crosslink density and therefore final properties of the polymer network. With small loadings (1-5 wt%) high crosslinking percentage is obtained.[255] Throughout the literature, crosslinking was performed to produce thin films or spread over Petri-dishes to produce elastomers in the shape of the container. Inspired by the tunability of the polymer particles we have produced with our droplet-based microfluidic system, we aimed to reimagine the capabilities of our biodegradable elastomer particle production for drug delivery.

Our goal was to perform the urea-anion catalyzed ROP of δ-valerolactone and bis(ε-caprolactone-4-yl)propane to influence the chemical and physical properties of the polyester particles we produce. By crosslinking the linear polymer systems, we can modulate the degradation time and decrease the amount of mass loss over time by targeting surface erosion over bulk erosion.

Additionally, we tether the drug to the polymer which will require surface erosion and hydrolytic cleavage of the drug from the polymer chain leading to a slower drug release. To tether the drugs to the polyester chains, we must utilize a drug that contains an alcohol group, which can act as an initiator during the ROP, *Scheme 5.2.* We chose to stay with the urea-anion catalyst, but the choice of which urea catalyst was an important decision. We needed to choose a catalyst that could copolymerize δ-valerolactone (VL) and ε-caprolactone (CL) with fast kinetics. From our previous study in **Chapter 3,** we knew that 1-cyclohexyl-3-phenylurea anion catalyst could polymerize VL to full conversion within 5 seconds and CL to full conversion within 30 seconds. Therefore we decided to move forward with 1-cyclohexyl-3-phenylurea as our catalyst of interest for the rest of this study. A detailed description of the synthesis of this urea can be found in *Appendix C.*

The urea-anion ROP operates via a bifunctional activation of the alcohol initiator through hydrogen bonding to the anionic portion of the urea catalyst and of the cyclic ester through hydrogen bonding to the N-H of the urea catalyst.[50] Then nucleophilic attach by the hydrogen-bonded activated alcohol leads to ring-opening and regeneration of an alcohol/urea anion adduct. The two drugs we chose to focus on were FDA-approved and commercially available chemotherapeutics Docetaxel and Paclitaxel. Docetaxel is a chemotherapeutic most used to treat breast, lung, prostate, stomach, and neck cancers. Paclitaxel is a chemotherapeutic most used to treat lung, ovarian, and breast cancers. Both chemotherapeutics have multiple alcohols that can act as initiators for polymer growth; however, the secondary alcohol is the most reactive for polymerization.[256] An additional advantage is that the ROP of lactide with Paclitaxel has been shown to produce polymer-drug conjugates that had controlled release profiles.[257] This prior work performing ROP made Docetaxel and Paclitaxel attractive drugs for our preliminary studies of drug release from our elastomeric particles.

Scheme 5.2: Urea anion ring-opening copolymerization of δ-valerolactone and bis(ε-caprolactone-4-yl)propane via the 1-cyclohexyl-3-phenylurea anion catalyst is a bifunctional activation of the initiator (alcohol group) and cyclic monomer. Two chemotherapeutics, Docetaxel and Paclitaxel, contain alcohol groups (circled in orange)that can act as initiators for the ROP. 9-anthracenemethanol is a model molecule that we will use for preliminary polymerization.
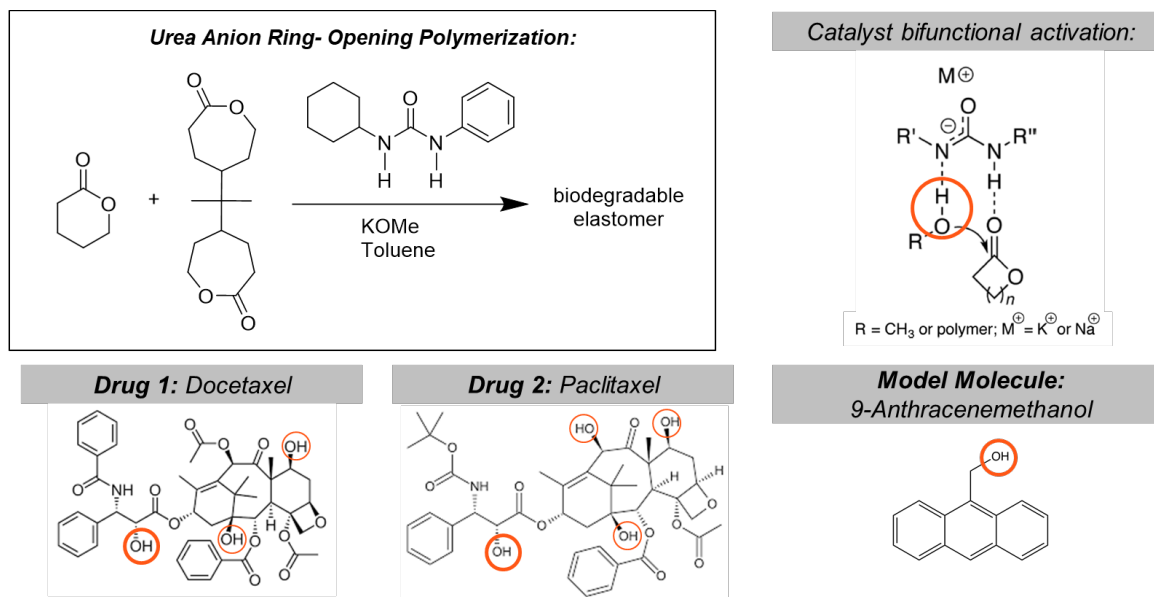
To compare the effect of crosslinking and tethering, we produce three different particles, *Figure 5.6.* Firstly, the 'simple drug dispersion' particle contains the drug of interest dispersed within the pre-polymerized polyester solution. The combined polymer and drug are supplied to our droplet-based microfluidic device to produce particles in a continuous phase. Secondly, the 'tethered drug dispersion' particles utilize the drug as the initiator for the ring-opening polymerization. The tethered polymer-drug conjugate in solution will be supplied to the microfluidic device to produce particles dispersed in the continuous phase. Lastly, the 'crosslinked drug dispersion' particles will utilize the drug as the initiator for the ROP with the addition of the BCP crosslinker. This ROP and crosslinking will be performed within the device and subsequent droplets to produce biodegradable elastomer-drug conjugates in flow.
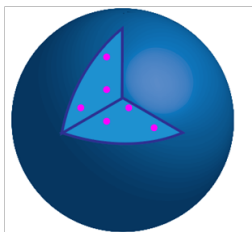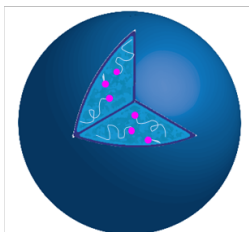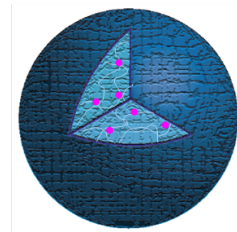
Figure 5.6: Three polyester particle variations to compare the effects of tethering and crosslinking on drug release kinetics, including a simple drug dispersion, tethered drug dispersion, and crosslinked drug dispersion. The drug is represented as the pink particles dispersed within the polyester matrix in blue.

5.5 Preliminary Results and Discussion

Droplet-Based Microfluidic Device Modifications

Slight modifications to the droplet-based microfluidic device were made to ensure that the crosslinking chemistry would not clog the device, ***Figure 5.7.*** In the original design a short 3" piece of small ID tubing (1/16" OD x 0.007" ID (0.178mm)) before being connected to a 3" piece of 25G thin wall stainless steel hypodermic tubing (0.02" OD, 0.012" ID (0.305mm)). With the modification the small ID tubing was removed to decrease the chances of pressure buildup and subsequent clogging within the small internal diameter tubing. The rest of the setup stayed the same, and depending on the formulation we can easily change the composition of the feeds into the cross-tee. For the simple drug dispersion formulation, ***Figure 5.7a***, the pre-polymerized polymer solution will sheath the alcohol/drug which will be supplied through the middle inlet of the tee. For the tethered-drug dispersion, ***Figure 5.7b***, the drug-polymer conjugate solution will be supplied through all three inlet tees. Lastly, for the crosslinked drug dispersion, ***Figure 5.7c***, the urea catalyst and the alcohol/drug (initiator) will be sheathed between two streams containing the

monomer and the BCP crosslinker. All formulations will employ a 1 wt% loading of Pluronic as the amphiphilic block copolymer shell based on our results from **Chapter 4**.
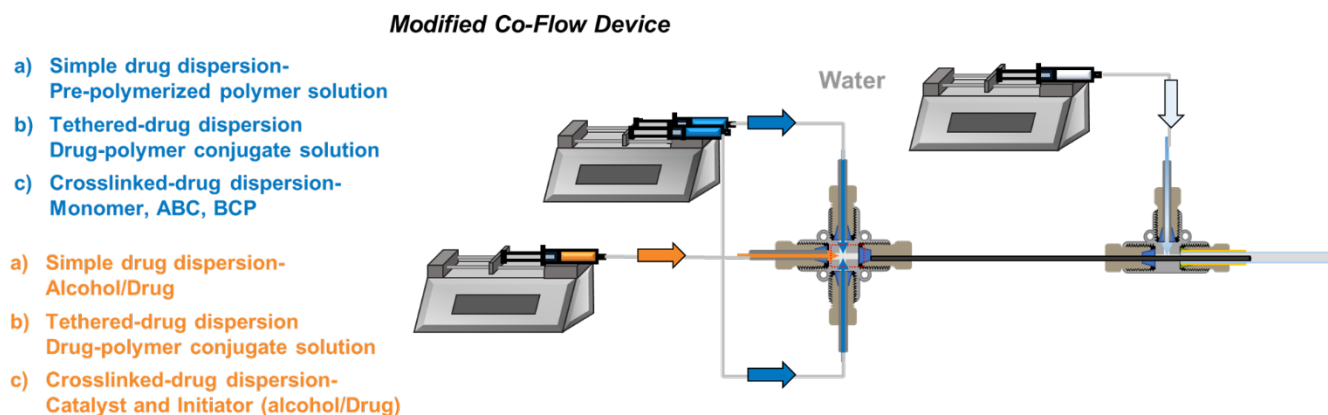
Modified Co-Flow Device

a) **Simple drug dispersion-**
   Pre-polymerized polymer solution
b) **Tethered-drug dispersion**
   Drug-polymer conjugate solution
c) **Crosslinked-drug dispersion-**
   Monomer, ABC, BCP

a) **Simple drug dispersion-**
   Alcohol/Drug
b) **Tethered-drug dispersion**
   Drug-polymer conjugate solution
c) **Crosslinked-drug dispersion-**
   Catalyst and Initiator (alcohol/Drug)

Figure 5.7: Droplet-based microfluidic modifications removing the small diameter tubing after the cross tee and replacing it with an extended hypodermic tubing.

Batch Polymerization with Docetaxel, Paclitaxel, and 9-Anthracenemethanol

Before moving into flow experiments, we first had to confirm that the two chemotherapeutics (Docetaxel and Paclitaxel) and the model molecule (9-anthracenemethanol) did not negatively impact the chemistry or the reaction kinetics. The reaction kinetics must be fast because the rate of polymerization will still be competing with water diffusion for the crosslinked drug dispersion particles. First, we replaced half the loading of our initiator potassium methoxide (KOMe) with Paclitaxel. We still need the potassium anion species for our polymerization to proceed, so we cannot fully replace the initiator with our drug of interest. After adding the Paclitaxel as a co-initiator we monitored the kinetics in batch, *Figure 5.8.* The ROP chemistry nor the polymerization kinetics were negatively impacted by the addition of the chemotherapeutic, which was very promising. The reaction reached 93% conversion within 30 s and produced a 19.5 kg mol^{-1} with a dispersity of 1.4. It should be mentioned that we were targeting around ~30 kg mol^{-}

89

[1] polymer product and we attribute the smaller molecular weight as additional initiation off the

multiple alcohol groups on the drug.

Figure 5.8: ROP of δ-valerolactone via 1-cyclohexyl-3-phenylurea potassium methoxide (KOMe) and Paclitaxel as initiators. The molecular weight and dispersity were determined by GPC against PS standards. The loading of KOME:drug:catalyst:monomer was 0.5:0.5:3:300.

After showing that Paclitaxel was a successful initiator for the ROP of VL we confirmed

that Docetaxel did not negatively impact the reaction kinetics or the ROP. Similarly, we replaced

half the loading of our initiator potassium methoxide (KOMe) with Paclitaxel and monitored the

kinetics in batch, *Figure 5.9.* In batch, the ROP kinetics were fast (X~91% in 30s) and reached

19.2 kg mol^{-1}. The actual molecular weight was less than the targeted MW and dispersity of the

polymer was 1.4 both indicative of the potential initiation of multiple alcohol groups on the
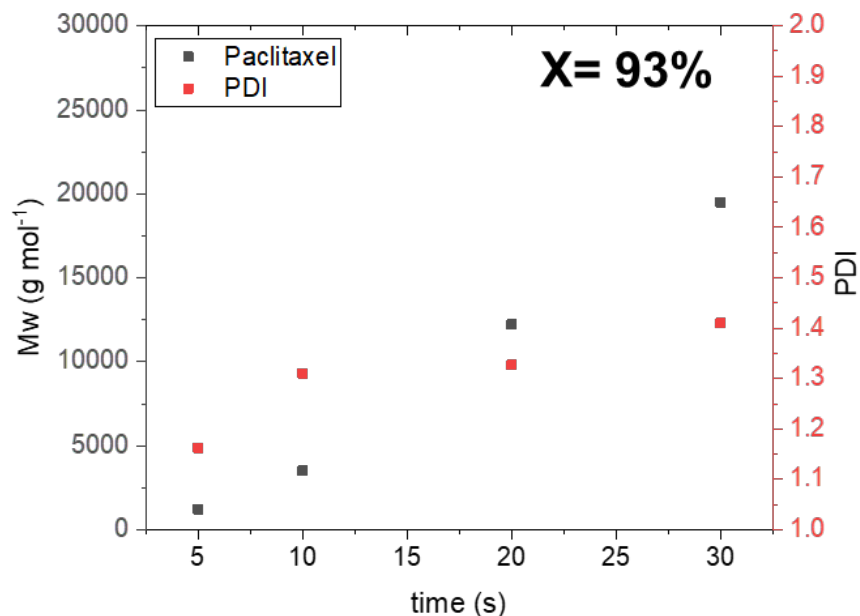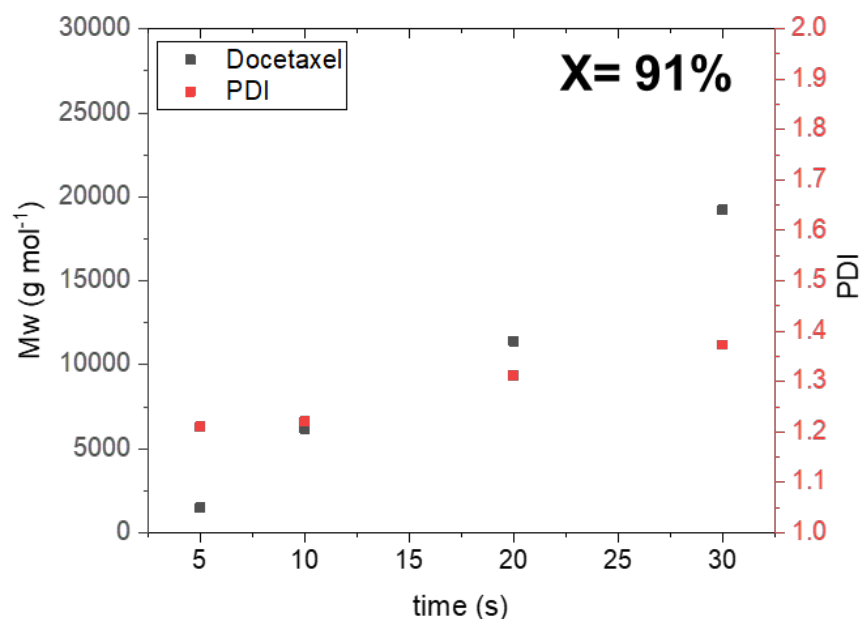
docetaxel.

Figure 5.9: ROP of δ-valerolactone via 1-cyclohexyl-3-phenylurea potassium methoxide (KOMe) and Docetaxel as initiators. The molecular weight and dispersity were determined by GPC against PS standards. The loading of KOME:drug:catalyst:monomer was 0.5:0.5:3:300.

In addition to Docetaxel and Paclitaxel we also investigated a model molecule, 9-anthracenemethanol. Observed diffusion of model drug molecules for drug delivery systems has been successfully used to accurately quantify the molecule release concentration through spectroscopy or other optical analysis.[258–260] This molecule was chosen for preliminary formulation studies as it would act as a drug analog in the ROP. The singular alcohol group also allows us to better control initiation and produce high molecular weight polymer products. Testing the model molecule in batch the ROP kinetics were fast reaching 95% conversion in 30 seconds, *Figure 5.10.* Additionally, the molecular weight of the polymer (28.1 kg mol^{-1}) was close to the target molecular weight (30 kg mol^{-1}) with a narrow dispersity (<1.14). Now that we have shown all three initiators are compatible with the ROP chemistry we can move away from batch and implement different formulations in flow.
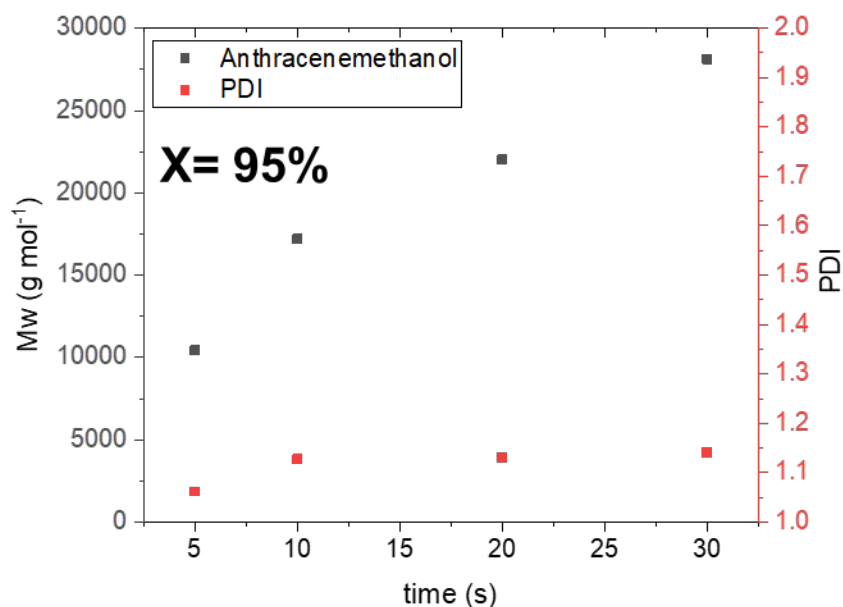
Figure 5.10: ROP of δ-valerolactone via 1-cyclohexyl-3-phenylurea potassium methoxide (KOMe) and the model molecule 9-anthracenemethanol as initiators.The molecular weight and dispersity were determined by GPC against PS standards. The loading of KOME:anthracenemethanol:catalyst:monomer was 0.5:0.5:3:300.

Comparison of Drug Release Between Three Variations of Polyester Particles

To determine the release kinetics of the active ingredient (ai), 9-anthracenethanol, from the three particles we had to produce droplets with each formulation within our microfluidic device. We first started with the simple ai dispersion. The ai was dispersed within a pre-polymerized VL polymer with a MW of 29.2 kg mol^{-1} and dispersity of 1.12. Next, particles were formed within a continuous phase of water and methanol 50:50. The particles were collected for 1 min within a total continuous phase volume of 20 mL. After particle collection, the timer was started, and samples were taken at intervals and analyzed via UV-VIS. The characteristic peak for 9-anthracenemethanol at 255 nm was measured over time. When the samples were not being analyzed the samples were kept on a shaker plate. The first timepoint at 5 minutes showed that

over 80% of the ai was released from the particle, *Figure 5.11a*. Over the course of the next hour, there was 97% cumulative drug release from the particle. As the ai was not tethered to the polymer chains it was not surprising that the ai would diffuse into the water:methanol continuous phase very quickly.
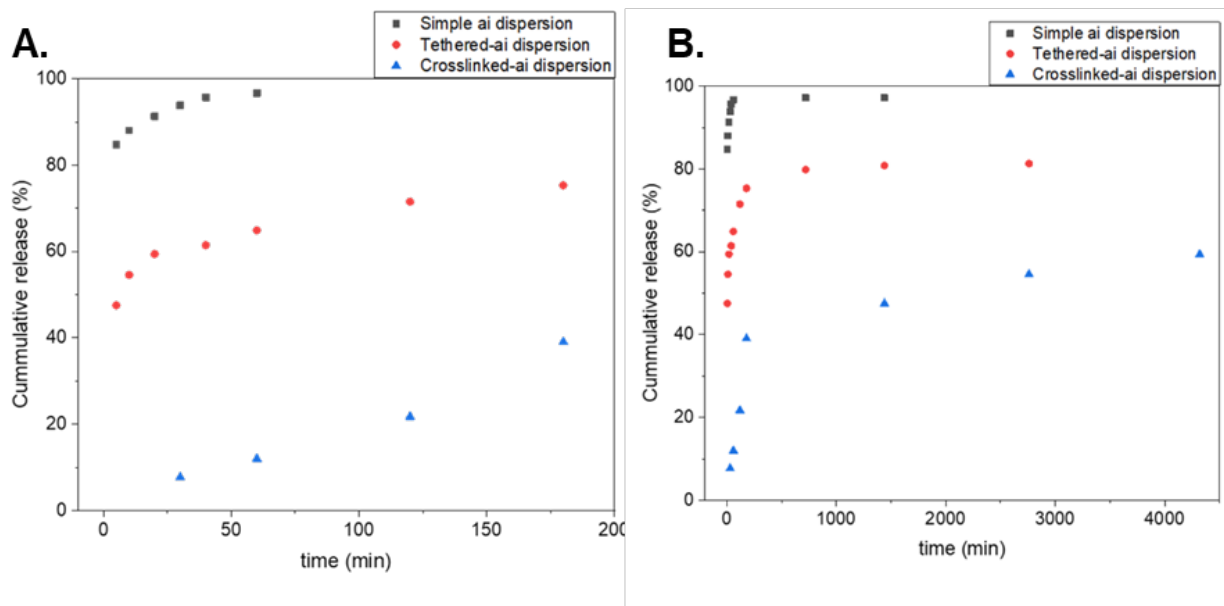
Figure 5.11: Active ingredient (ai), 9-anthracenemethanol, release from 3 different particle dispersions including simple dispersion, tethered-ai dispersion, and crosslinked-ai dispersion. A) Shows the cumulative release of the ai over 3hrs. b) Shows the cumulative release over a longer period, 72 hrs.

Next, the tethered-ai dispersion was generated via the droplet-based microfluidic system. The ai was used to pre-polymerize VL resulting in a polymer product with a MW of 28.1 kg mol^{-1} and a dispersity of 1.14. The polymer solution was fed through the reactor and the particles were collected in the same water and methanol 50:50 mixture. Particles were collected over 1 minute with a total continuous phase volume of 20 mL. Similarly, samples were taken at intervals and the characteristic peak for 9-anthracenemethanol was analyzed via UV-VIS. When the samples were

not being analyzed the samples were kept on a shaker plate. For the tethered dispersion, we report that the initial release within the first 5 minutes was decreased from over 80% with the simple dispersion to 47% with the tethered-ai formulation, *Figure 5.11a*. Sustained release of the ai was observed over the course of the next 3 hrs reaching 75%. We continued to monitor the release into the continuous phase for the next 45 hrs and we saw a plateau in the release. At a total of 48 hrs, our release was 81.2%, *Figure 5.11b*. We are still investigating why the release from the tethered particles drastically plateaued. It should be noted that after this length of time some began to break apart and form a film at the bottom of the vial, since the particles were not crosslinked. Our next steps are to analyze the film by dissolving the leftover polymer and determining whether we can recover the rest of the unreleased ai through UV-VIS analysis.

Finally, we produced the crosslinked-ai dispersion where the urea-anion ROP chemistry of VL and BCP is initiated by the ai within the device and subsequent droplets. The catalyst, KOMe, and ai were dispersed within the organic phase entering the middle inlet of the cross tee, while the monomer (VL) and crosslinker (BCP, 0.5wt% loading) were dispersed within the organic phase supplied through the two side tees allowing the solution to sheath the catalyst phase. The particles were collected over 1 minute in a water and methanol 50:50 mixture (20 mL). The particles were then analyzed via UV-VIS over the next 72 hours. Over the first 30 minutes, the amount of ai released into the continuous phase was below our level of detection with the UV-VIS, however, at 30 minutes we started to see the ai characteristic peak and determined an 8% release, *Figure 5.11a*. The crosslinked ai dispersion displaced a sustained release over the next 72 hours resulting in a max release of 59%. Similarly, to the tethered ai release our next steps are to degrade the crosslinked particle and see if we can recover the remaining ai via UV-VIS analysis. By analyzing the three release profiles it is apparent that the formulation changes drastically affect the release

kinetics and cumulative release over time. The simple ai dispersion resulted in the fastest release while tethering the ai and subsequently tethering and crosslinking slowed the cumulative release of the ai into the continuous phase. These results are very exciting and highlight the power and versatility of our droplet-generating device for comparing a range of formulations of polymer-drug delivery systems.

Ongoing Work- Biodegradable Elastomer Crosslink Density to Tune Release Kinetics

The preliminary results showing that drug release kinetics can be tuned by employing tethering and subsequent crosslinking of an active ingredient within a polymer particle are very exciting. We are currently working on reproducing our experiments and increasing the length of time that we monitor the ai release into the continuous phase. Additionally, we will be dissolving the tethered-ai polymer that is left over in the continuous phase to recover the unreleased ai. Similarly, we will speed up degradation by breaking down the crosslinked particles remaining and recovering the unreleased ai. Next, we can start changing the formulation of the crosslinked ai system. We can easily increase and decrease the loading of the BCP crosslinker to produce particles with varying degrees of crosslinking density. By increasing the crosslinking density of the particles, we may be able to further slow down the release of the ai into the continuous phase and increase the amount of time needed for cumulative release. Aside from crosslinking, many other parameters can be tuned within the formulation to tune drug release parameters, which I will go into detail about in my future work section of **Chapter 6.**

5.6 Conclusions

Utilizing a polymer-based delivery system is a very promising avenue to control release kinetics for controlled drug delivery. Synthetic biodegradable polymers, specifically polyesters, come with many advantages including chemical tunability, diversity, biocompatibility, and mechanical strength, which makes them successful drug delivery materials for biomedical applications. In this chapter, I focused on implementing our droplet-based microfluidic platform to produce three different formulations of polymer particles including a simple drug dispersion, a tethered-drug dispersion, and a crosslinked-drug dispersion. Our preliminary results show that the drug release kinetics can be improved by tethering and encapsulating the drug within our biodegradable elastomer droplets. Using 9-anthracenemethanol as a model molecule we report that the simple ai dispersion particles showed over 80% release within the first 5 minutes of particle formation, and 97% cumulative release within the first hour. The release kinetics were slowed significantly by tethering the ai to the polymer. The tethered-ai polymer particles showed 47% release within the first 5 minutes and 75% release over 48 hrs. Lastly, the crosslinked and tethered ai particles showed 8% cumulative release in 30 min and 59% cumulative release within 72 hrs. By altering the particle formulation, we were able to slow the release of an active ingredient from the polymer particle delivery system. This work is ongoing, specifically analyzing how the crosslinking density of the particles could be utilized to tune drug release kinetics.

CHAPTER 6: Conclusions and Future Directions

6.1 Conclusions

In this work, we sought to develop a catalyst encapsulation methodology to perform the water-sensitive ring-opening polymerization (ROP) in an aqueous dispersion to expand biodegradable polymerization techniques. Our encapsulation methodology is comprised of a droplet-based microfluidic process that methodically encapsulates the catalyst within the center of micron-sized droplets. The success of this approach relies on precise simultaneous control of the kinetics of polymerization, the rate of mass transfer rates, and fluid mechanics. We report, for the first time, the production of biodegradable polyester particles dispersed in water. Additionally, we develop a set of design rules for the process and formulation parameters that govern the stability of the micro-droplets during generation, flow, and collection. This framework allowed us to expand into other water-sensitive chemistries and perform the ROP of an epoxide monomer to produce polyether particles in water. The power of this encapsulation methodology can be realized through our production of novel polymeric materials that could not be made through any other means, including spherical crosslinked polyether particles dispersed in water and spherical biodegradable elastomers produced in continuous flow. Lastly, we expanded the application of our biodegradable elastomers to the field of controlled drug delivery, but tuning drug release profiles through drug tethering and crosslinking within different formulation microparticles. Overall, our droplet-based microfluidic device, encapsulation methodology, and design rules have shown their potential to expand polymerization techniques for water-sensitive chemistries, broadening the types of polymeric materials accessible.

In **Chapter 1**, I discussed the ROP of heterocyclic monomers, the general mechanisms, the thermodynamics and kinetics governing ROP, and the effect of monomer ring-strain. I then

focused more specifically on organocatalyzed ROP and the current microflow technologies being employed and their limitations. Lastly, I outlined our efforts to overcome these limitations and broaden the types of polymeric materials attainable with ROP in flow. **Chapter 2** focused primarily on the device design theory and fluid mechanics for microflow reactors, which informed the final design of our encapsulation system. The three types of forces that influence droplet generation (i.e. velocity, viscosity, and surface tension) are discussed in length and concurrently how our system allows easy tuning of each parameter. This chapter gave a detailed description of the design and development of our droplet-based microfluidic device, including device materials and geometry, operation parameters, and configurations. A central feature is the secondary fast quench configuration, which allows precise determination of the conversion at the end of the outlet tip at each flow rate before droplet formation. These first two chapters laid the foundation for our encapsulation framework which is the focus of the remainder of the thesis.

In **Chapter 3**, we established the proof-of-concept for performing the water-sensitive urea-anion ROP of the cyclic ester δ-valerolactone, in an aqueous dispersion.[127] The organic phase formulation requirements include hydrophobic solvent choice, catalyst and initiator loading, monomer selection, and monomer concentration are reported in depth. Through proper formulation selection, we produced 300 μm sized particles over a large range of residence times (1-22s). We performed a systematic study where the molecular weight of the polymer synthesized at several residence times was compared between the fast quench and droplet configuration. At each tested rt, the droplet encapsulation technique produced higher molecular weight polymers compared to fast quench. The droplet ROP encapsulation was able to produce a maximum molecular weight of 20.6 kg mol^{-1} compared to the fast quench configuration maximum of 15.3 kg mol^{-1}. This higher molecular weight demonstrates, for the first time, successful ring-opening polymerization of

biodegradable cyclic esters in an aqueous dispersion. To demonstrate the benefit of performing a ROP in dispersion, we synthesized biodegradable elastomer particles by introducing a crosslinking monomer within the dispersed phase. A 1 wt% loading of the bis(e-caprolactone-4-yl)propane (BCP) crosslinker produced particles with a molecular weight of 65.3 kg mol^{-1} and dispersity of 2.6. Through the deep understanding of our system and the fluid mechanics within microflow reactors, we expanded the use of the encapsulation technique to produce crosslinked biodegradable materials in flow that couldn't be produced through any other means.

The process and formulation parameters that govern the stability of the micro-droplets during generation, flow, and collection were explored in-depth within **Chapter 4**.[174] Specifically, we showed how our device allowed quick and efficient probing of the droplet viscosity, surface tension, and hydrophobicity through the addition of amphiphilic block copolymers (ABC). First, we explored ABC loading and its impact on catalytic activity. We observed a positive correlation between the molecular weight and conversion attainable at each residence time with the increase in Pluronic loading from 0.25 wt% to 1 wt%. Next, we tested three different compositions of block copolymers, including poly(ethylene glycol)- poly(valerolactone) (PEG-PVL), poly(ethylene glycol)-poly(caprolactone) (PEG-PCL), and Pluronic (PEG-PPG-PEG) and their effect on catalytic activity. We established that the Pluronic, which had the highest hydrophilic-lipophilic balance of the ABCs tested, is water-soluble and could therefore migrate to the interface of the particle and the aqueous phase to stabilize the droplets during flow and collection. These experiments revealed that the composition of the ABC impacts the catalyst protection efficiency, which affects the catalyst activity within the droplet before quenching. Furthermore, the design rules we developed were applied to the ROP of propylene oxide to produce polyether particles in an aqueous dispersion.

The production of crosslinked biodegradable elastomers motivated the work in **Chapter 5**, where we applied these materials to drug delivery. This chapter outlines the benefits of utilizing polymers in drug delivery systems and how drug release kinetics can be tuned via degradation mechanisms. We produced three polymer-based particles to explore the effect of dispersed drug release, tethered drug release, and crosslinked/tethered drug release. The preliminary results show that the drug release kinetics can be improved by tethering and encapsulating the drug within our biodegradable elastomer droplets. This example of utilizing our droplet-based microfluidic encapsulation device to solve other problems outside of the field of polymer science highlights the versatility and robustness of our system.

6.2 Future Directions

Thus far, I explored the use of a droplet-based microfluidic platform for the expansion of biodegradable polymer technologies. Throughout the development of the device and subsequent analysis of two water-sensitive ring-opening polymerizations in aqueous dispersions, we recognized the versatility of this device to influence other areas of research. For example, during our brief comparison of three amphiphilic molecular shells, we observed an effect of the composition on catalyst protection efficiency. Additionally, while utilizing these particles for drug delivery applications, we observed distinct release profiles when comparing a simple drug dispersion, a tethered drug-polymer conjugate, and a tethered and crosslinked drug-polymer network. These observations inspired us to utilize our device for other encapsulation applications, including encapsulation of a highly active catalyst to induce latency. Within this section, I will break down three potential avenues of research utilizing our droplet-based microfluidic device and encapsulation methodology.

Further Exploration into the Effect of Amphiphilic Block-Copolymer Shell Composition

In this work, we demonstrated that catalyst protection efficiency would be tuned by changing the composition of the amphiphilic block copolymer (ABC) shell. In **Chapter 4** we compared three amphiphilic block copolymers, PEG-PCL, PEG-PVL, and a Pluronic. From our comparison, we found that changing the composition of the block copolymers played a role in the catalyst protection efficiency. More specifically, we observed a difference in the conversion and ultimate polyester molecular weight between the three ABCs. We tentatively attributed the difference in performance to the difference in hydrophilic-lipophilic balance (HLB) values.[189] HLB values range between 0 and 20, where an HLB of 20 represents a completely hydrophilic molecule and an HLB of 0 is a completely hydrophobic agent.[261] The Pluronic, which performed the best, has an HLB consistent with surfactants utilized as oil/water emulsifying agents. Since we are generating an oil/water dispersion, it is consistent that the micro-droplets and subsequent dispersion are most stable with the Pluronic as the ABC versus the other two compositions. Overall, our results revealed that the composition of the ABC impacts the catalyst activity within the droplets before quenching. One potential avenue of research would be to further investigate how composition affects catalyst protection efficiency. By varying composition, block length, and functionalization capabilities a suite of ABC can be analyzed to determine the effects of composition, ***Figure 6.1***.
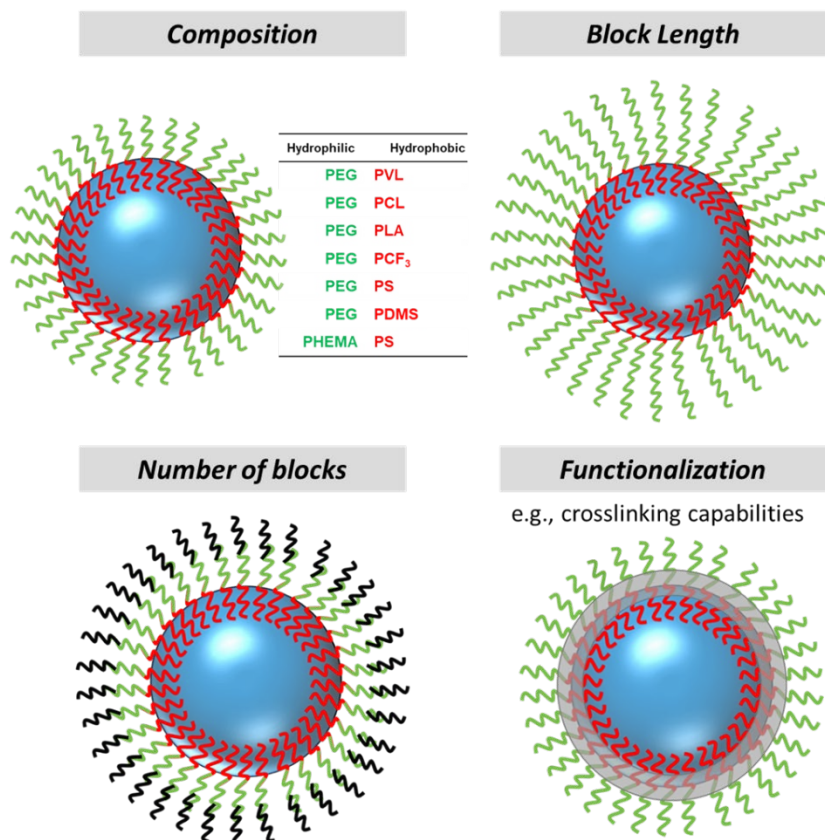
Figure 6.1: Amphiphilic block copolymer (ABC) tuning parameters, including composition, block length, number of blocks, and functionalization capabilities.

The self-assembly of the ABCs at the interface between the aqueous and the dispersed phase is driven by the polar headgroup interacting with the water while the nonpolar tail interacts with the nonpolar organic phase.[262–264] We have shown that increasing the number of hydrophilic groups compared to hydrophobic groups (i.e., high HLB) showed better catalyst activity in the droplets. By simply changing the composition and length of the blocks you can access a variety of molecules with varying HLB values allowing a deeper dive into the effect of the number of hydrophilic to hydrophobic repeating units on the catalyst activity within the droplet. We have shown that the addition of an ABC decreases the surface tension of the droplet allowing clean and

consistent droplet generation at the outlet tip, and improves the droplet generation and stability during flow and subsequent collection; however, we have not yet uncovered if any other parameters besides HLB value can increase the amount of time for catalytic activity before complete quenching of the catalyst via water diffusion into the particle. If we look at the drug delivery literature, many groups have shown the impact of ABC composition and block length on the stability of different block copolymer systems.[265–277] Thus, determining the importance of composition and HLB on the stability of our droplets and the catalyst protection efficiency would be valuable information for future encapsulation efforts.

Establishing Robust Formulation Rules for Controlling Drug Delivery via Biodegradable Elastomers

In **Chapter 5**, we expanded the applications of our biodegradable particles and biodegradable elastomers to drug delivery applications. Our preliminary results showed that tethering the drug to create a drug-polymer conjugate and subsequently crosslinking the polymer network resulted in a sustained release of the active ingredient over time. These results show the promising application of our encapsulation methodology to influence the release profiles of active ingredients for controlled drug delivery. A prominent advantage of our system for the generation of spherical polymeric particles is the ease of formulation modification. Through simple formulation changes, we can access a wide variety of polymeric particles with varying surface properties, degrees of crosslinking, sizes, and shapes, ***Figure 6.2.***

TUNING POLYMER PARTICLE PARAMETERS FOR DRUG DELIVERY

Size

100 nm

100 µm

Large: prolonged release
Small: long circulation times

Crosslinking

Crosslinking affects erosion rate
More crosslinking slows the diffusion of the drug

Surface Properties

PEG

Modulates interactions with macrophages
Reduces capture by immune cells

Shape

*Affects interactions
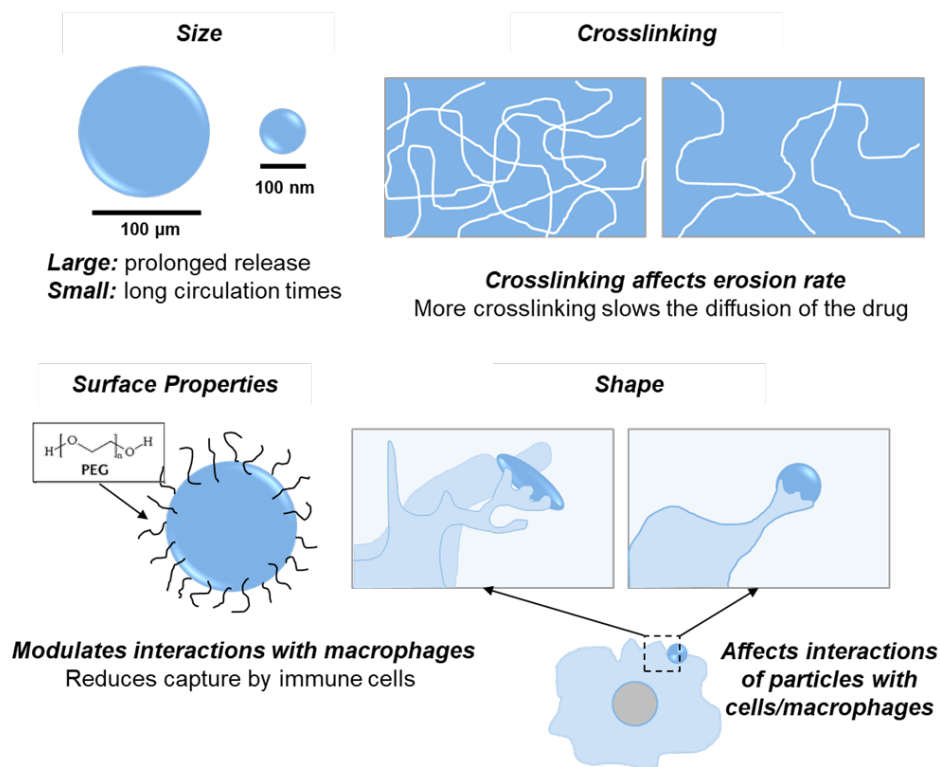of particles with
cells/macrophages*

Figure 6.2: A) Droplet-based microfluidic device configuration for encapsulating highly active catalysts within polymer solution. B) Graphic showing the methodology for encapsulation of the highly active catalyst within a polymeric sphere allowing a triggerable release of the catalyst.

The size of polymeric particles is a very important parameter for drug delivery applications.[278,279] has been shown that particles size can directly impact drug loading, release profiles, and delivery efficiency.[279–282] The optimal diameter varies between applications and carrier design/formulation, for example, polymeric nanoparticles (20-250nm), liposomes or lipid nanoparticles (50-1000nm), dendrimers (1-10nm), hydrogels (50-150nm), and inorganic nanoparticles (1-20nm)[283–290]. Currently, we are operating on the micron-scale with our droplet-based system, however, microfluidics has been utilized successfully to generate nano-sized particles in continuous flow.[291–295] With our device, size can be controlled via the outlet tip diameter and through flow rate. If we decrease the outlet tip diameter or increase our flow rate to

operate in the jetting regime we could decrease the diameter of our particles. It should be noted that our particles being on the micron scale can also open up applications for post-processing of the particles via thermoforming or molding into desired shapes for medical implants.
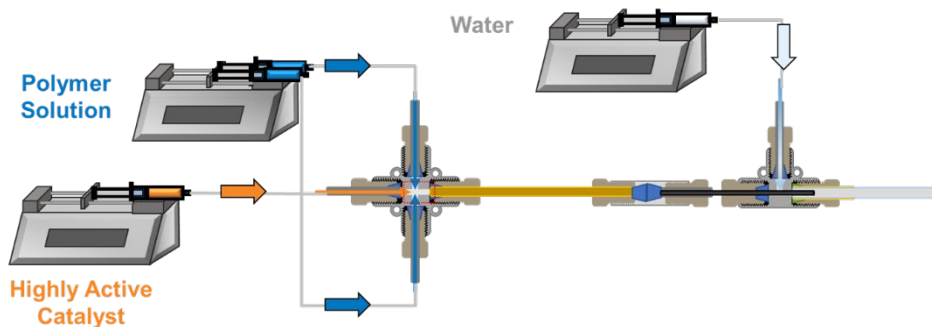
Crosslinking matrixes for drug delivery have been utilized to control the release of drugs from delivery systems.[296–298] Crosslinking has been used to enhance the biomechanical properties of scaffolds, modulate the release rates of incorporated active agents, and implement surface erosion of particles in a physiological environment.[299–301] Additionally, tuning crosslinking density of cyclic ester systems has been shown to impact drug release and drug loading properties.[302–304] In our aforementioned work, we explored the crosslinking of cyclic esters within spherical particles, which resulted in sustained release profiles compared to the non-crosslinked systems. The loading of the bis(e-caprolactone-4-yl)propane (BCP) crosslinker was kept constant (0.5 wt%), the ABC composition and the loading constant (Pluronic at 1wt%), and the size of the particle constant (300μm), and a spherical shape. The next step would be to thoroughly conduct an investigation into the impact of crosslinking density by varying the loading of BCP within the particle formulation.

In addition to the size and crosslinking density of our particles, another potential area of research could be a deep dive into the physical and chemical properties of our particles and their effect on drug delivery efficacy. The physical and chemical properties of drug carriers affect the *in vivo* circulation time of drug delivery systems.[305–308] The final circulation time of carriers is determined by the balance between blood vessel penetration, urine excretion, and macrophage recognition.[309–311] Surface charge and surface properties can be tuned via the amphiphilic block copolymer shell. Other chemical properties such as stimuli responsiveness or triggered release could lead to more advanced applications of these drug delivery systems.[312,313]

Employing the Encapsulation Design Principles to Induce Catalyst Latency

The droplet-based microfluidic device has potential for other encapsulations outside of ring-opening polymerization catalysts. The excellent control over flow rates and ease of formulation alteration leaves open opportunities for encapsulation of any material. For example, we have briefly investigated utilizing our encapsulation methodology to encase a highly active catalyst within a polymer particle. The highly active catalyst was supplied through the middle inlet of our droplet-based microfluidic device, while a polymer solution was supplied through the two side inlets allowing the catalyst to be protected within the core of the particles produced, *Figure 6.3a.* The methodology was to systematically encapsulate the catalyst within a polymer particle with a desired composition, which would allow a triggered release of the catalyst, *Figure 6.3b.*
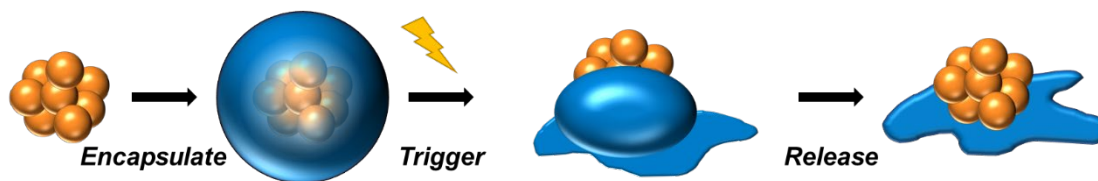

Figure 6.3: A) Droplet-based microfluidic device configuration for encapsulating highly active catalysts within polymer solution. B) Graphic showing the methodology for encapsulation of the highly active catalyst within a polymeric sphere allowing a triggerable release of the catalyst.

For a proof-of-concept, we chose to encapsulate a highly active catalyst (*not disclosed due to confidentiality*) that reaches over 90% conversion within 10min, within a polymer with a glass transition temperature (T_g) above room temperature, ***Figure 6.4.*** By using a high T_g polymer, the polymer will be in a glassy state after droplet formation which we hypothesized would slow the diffusion of the highly active catalyst out of the polymer particle. Additionally, having a high T_g polymer would allow a triggered release via breaking down the particle (e.g. shear) or via a temperature trigger above the T_g value. Without stirring the catalyst encapsulated within the polymer particles exhibited 14 hours of latency before the polymerization took off. We also observed a triggerable release via shear after stirring the catalyst encapsulated particles for an hour. These results demonstrate the versatility of our encapsulation methodology for other catalyst encapsulation applications.

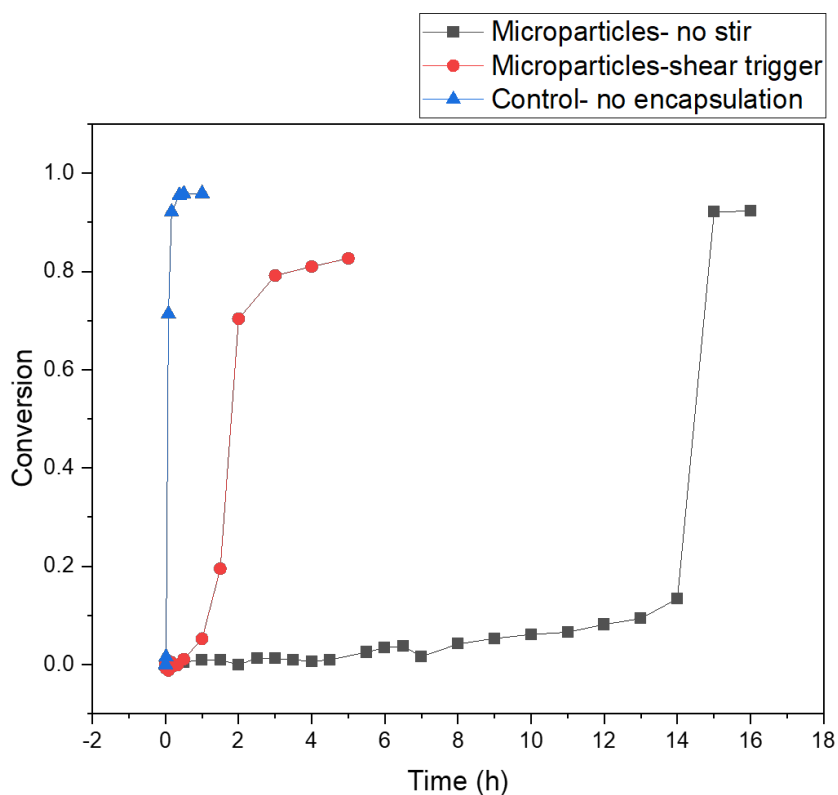**Figure 6.4:** Polymerization conversion over time for a highly active catalyst encapsulated within

Figure 6.4: (cont.) polymer microparticles. The 'control' is the catalyst not encapsulated within the polymer particle and shows complete conversion in less than an hour. The two microparticles curves show a shear triggered release with stirring after an hour and catalyst latency for over 14 hours without stirring.

APPENDIX A: Supplemental Information for Chapter 3

Materials:

The monomers of interest δ-valerolactone (VL) and ε-caprolactone (CL), 1,3 diphenylurea **Urea (1**), and reactants for the synthesis of **Urea (2)** and **Urea (3)** including cyclohexyl isocyanate, aniline, phenyl isocyanate, and N-methylcyclohexyl amine were purchased from Sigma Aldrich. All necessary solvents and Tergitol™ (surfactant/stabilizing agent) were also purchased from Sigma Aldrich.

General Procedure for Solution Preparation and Storage:

Care was taken for monomer preparation to ensure that monomer solutions were free of impuries and dry. δ-valerolactone (VL) was distilled and stored at 4˚C under anhydrous conditions. ε-caprolactone (CL) was distilled and stored over seives for 24 hours before use under anhydrous conditions. All catalyst, preparation materials (syringes, vials, needles, etc.), and solvents (THF and toluene) were dried and stored under anhydrous conditions. All batch polymerizations were performed inside the glovebox, while all subsequent fast quench, and droplet generation experiments the solutions were prepared inside the glovebox, loaded onto the appropriate glass syringes, and the capped syringes were brought out of the glovebox and attached to the microfluidic device.

General Procedure for Batch Testing Urea Organocatalyzed Ring-Opening Polymerization of Cyclic Esters:

The primary constraint for the success of the project is the selection of a catalyst system with a high rate of polymerization. Urea organocatalysts were chosen as the catalysts of interest

because they exhibit fast polymerization kinetics for the ring-opening polymerization of cyclic esters, specifically our monomers of interest, δ-valerolactone (VL) and ε-caprolactone (CL). With a wide variety of urea catalysts to choose from, we focused on testing three ureas that have been previously reported to reach full conversion in under 10 seconds.[50,314] We tested commercially available 1,3-diphenylurea (**Urea (1)**) as well as two ureas we prepared by reacting the corresponding isocyanates and amines for 3-cyclohexyl-1-phenylurea (**Urea (2)**) and 3-cyclohexyl-3-methyl-1-phenylure (**Urea (3)**).[315]

To probe the polymerization behavior under our formulation requirements we ran a series of batch polymerizations, **Table A.1**. All solutions were prepared under anhydrous conditions (glove box) and the results showed that all three ureas polymerized VL in under 10 seconds, while **Urea (2)** and **Urea (3)** were able to polymerize CL in under 30 seconds. At high conversion **Urea (2)** and **Urea (3)** were shown to produce polymers with a larger dispersity, therefore we chose to move forward with **Urea (1)** as our catalyst of interest for the remainder of the study. Having a catalyst system that is able to produce well defined polymers would allow us to better analyze any adverse effects of the flow system and subsequently the exposure to water.

Table A.1: Results from testing three urea organocatalyst with hydrophobic solvent

Entry	Monomer	Catalyst	Catalyst/initiator	Time (s)	X (%)	$M_{n,theoretical}$ (g*mol^{-1})	M_n (g*mol^{-1})	PDI
1	VL	Urea (1)	3	<10	>90	18,000	16700	1.12
2	CL	Urea (1)	3	10	5	1,050	1200	1.13
3	VL	Urea (2)	3	<5	>90	18,000	19900	1.43
4	CL	Urea (2)	3	30	>90	18,900	18000	1.21
5	VL	Urea (3)	4	<10	>90	18,000	20000	1.45
6	CL	Urea (3)	4	30	72	15,100	16300	1.23

Table SI notes. conversion calculated via 1H NMR, molecular weight/PDI reported via GPC against polystyrene standards. Room temperature. Stir plate at 800 rpm. Quenched with benzoic acid. Catalyst solvent is tetrahydrofuran and solvent for monomer solution is toluene. [Monomer]=2M. [Initiator (KOMe)]:[Monomer] [1]:[200].

Urea (1) and VL were chosen for subsequent reactions because the polymerization reached full conversion in under 10 seconds and produced the narrowest dispersity polymer, **Figure A.1**. Having fine control over the polymer produced allows us to better see any increase in polymerization during droplet formation in the aqueous dispersion.
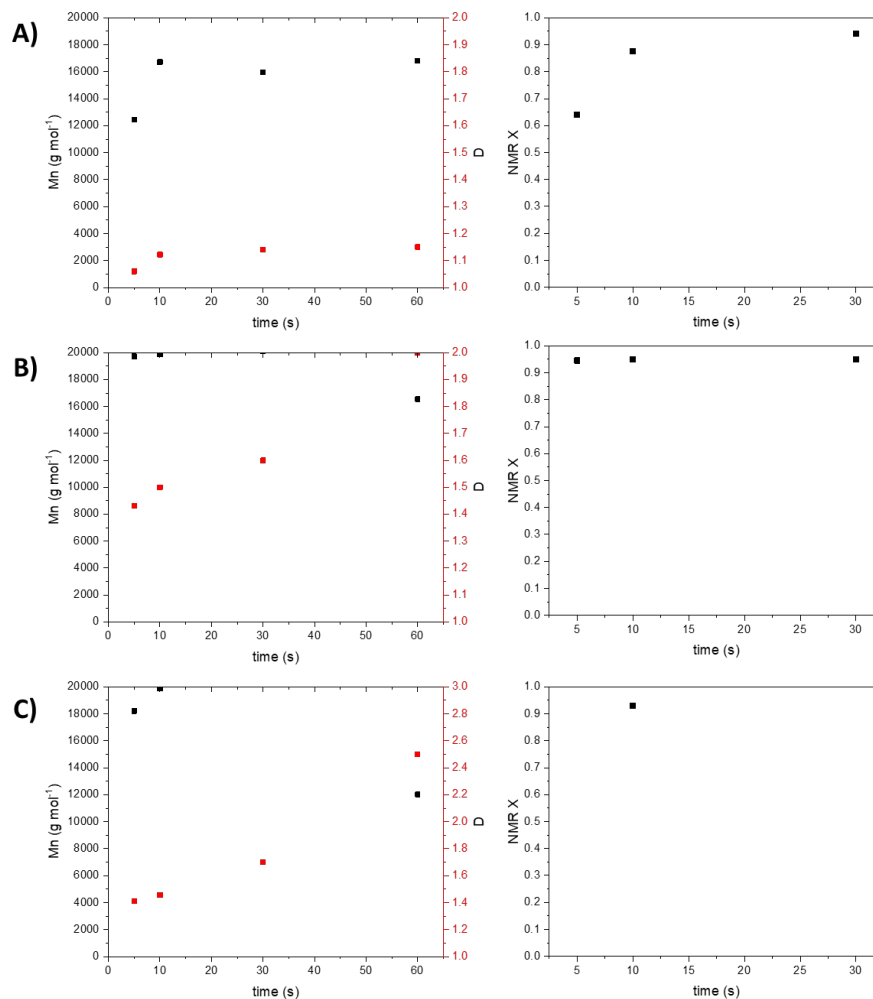
Figure A.1: Results from batch experiments comparing the three catalysts rate of polymerization of VL. A) Urea 1 B) Urea 2 C) Urea 3. Room temperature. Stir plate at 800 rpm. Quenched with benzoic acid. Initiator:Catalyst:Monomer. Urea (1) 1:3:200. Urea (2) 1:3:200. Urea (3) 1:4:200.

Diameter of Tubing Effect on Molecular Weight and Conversion:

The choice of tubing diameter after the cross tee plays an important roll in the mixing via diffusion between the catalyst/initiator and monomer streams. As we decreased the inner tubing diameter from 304.8 μm to 177.8 μm we saw a linear increase in MW with residence time, **Figure A.2.** The smaller ID decreases the diffusion distance and therefore increases the homogenization

between the two organic streams. Therefore, moving forward the design implemented a 177.8 μm ID tubing after the cross tee.
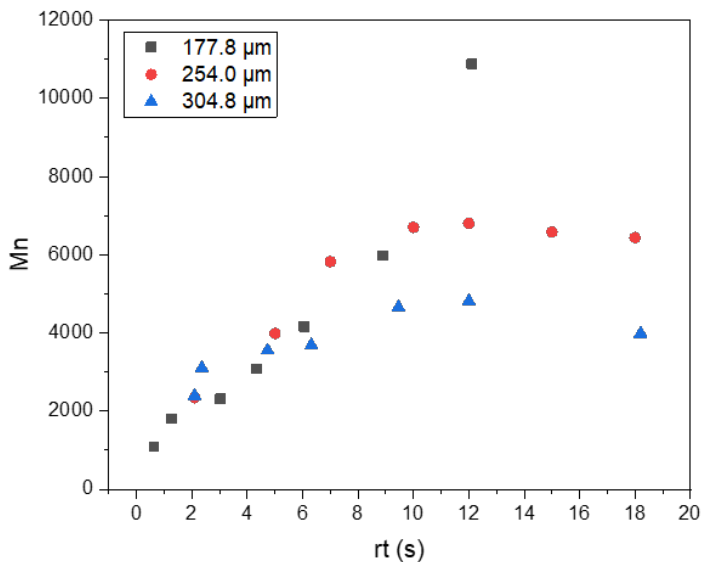

Figure A.2: Shows the effect of the diameter of the tubing after the cross tee on the molecular weight, polydispersity, and conversion of the polymer produced. Operating the device in the fast quench configuration. Catalyst is Urea (1), initiator is KOMe, and monomer is VL. Initator:Catalyst:Monomer 1:3:200. [Monomer]=3M. Quenching solution is acetic acid/THF.

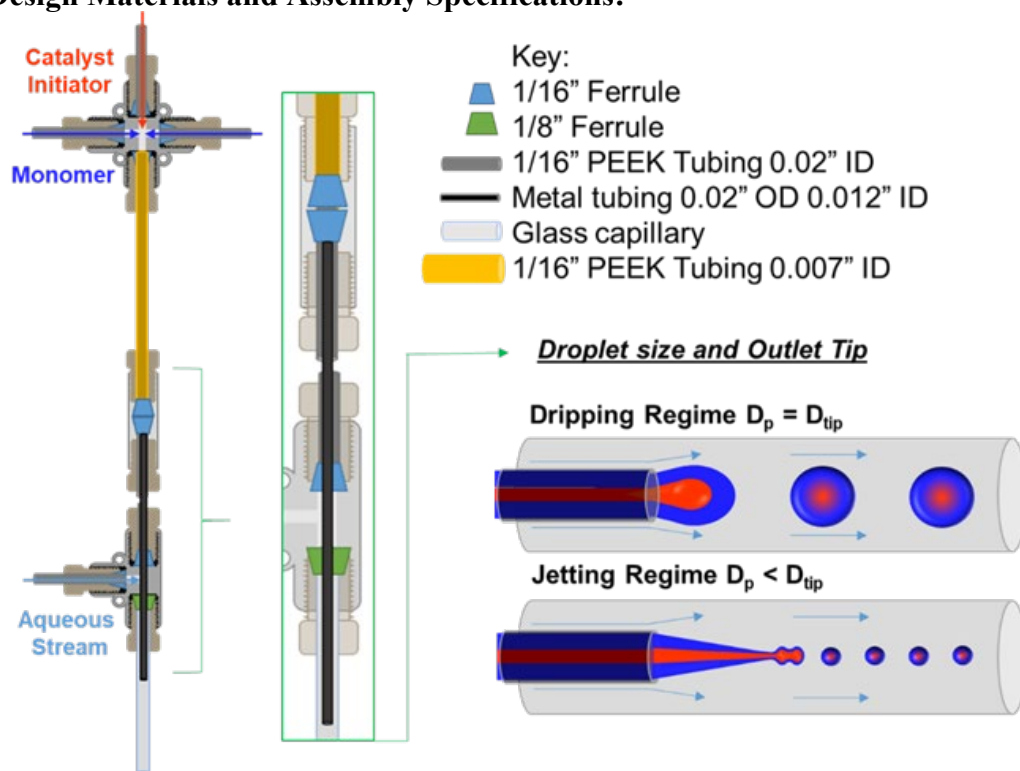**Device Design Materials and Assembly Specifications:**

Figure A.3. Droplet generating co-flow microfluidic device with all components listed

The microfluidic device utilized is made from all commercially available components. **Figure A.3** shows a cross-section of both intersecting flow points at each end of the co-flow droplet generating microreactor. The microreactor consists of one PEEK 0.02" thru hole cross assembly and one PEEK 0.02" thru hole tee fitting purchased from IDEX Health & Science. Input flow was supplied by three syringe pumps with glass syringes connected to 1/16" OD, 0.02" (177.8 µm) ID PEEK tubing, which was also purchased from IDEX. The outlet of the 177.8 µm ID tubing after the cross tee.

Connecting the two fittings is a 3" piece of 25G stainless steel hypodermic tubing with a 0.02 OD, 0.012 ID purchased from Component Supply. One end of the metal hypodermic tubing was connected to the outlet of the cross tee, while the other end of the metal tubing was entirely

threaded through the subsequent tee and into the center of the glass capillary tube. (The ends of the hypodermic tubing were inserted into a piece of the 1/16" PEEK tubing to seal the 1/16" ferrule). The glass capillary was inserted into 1/8" PEEK tubing and positioned at the opposite end of the tee. This allowed enough space for the water to flow through the gap around the metal tubing to shear off the droplets.

Testing Hydrophobic Solvents:

At such a small scale, the effects of surface forces are significantly greater than other forces that the droplet will experience, such as the viscous force. Shearing by dominating interfacial tension force is advantageous for continuous and stable formation of monodispersed droplets.[316] The interfacial tension between the two phases (γ) is a set value depending on the composition of the two phases. To tune the interfacial tension between the two phases, we analyzed the compatibility of different solvents with the ROP chemistry, **Figure A.4**.
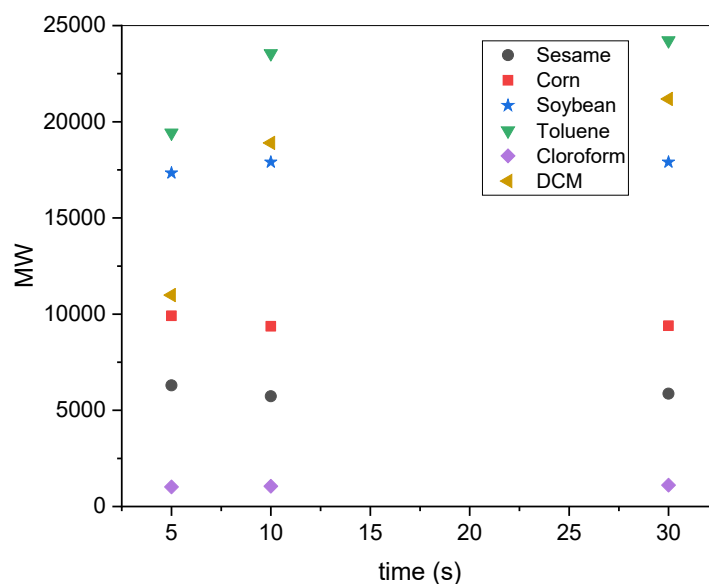
Figure A.4. Testing hydrophobic solvents' compatibility with ROP in batch. Room temperature. Stir plate at 800 rpm. Quenched with benzoic acid. Catalyst is Urea (1), initiator is KOMe, and monomer is VL. Initator:Catalyst:Monomer 1:3:200. [Monomer]=3M.

The benefit of using a hydrophobic solvent is two-fold first, its immiscibility with water aids in controlled droplet generation, and secondly, it protects the catalyst from water diffusion. However, the catalyst and initiator have limited solubilities in these apolar solvents, which can slow the polymerization too much. Therefore, a fine balance between fast polymerization within the droplet and immiscibility with water must be met. We started by looking at two different classes of hydrophobic solvents: biobased oils and organic solvents. The biobased oils of interest were sesame, corn, and soybean. The polymerization within all three of these oils reached full conversion within 5 seconds, but the molecular weight of the polymer produced varied drastically. Corn and soybean oil produced higher molecular weight than the sesame oil, 10k and 17k, respectively. However, the soybean oil was the only oil that produced a monophasic product with the polymer. The organic solvents of interest were toluene, chloroform, and DCM. Toluene and

116

DCM yielded the highest molecular weight, 24K and 20K, respectively. However, toluene had a significantly faster rate than the other two organic solvents. After analyzing the six hydrophobic solvents in batch polymerizations, we toluene as our hydrophobic solvent.

Stability of Urea Catalyst Activity During Flow:

In order to determine if the chemistry is affected by the inhomogeneity in the flow device, we ran stability studies at three different flow rates for multiple residence times in the fast quench configuration with toluene as the hydrophobic solvent. We observed that the polymer conversion remained consistent at all three flow rates for over 250 residence times, showing that the chemistry within the device is stable and reproducible, **Figure A.5**.
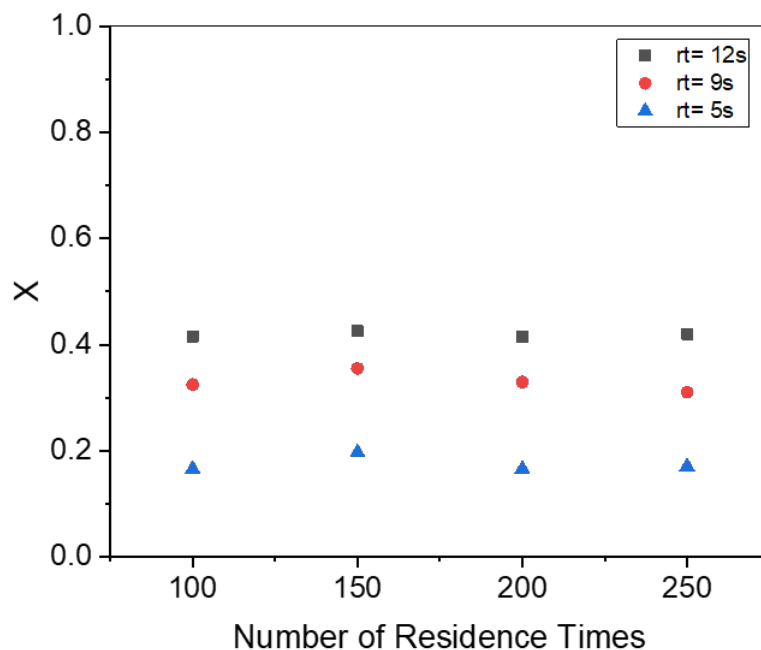

Figure A.5. Stability study of the polymerization of VL by **Urea (1)** over 250 residence times for three flow rates within the flow device. Quenched with acetic acid/THF. Catalyst is Urea (1), initiator is KOMe, and monomer is VL. Initator:Catalyst:Monomer 1:3:200. [Monomer]=3M.

Increase in Dispersity for Droplet Generation Over Fast Quench Analysis:

Interestingly when comparing the fast quench configuration samples to their droplet configuration counterparts we saw an increase in dispersity in the polymer produced after droplet formation. **Figure A.6** gives an example of a sample collected during fast quench versus a sample collected during droplet formation at the same residence time. One can see the increase in dispersity for the droplet configuration and a slight tailing towards the lower molecular weight. This tailing can be explained by the initiation of small polymer chains by the water after droplet formation, and nonhomogenous quenching of the catalyst within the particle due to water diffusion.
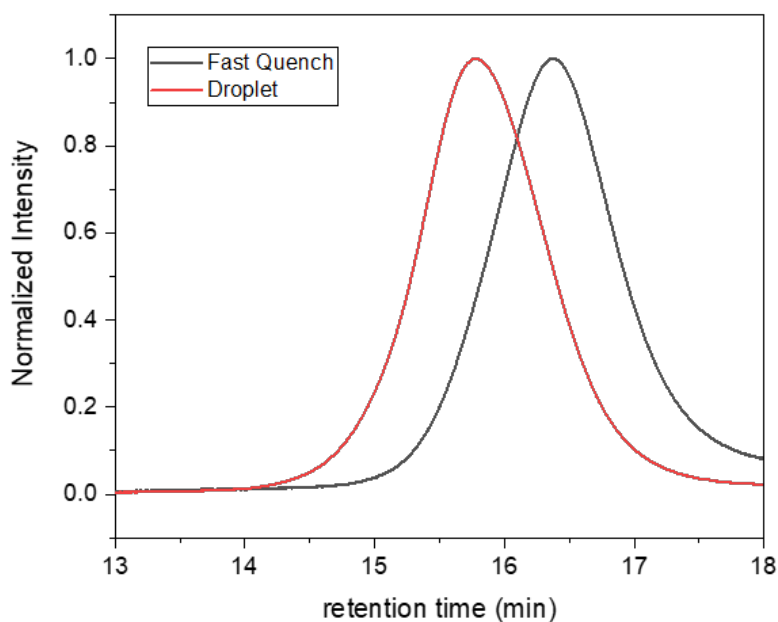
Figure A.6. GPC comparison between the fast quench configuration and the droplet configuration (rt=12.7s)

Droplet Collection for Analysis:

In order to collect the droplets for GPC and NMR analysis we utilized glass GPC vial inserts (Thermo-Fisher). The glass vial insert was placed at the end of the glass capillary outlet and the droplets were collected for subsequent analysis, **Figure A.7**.

Figure A.7. Droplet collection was performed by utilizing a GPC sample insert at the end of the glass capillary.

BCP Crosslinked Droplets:

The bis(e-caprolactone-4-yl)propane (BCP) was synthesized following previously reported methods. [92,166]

Device Design Modification:

Small modifications were made to the droplet generating microfluidic device to allow the implementation a crosslinker into the ROP chemistry. We knew the viscosity of the solution was going to increase within the device due to the crosslinking chemistry. By removing the smaller diameter tubing (1/16" OD 0.007" ID) we could remove the area of the device most prone to pressure buildup and subsequent clogging. In the new design, **Figure A.8**, the metal hypodermic tubing is attached directly to the cross tee and fed through the subsequent tee that supplies the

continuous water phase. Lastly, the length of the hypodermic tubing was increased from 3" to 4" to keep the overall reaction volume and the previously used residence times consistent.
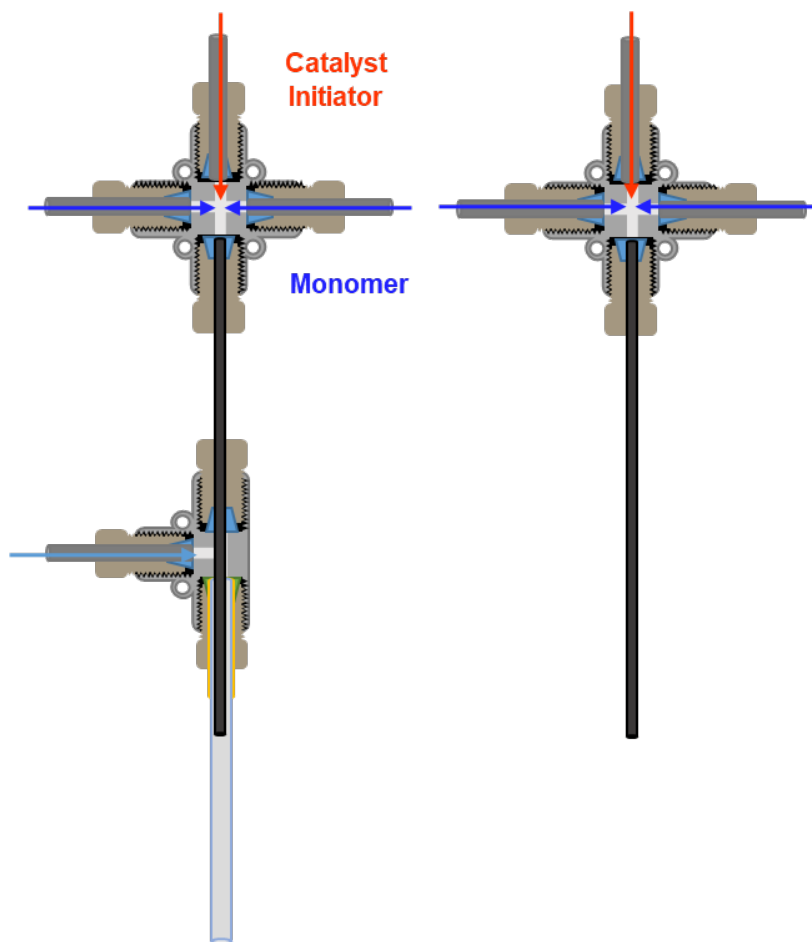
Figure A.8. Modified device design, removing small diameter tubing after the cross tee.

BCP Polymerization Results in Flow:

With the new device design, we ran three trials with varying amounts of BCP crosslinker, 0, 0.5, and 1%. The droplets were collected in a vial containing 50:50 ratio of water to methanol, allowing the toluene to diffuse out into the aqueous phase and therefore solidifying the droplets. After collection, the droplets were left in solution until they sank to the bottom of the vial (indicating the removal of toluene). Next, the particles were dissolved in THF with vigorous shaking for 10 minutes. The solution was then filtered through 0.45um filters to remove insoluble

crosslinked polymer that could damage the GPC column. The results showed a significant increase in molecular weight and dispersity for the polymer produced with the 0.5 and 1% BCP crosslinker over the control with no crosslinker present. However, there was not much difference in the molecular weight between the 0.5 and 1% trials, **Figure A.9**.
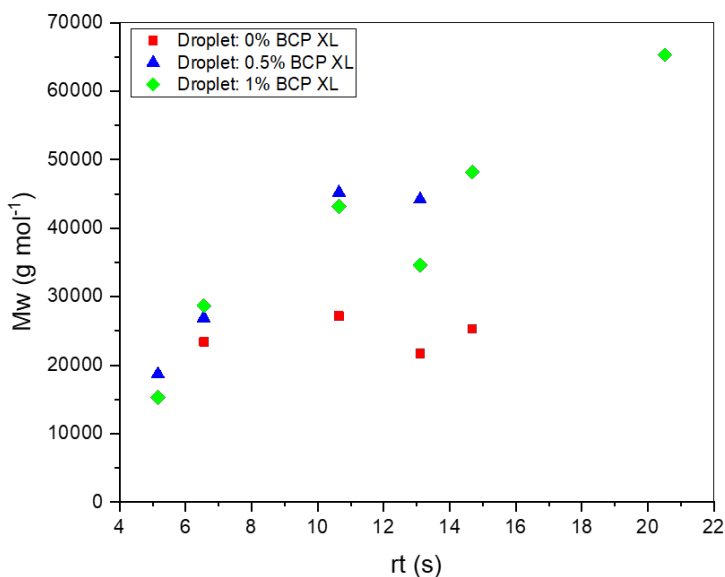
Figure A.9. Comparison between droplets containing 0, 0.5, and 1% BCP crosslinker. Catalyst is Urea (1), initiator is KOMe, and monomer is VL. Initator:Catalyst:Monomer 1:3:200. [Monomer]=3M.

Looking specifically at the 0.5% loading of BCP crosslinker, we confirmed that the increase in molecular weight and crosslinking occurred while the droplet was in the aqueous phase, by operating the device in the fast quench configuration and comparing the two results, **Figure A.10**. The drastic increase in both molecular weight and dispersity is indicative of the ROP and crosslinking within the droplets.

Figure A.10. Molecular weight and dispersity of 0.5% BCP crosslinked droplets over a range of residence times for both the fast q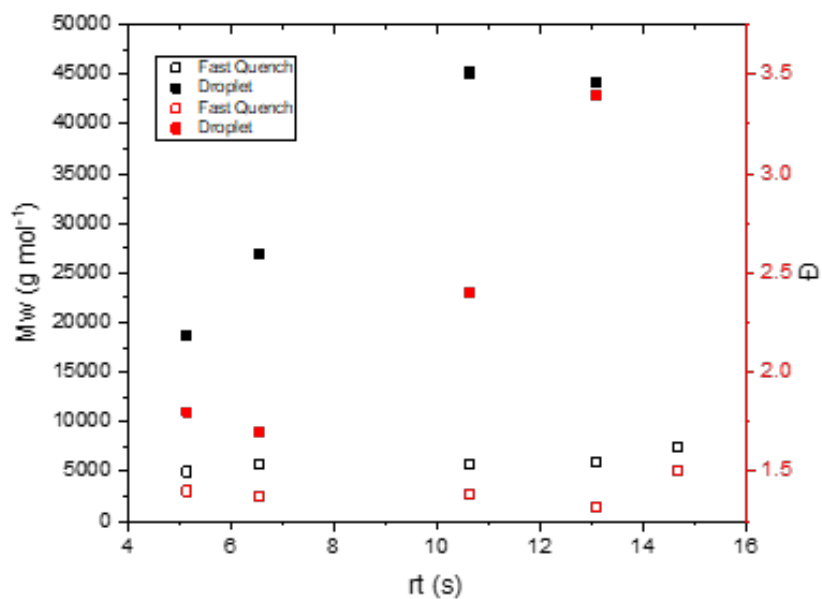uench and the droplet polymerizations. Catalyst is Urea (1), initiator is KOMe, and monomer is VL. Initator:Catalyst:Monomer 1:3:200. [Monomer]=3M. Fast quench quenching solution was acetic acid/THF.

APPENDIX B: Supplemental Information for Chapter 4

Materials and Reactant Preparation and Storage

ROP of Delta-Valerolactone:

The reactants δ-valerolactone (VL), 1,3 diphenylurea, and potassium methoxide (KOMe) were purchased from Sigma Aldrich. Proper monomer preparation is vital to ensure that the monomer solutions are free of impurities and completely dry. The δ-valerolactone (VL) was distilled and stored at 4°C under anhydrous conditions. All preparation materials (syringes, vials, needles, etc.), and solvents (THF and toluene) were dry and stored under anhydrous conditions. All batch polymerizations were performed inside the glovebox. While all subsequent solutions used during the fast quench and droplet generation experiments were prepared inside the glovebox, loaded onto the appropriate glass syringes, and the capped syringes were brought out of the glovebox and attached to the microfluidic device.

ROP of Propylene Oxide:

The reactants propylene oxide, tributylborane, phosphazene base P2-Et, and octanol were purchased from Sigma Aldrich. All reactants were stored under inert atmosphere. The octanol was distilled before storage and subsequent use. All solutions were prepared inside the glovebox, loaded onto appropriate glass syringes, and the capped syringes were brought out of the glovebox and attached to the microfluidic device.

Amphiphilic Block Copolymers:

The Pluronic (14600 g mol^{-1}) and all reactants needed for the synthesis of the amphiphilic block copolymers (PEG-PVL, PEG-PLA, and PEG-PCL) including methoxy poly(ethylene

glycol), 3,6-dimethyl-1,4-dioxane-2,5-dione, ε-caprolactone, triazabicyclodecene, and tin(II) 2-ethylhexanoatemethoxypolyethylene glycol, δ-valerolactone, were purchased from Sigma Aldrich. All synthesis were performed under inert atmosphere.

Droplet-Based Microfluidic Device

Fast Quench vs Droplet Configuration:

The off-the-shelf droplet-based microfluidic device can be operated in two configurations.[127] The first is the fast quench configuration where the hypodermic tubing dispersed phase outlet tip can be inserted into the quench solution. This configuration allows us to precisely determine the conversion and molecular weight at each specific flow rate before droplet formation. The second configuration is the droplet generating configuration where the hypodermic tubing is threaded through a secondary cross tee where the continuous aqueous phase is being supplied. On the opposite end of the tee the hypodermic tubing is centered inside the glass capillary allowing water to completely sheath the hypodermic tubing and shear the dispersed phase off into droplets continuously, *Figure B.1*.
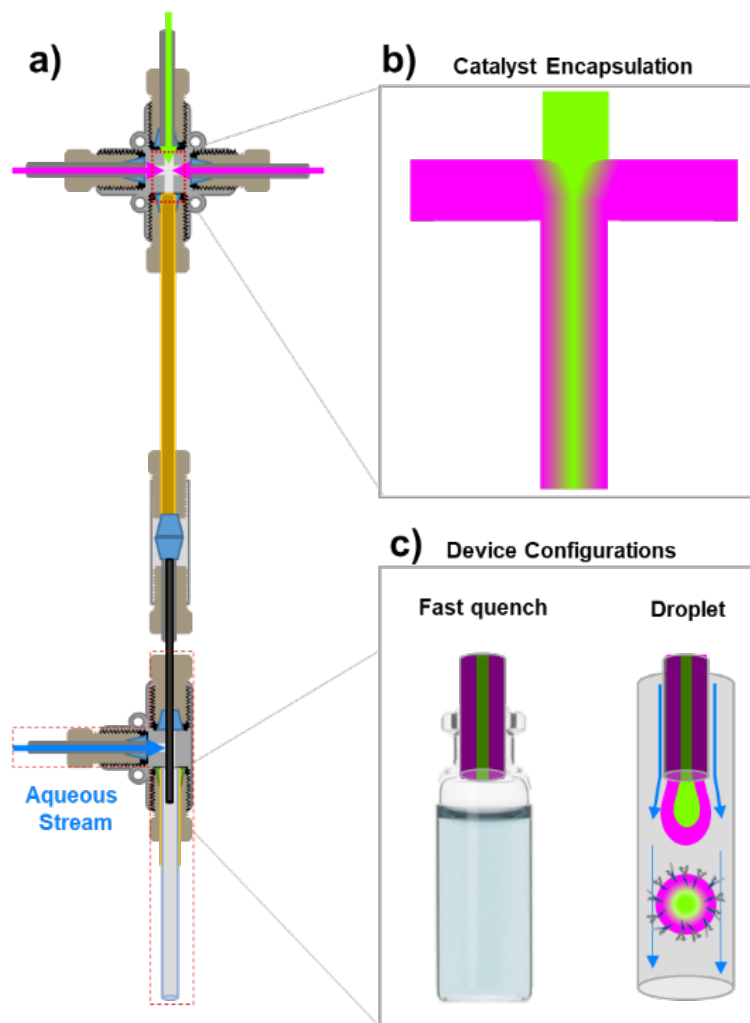
Figure B.1: a) Off-the-shelf droplet-based microfluidic device. b) The water-sensitive catalyst is sheathed between two streams of monomer solutions c) Graphic showing the fast quench configuration and droplet generating configuration that the device can be operated in.

Device Design Materials and Assembly Specifications:

The microfluidic device we designed is made from all commercially available components.

Figure B.2 shows a cross-section of both intersecting flow points the co-flow droplet generating

microreactor. The microreactor consists of one PEEK 0.02" thru hole cross assembly and one

PEEK 0.02" thru hole tee fitting purchased from IDEX Health & Science. Input flow was supplied

by three syringe pumps with glass syringes connected to $^1/_{16}$" OD, 0.02" (177.8 μm) ID PEEK

tubing, which was also purchased from IDEX. Connecting the two fittings is a 3" piece of 25G

thin wall stainless steel hypodermic tubing with a 0.02 OD, 0.012 ID purchased from Component Supply. One end of the metal tubing was inserted into a piece of the $^1/_{16}$" PEEK tubing to seal an end on both fittings, while the other end of the metal tubing was entirely threaded through the tee. The glass capillary was inserted into 1/8" PEEK tubing and positioned at the opposite end of the tee. This allowed enough space for the water to flow through the gap around the metal tubing to shear off the droplets.
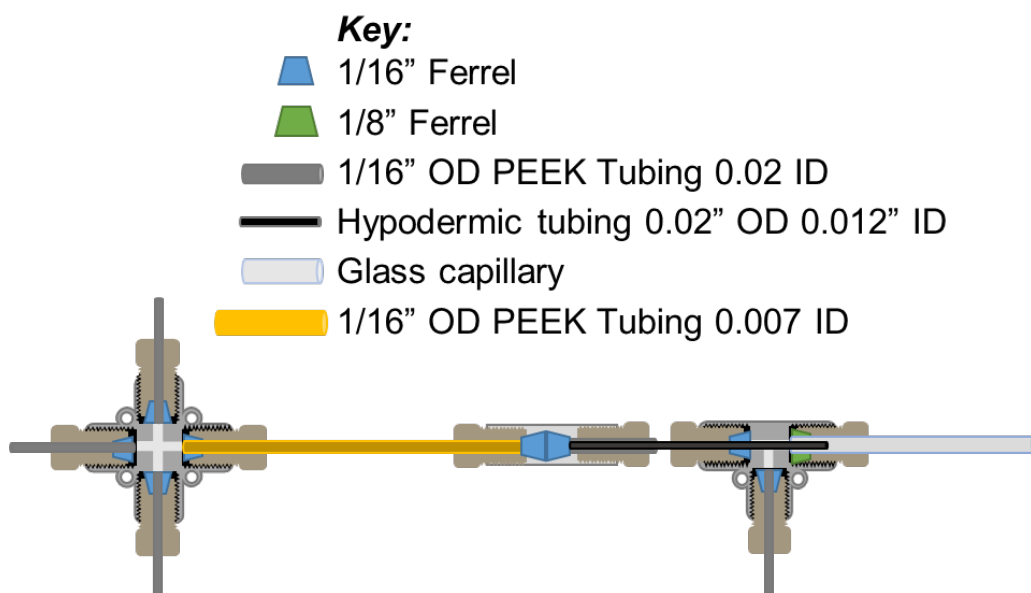
Figure B.2: Droplet generating co-flow microfluidic device with all components listed

Dripping Flow Regime:

To successfully encapsulate the catalyst within the center of the droplet and allow the catalyst the longest amount of time for polymerization we must operate in the dripping regime. In the dripping regime the droplets are formed close to the tip of the tube with strict periodicity.[317] Whereas the jetting regime has droplet formation at the end of a jet, ***Figure B.3a.*** In the jetting regime there is a larger surface area being exposed to the aqueous phase before droplet formation, which leads to faster quenching of the catalyst.
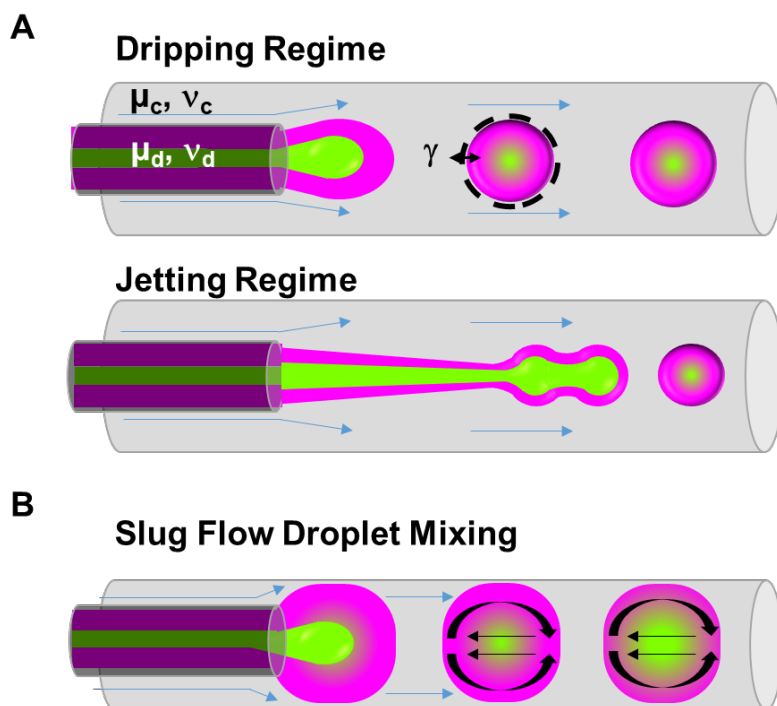
Figure B.3: A)Undesired jetting regime versus desired dripping regime B) Droplet mixing induced from slug flow

It is also undesirable for the regime to switch into the slug flow regime, where the droplets fill the cross-section of the glass capillary tube. In this regime the slug's internal fluid circulates very effectively due to high shear interactions with the glass capillary wall. The faster mixing owing to the twirling effect and recirculating flow would lead to faster quenching of the catalyst within the droplet, ***Figure B.3b.***[125,126]

General Synthesis of Amphiphilic Block Copolymers (ABC):

PEG-PLA:

A solution of the catalyst DBU (0.069 mmol 1eq) and 3000 g mol^{-1} mPEG (1eq) in 3mL of DCM was prepared in a glovebox in a 20 mL vial. A separate solution of the lactide (100eq) in 5 mL of DCM was also prepared in a separate vial. The two solutions were mixed and quenched after 15

min with benzoic acid.[186] The ABC is then precipitated in diethyl ether and hexane (1:1) and dried via high vacuum.

PEG-PVL:

Similarly a solution of the 1,3 diphenylurea (3eq), potassium methoxide (0.142 mmol 1eq) and 2000 g mol^{-1} mPEG (1eq) were dissolved in THF in a glovebox. A separate solution of δ-valerolactone in THF was also prepared. The two solutions were mixed and quenched after 60s with benzoic acid. The ABC is then precipitated in diethyl ether and hexane (1:1) and dried via high vacuum.

PEG-PCL:

A solution of the tin(II) 2-ethylhexanoate(0.098mmol 1eq), 5000 g mol^{-1} mPEG (1eq), and ε-caprolactone were added to a round bottom flask with a stirbar and sealed with a septum. The round bottom flast was taken out of the glovebox, attached to a Schlenk line under N$_2$, and the temperature was brought to 120˚C for 6hrs. The reaction was quenched with benzoic acid.[318] The ABC is then precipitated in diethyl ether and hexane (1:1) and dried via high vacuum.

Table B.1: Amphiphilic block copolymer composition and block molecular weights

Composition	PEG wt%	Mw$_{total}$	Mw$_{blockA\_PEG}$	Mw$_{blockB}$	HLB
Pluronic^a	82.5	14600	12000	2600	16.5
PEG-PCL	35.4	13300	5000	8300	7.08
PEG-PVL	33.1	6500	2000	4500	6.12
PEG-PLA	43.1	7300	3000	4300	8.6

Polymer Product Analysis and Characterization

To measure the success of the catalyst encapsulation and protection from the aqueous phase, we analyzed both the fast quench and droplet samples with gel permeation chromatography (GPC) for the molecular weight and gas chromatography (GC) for monomer conversion. The GC analysis of conversion is a powerful tool to monitor the decrease in monomer with respect to an internal standard. The validity of this method relies on an accurate determination of the initial monomer-to-internal standard ratio,[3] which we obtained by taking a preliminary sample of the solution before starting the polymerization. For our system, we employed decane as our internal standard as it is stable during the polymerization and analysis. It is important to note that the internal standard was added to the monomer phase so the initial monomer-to-internal standard ratio sample would be taken from the same solution. Additionally, the quantity of the internal standard was shown to be an important factor, as too small of a quantity of internal standard does not allow sufficient precision for the accurate determination of conversion over time.

GPC Data Processing and Dispersity:

We utilize the EcoSEC software associated with our GPC to perform the data processing associated with obtaining molecular weight and dispersity. We do not rely on the automatic integration of each peak, instead we edit every peak individually to ensure we include the entirety of the peak and any peak tailing. We draw a straight baseline from the furthest left bound of the peak to the furthest right bound of the peak. Care is taken to make sure that our baseline is not is not higher than the original baseline or sloping.

We have found that the dispersity of the polymers obtained from the microfluidic droplet-based system are higher than in batch. Additionally, when comparing the fast quench configuration

samples to their droplet configuration counterparts we also see an increase in dispersity of the polmer produced, ***Figure B.4.*** We attribute the increase in dispersity to the initiation of small polymer chains by the water after droplet formation, and nonhomogeneous quenching of the catalyst within the particle due to water diffusion.
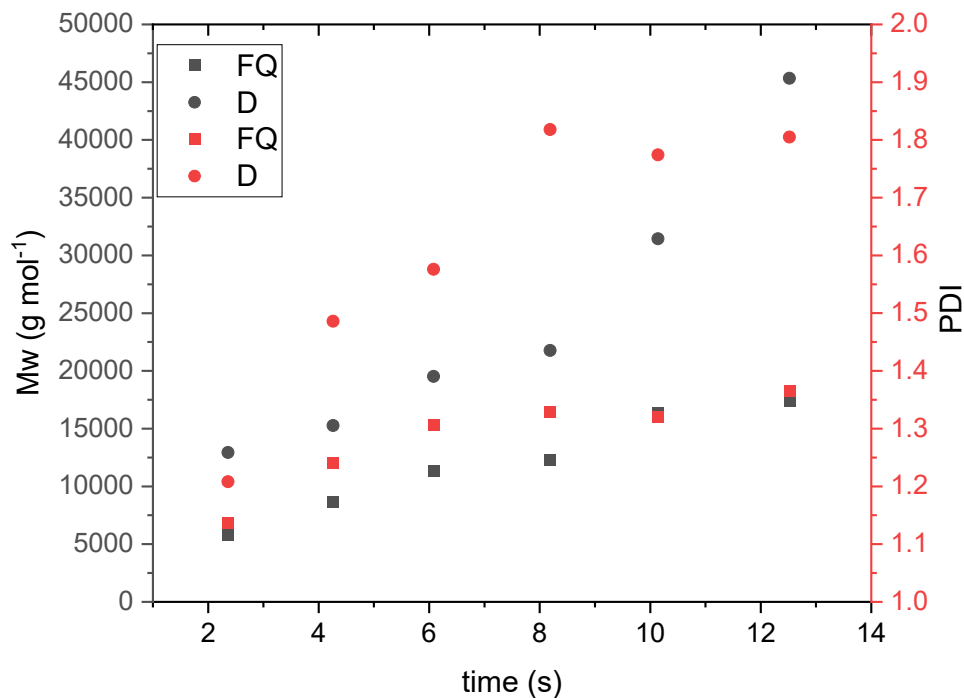
Figure B.4: Fast quench and droplet molecular weight and dispersity (PDI) obtained from the GPC. The droplet configuration produces more dispersed polymer than the fast quench due to small polymer chain initiation and nonhomogenous quenching of the catalyst.

We start our polymerization with a living system, but because the initiation and quenched are occurring in a non-homogeneous mixture we observe tailing in the MWD. The dispersity is indicative of this tailing but the visual of the GPC traces is more insightful. ***Figure B.5.*** In this figure you can see broadening of the peaks with increase in rt within the reactor.
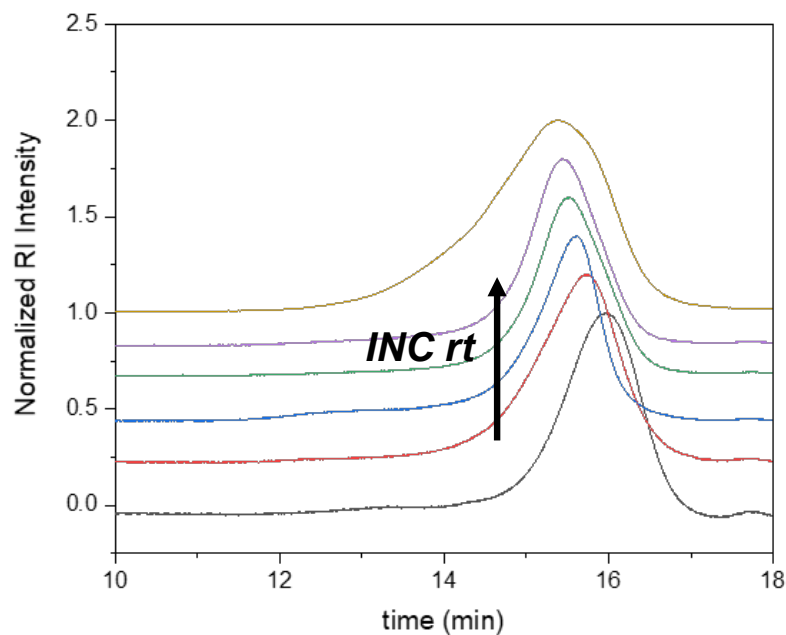
Figure B.5: A series of GPC traces showing the molecular weight distribution broadening an tailing due to the initiation and quenching happening simultaneously in the non-homogeneous disperse phase.

ROP of δ-Valerolatone with the Addition of ABCs and Hydrophobes

To ensure that the addition of amphiphilic block copolymers (ABC)s did not negatively affect the ring-opening polymerization kinetics we first tested the formulation in batch. With a 1 wt% loading of ABC we saw that the PEG-PVL, PEG-PCL, and Pluronic all reached high molecular weight (20 kg mol^{-1}) and high conversion (X>90%) in 20 seconds, ***Figure B.6***. The only ABC that showed a negative impact on the ROP kinetics was PEG-PLA where the maximum molecular weight was around 6 kg mol^{-1} and the maximum conversion attainable was around 30%.
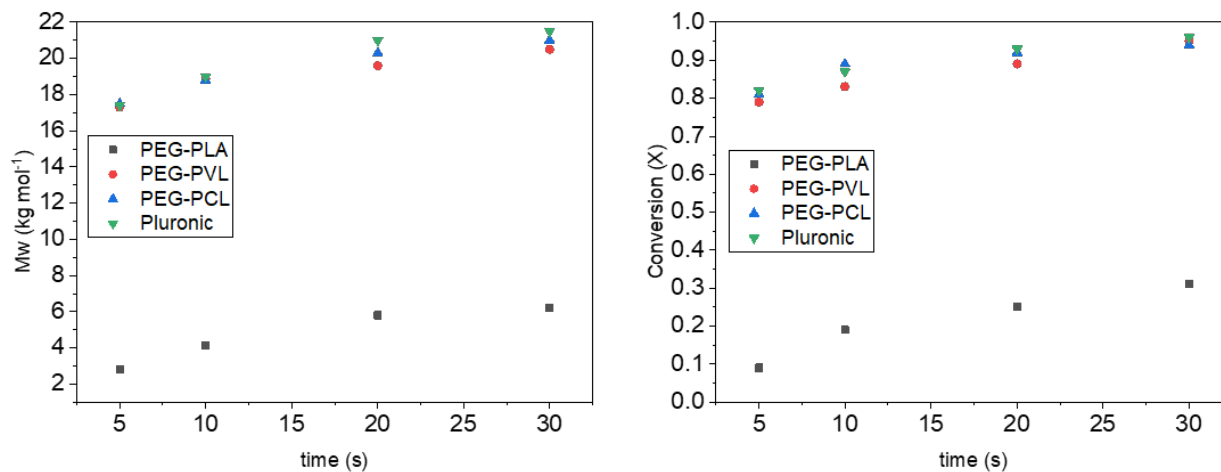
Figure B.6: Batch polymerization results from the ROP of delta-valerolactone with 1,3 diphenylurea with the addition of the amphiphilic block copolymers

Similarly the addition of hydrophobes was tested in batch. The hydrophobe that showed the least negative impact to the ROP kinetics was hexadecane. We saw that with the addition of 0.4M hexadecane the batch polymerization was still able to reach high molecular weight (20 kg mol^{-1}) and high conversion (X>90%) in 20 seconds, *Figure B.7*.
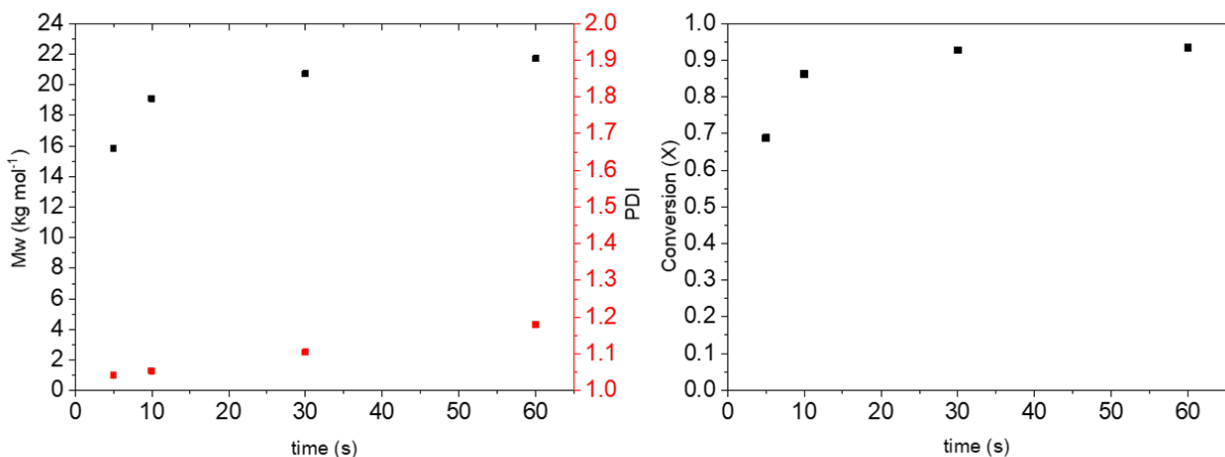
Figure B.7: Batch polymerization results from the ROP of delta-valerolactone with 1,3 diphenylurea with the addition of the amphiphilic block copolymers and hexadecane.

ROP of Propylene Oxide with Organobase and Tributylborane

To illustrate the versatility of our system we expanded to another water-sensitive ROP chemistry, ***Scheme B.1***. The ROP of propylene oxide via an organobase and tributylborane with octanol as an initiator was chosen for two reasons: firstly, this chemistry is also known for being able to reach high molecular weight polymer with low dispersity, and secondly, the reaction is highly reactive and exothermic. By choosing a very reactive chemistry we could show the benefit of using a small reaction volume flow system such as our droplet-based microfluidic device. We can safely increase the co-catalyst loading within our device to levels that in batch would be unsafe and highly exothermic.

Scheme B.1: Ring-opening polymerization of propylene oxide
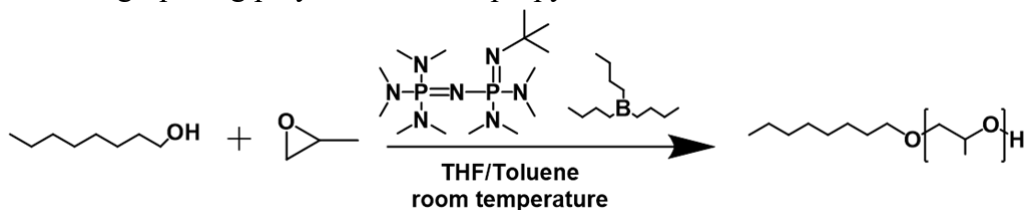
Device Design Modification for the ROP of Epoxides

Small modifications were made to the droplet generating microfluidic device to allow the implementation of the epoxide ROP chemistry, **_Figure B.8_**. The possibility of clogging the device due to the high reaction rate and quick increase in viscosity combined with the high exothermicity of the polymerization of propylene oxide prompted us to optimize the device. Firstly, we moved the flow system into a chemical reaction hood as the first safety measure. Secondly, we increased the length of the tubing entering the main cross-tee to 3ft coils. Increasing these portions of tubing would ensure that if the device did clog there would not be any backflow into the syringes leading to a runaway reaction.
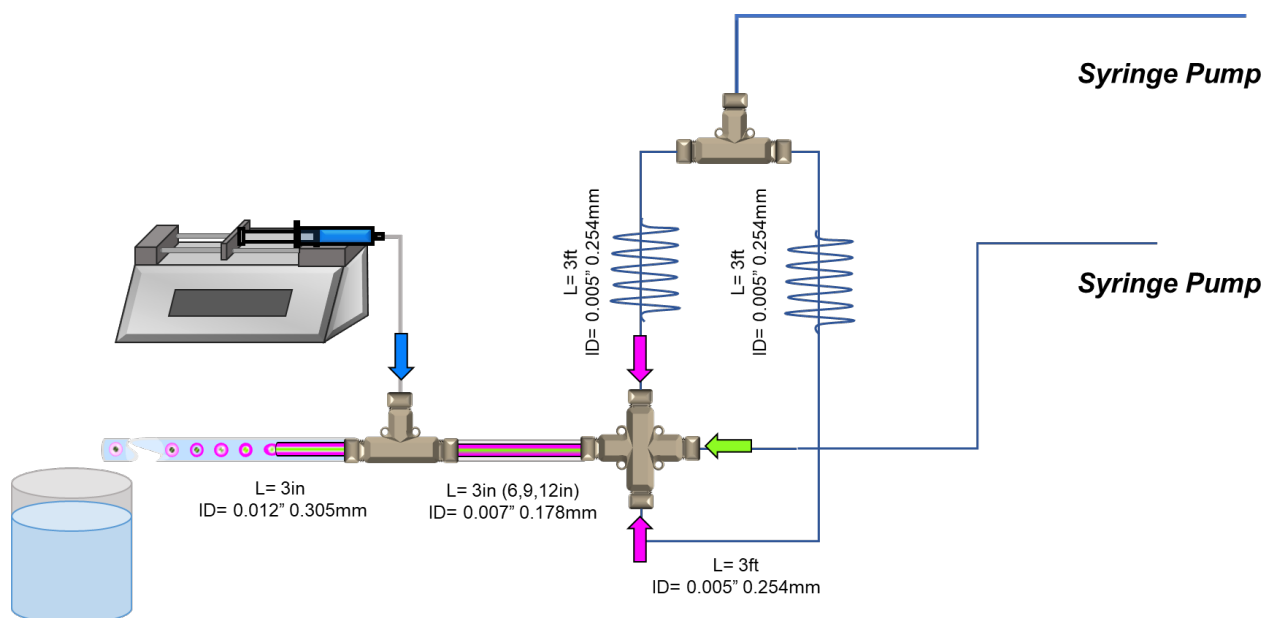
Figure B.8. Modified device design, removing small diameter tubing after the cross tee.

In an attempt to further increase the molecular weight attainable with the PO ROP we added in a crosslinker, 1,4-butanediol diglycidyl ether. With a 1wt% addition of the crosslinker we saw a dramatic increase in viscosity of the solution compared to the formulation without the crosslinker. This increase in viscosity could very easily clog the system at longer residence times, therefore we only operated the system with flow rates that resulted in less than 10 second residence times within the device. With the addition of the crosslinker we saw an increase at rt = 9.5s from 26% to 41%, *Figure B.9.*
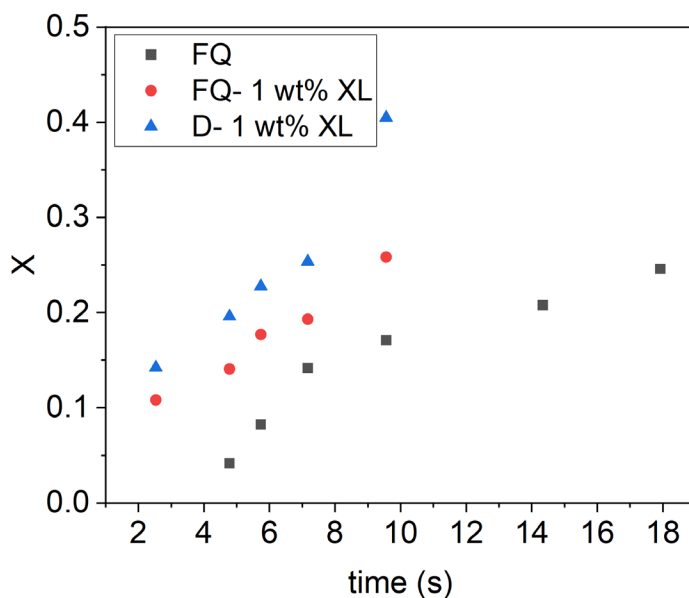
Figure B.9. Ring-opening polymerization of propylene oxide with the addition of 1wt% 1,4-butanediol diglycidyl ether as a crosslinker

APPENDIX C: Supplemental Information for Chapter 5

Materials and Methods

Copolymerizations of ROP of Delta-Valerolactone and Bis(ε-Caprolactone-4-yl)Propane:

The reactants δ-valerolactone (VL), 1,3 diphenylurea, and potassium methoxide (KOMe) were purchased from Sigma Aldrich. The bis(e-caprolactone-4-yl)propane (BCP) was synthesized following previously reported methods. [92,166] Proper monomer preparation is vital to ensure that the monomer solutions are free of impurities and completely dry. The δ-valerolactone (VL) was distilled and stored at 4˚C under anhydrous conditions. All preparation materials (syringes, vials, needles, etc.), and solvents (THF and toluene) were dry and stored under anhydrous conditions. All batch polymerizations were performed inside the glovebox. While all subsequent solutions used during the fast quench and droplet generation experiments were prepared inside the glovebox, loaded onto the appropriate glass syringes, and the capped syringes were brought out of the glovebox and attached to the microfluidic device.

Droplet Collection for Analysis:

In order to collect the droplets for GPC, NMR, GC and UV-vis analysis, we utilized glass 20mL vials. The glass vials were filled with 18 mL of a 50:50 mixture of methanol and DI water. The methanol helps remove the toluene solvent from the droplet allowing the polymer particles to precipitate into solid spheres. The glass capillary outlet tip was inserted into the collection vial and particle collection was done over a given period of time.

Crosslinked Biodegegradable Elastomers:

Scheme C.1: Copolymerization of bis(ε-caprolactone-4-yl)propane and δ-valerolactone via 1,3 diphenylurea to from crosslinked biodegradable elastomers tethered to the chemotherapeutics of interest, Paclitaxel or Docetaxel, or the model molecule 9-anthracenemethanol
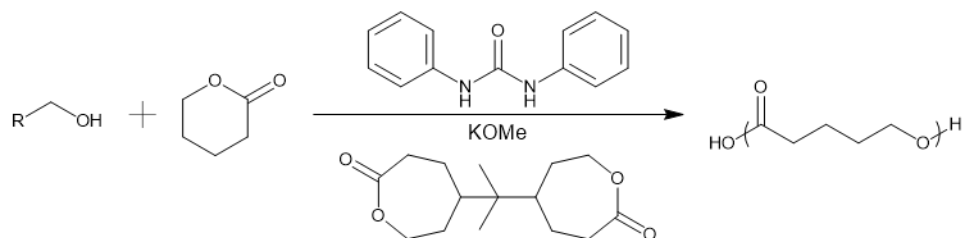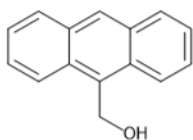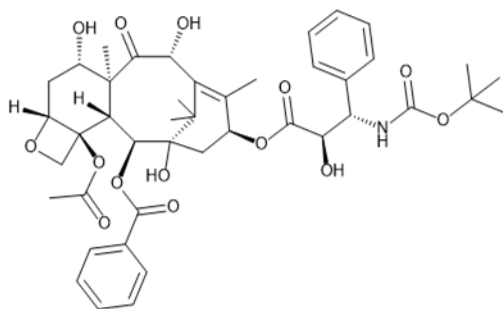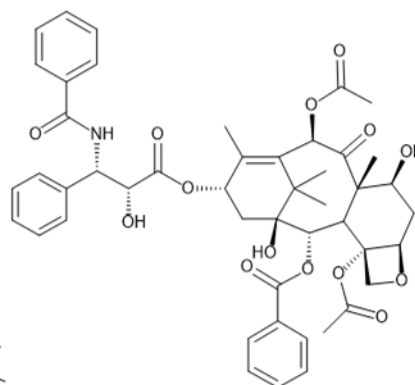
REFERENCES

(1)   Panchal, S. S.; Vasava, D. V. Biodegradable Polymeric Materials: Synthetic Approach. *ACS Omega* **2020**, *5* (9), 4370–4379.

(2)   Wang, J.; Wang, L.; Zhou, Z.; Lai, H.; Xu, P.; Liao, L.; Wei, J. Biodegradable Polymer Membranes Applied in Guided Bone/Tissue Regeneration: A Review. *Polym. 2016, Vol. 8, Page 115* **2016**, *8* (4), 115.

(3)   Luckachan, G. E.; Pillai, C. K. S. Biodegradable Polymers- A Review on Recent Trends and Emerging Perspectives. *J. Polym. Environ. 2011 193* **2011**, *19* (3), 637–676.

(4)   Park, J. H.; Ye, M.; Park, K. Biodegradable Polymers for Microencapsulation of Drugs. *Molecules*. Molecular Diversity Preservation International 2005, pp 146–161.

(5)   Gross, R. A.; Kalra, B. Biodegradable Polymers for the Environment. *Science* **2002**, *297* (5582), 803–807.

(6)   Hans, M. .; Lowman, A. . Biodegradable Nanoparticles for Drug Delivery and Targeting. *Curr. Opin. Solid State Mater. Sci.* **2002**, *6* (4), 319–327.

(7)   Lambert, S.; Wagner, M. Environmental Performance of Bio-Based and Biodegradable Plastics: The Road Ahead. *Chem. Soc. Rev.* **2017**, *46* (22), 6855–6871.

(8)   Vasanthi, K. Biodegradable Polymers - A Review. *Polym. Sci.* **2017**, *3* (1), 1–7.

(9)   Kaeb, H.; Aeschelmann, F.; Dammer, L.; Carus, M. Market Study on the Consumption of Biodegradable and Compostable Plastic Products in Europe 2015 and 2020. **2016**, No. April 2016.

(10)   Nuyken, O.; Pask, S. D. Ring-Opening Polymerization-An Introductory Review. *Polymers (Basel)*. **2013**, *5* (2), 361–403.

(11)   Hall, H. K.; Schneider, A. K. Polymerization of Cyclic Esters, Urethans, Ureas and

Imides. *J. Am. Chem. Soc.* **2002**, *80* (23), 6409–6412.

(12)   Walsh, D. J.; Hyatt, M. G.; Miller, S. A.; Guironnet, D. Recent Trends in Catalytic

Polymerizations. *ACS Catal.* **2019**, *9* (12), 11153–11188.

(13)   Saiyasombat, W.; Molloy, R.; Nicholson, T. M.; Johnson, A. F.; Ward, I. M.;

Poshyachinda, S. Ring Strain and Polymerizability of Cyclic Esters. *Polymer (Guildf).*

1998, *39* (23), 5581–5585.

(14)   Duda, A.; Kowalski, A.; Penczek, S.; Uyama, H.; Kobayashi, S. Kinetics of the Ring-

Opening Polymerization of 6-, 7-, 9-, 12-, 13-, 16-, and 17-Membered Lactones.

Comparison of Chemical and Enzymatic Polymerizations. *Macromolecules* **2002**, *35* (11),

4266–4270.

(15)   Dubois, P.; Coulembier, O.; Raquez, J. M. *Handbook of Ring-Opening Polymerization*;

John Wiley and Sons, 2009.

(16)   Living Polymerization. In *The IUPAC Compendium of Chemical Terminology*;

International Union of Pure and Applied Chemistry (IUPAC), 2008.

(17)   Stridsberg, K. M.; Ryner, M.; Albertsson, A.-C. Controlled Ring-Opening Polymerization:

Polymers with Designed Macromolecular Architecture. In *Degradable Aliphatic*

Polyesters; Springer Berlin Heidelberg: Berlin, Heidelberg, 2000; pp 41–65.

(18)   Su, W.-F. Ring-Opening Polymerization; Springer, Berlin, Heidelberg, 2013; pp 267–299.

(19)   Kamber, N. E.; Jeong, W.; Waymouth, R. M.; Pratt, R. C.; Lohmeijer, B. G. G.; Hedrick,

J. L. Organocatalytic Ring-Opening Polymerization. *Chemical Reviews*. December 2007,

pp 5813–5840.

(20)   Zhang, X.; Fevre, M.; Jones, G. O.; Waymouth, R. M. Catalysis as an Enabling Science

for Sustainable Polymers. *Chem. Rev.* **2018**, *118* (2), 839–885.

(21) Becker, G.; Wurm, F. R. Functional Biodegradable Polymers: Via Ring-Opening Polymerization of Monomers without Protective Groups. *Chemical Society Reviews*. Royal Society of Chemistry October 21, 2018, pp 7739–7782.

(22) Al-Shok, L.; Haddleton, D. M.; Adams, F. Progress in Catalytic Ring-Opening Polymerization of Biobased Lactones. **2022**.

(23) Hu, Y.; Daoud, W. A.; Cheuk, K. K. L.; Lin, C. S. K. Newly Developed Techniques on Polycondensation, Ring-Opening Polymerization and Polymer Modification: Focus on Poly(Lactic Acid). *Materials (Basel).* **2016**, *9* (3).

(24) Dove, A. P. Organic Catalysis for Ring-Opening Polymerization. *ACS Macro Letters*. 2012, pp 1409–1412.

(25) Maqsood, M.; Seide, G. Biodegradable Flame Retardants for Biodegradable Polymer. *Biomol. 2020, Vol. 10, Page 1038* **2020**, *10* (7), 1038.

(26) Hsu, S. H.; Hung, K. C.; Chen, C. W. Biodegradable Polymer Scaffolds. *J. Mater. Chem. B* **2016**, *4* (47), 7493–7505.

(27) Siracusa, V.; Rocculi, P.; Romani, S.; Rosa, M. D. Biodegradable Polymers for Food Packaging: A Review. *Trends Food Sci. Technol.* **2008**, *19* (12), 634–643.

(28) Bari, S. S.; Chatterjee, A.; Mishra, S. Biodegradable Polymer Nanocomposites: An Overview. *http://dx.doi.org/10.1080/15583724.2015.1118123* **2016**, *56* (2), 287–328.

(29) Hu, S.; Zhao, J.; Zhang, G.; Schlaad, H. Macromolecular Architectures through Organocatalysis. *Prog. Polym. Sci.* **2017**, *74*, 34–77.

(30) Kiesewetter, M. K.; Shin, E. J.; Hedrick, J. L.; Waymouth, R. M. Organocatalysis: Opportunities and Challenges for Polymer Synthesis. *Macromolecules*. March 9, 2010, pp 2093–2107.

(31) Piedra-Arroni, E.; Ladavière, C.; Amgoune, A.; Bourissou, D. Ring-Opening
      Polymerization with Zn(C6F5)2 -Based Lewis Pairs: Original and Efficient Approach to
      Cyclic Polyesters. *J. Am. Chem. Soc.* **2013**, *135* (36), 13306–13309.

(32) Li, X.-Q.; Wang, B.; Ji, H.-Y.; Li, Y.-S. Insights into the Mechanism for Ring-Opening
      Polymerization of Lactide Catalyzed by $Zn(C_6F_5)_2$ /Organic Superbase Lewis Pairs. *Catal.
      Sci. Technol.* **2016**, *6* (21), 7763–7772.

(33) Jeong, W.; Hedrick, J. L.; Waymouth, R. M. Organic Spirocyclic Initiators for the Ring-
      Expansion Polymerization of β-Lactones. *J. Am. Chem. Soc.* **2007**, *129* (27), 8414–8415.

(34) Chang, Y. A.; Waymouth, R. M. Ion Pairing Effects in the Zwitterionic Ring Opening
      Polymerization of δ-Valerolactone. *Polym. Chem.* **2015**, *6* (29), 5212–5218.

(35) Jeong, W.; Shin, E. J.; Culkin, D. A.; Hedrick, J. L.; Waymouth, R. M. Zwitterionic
      Polymerization: A Kinetic Strategy for the Controlled Synthesis of Cyclic Polylactide. *J.
      Am. Chem. Soc.* **2009**, *131* (13), 4884–4891.

(36) Culkin, D. A.; Jeong, W.; Csihony, S.; Gomez, E. D.; Balsara, N. P.; Hedrick, J. L.;
      Waymouth, R. M. Zwitterionic Polymerization of Lactide to Cyclic Poly(Lactide) by
      Using N-Heterocyclic Carbene Organocatalysts. *Angew. Chemie Int. Ed.* **2007**, *46* (15),
      2627–2630.

(37) Pothupitiya, J. U.; Dharmaratne, N. U.; Jouaneh, T. M. M.; Fastnacht, K. V.; Coderre, D.
      N.; Kiesewetter, M. K. H-Bonding Organocatalysts for the Living, Solvent-Free Ring-
      Opening Polymerization of Lactones: Toward an All-Lactones, All-Conditions Approach.
      Macromolecules **2017**, *50* (22), 8948–8954.

(38) Lohmeijer, B. G. G.; Pratt, R. C.; Leibfarth, F.; Logan, J. W.; Long, D. A.; Dove, A. P.;
      Nederberg, F.; Choi, J.; Wade, C.; Waymouth, R. M.; et al. Guanidine and Amidine

Organocatalysts for Ring-Opening Polymerization of Cyclic Esters. *Macromolecules* **2006**, *39* (25), 8574–8583.

(39)   Pratt, R. C.; Lohmeijer, B. G. G.; Long, D. A.; Waymouth, R. M.; Hedrick, J. L. Triazabicyclodecene: A Simple Bifunctional Organocatalyst for Acyl Transfer and Ring-Opening Polymerization of Cyclic Esters. *J. AM. CHEM. SOC* **2006**, *128*, 4556–4557.

(40)   Zhang, L.; Nederberg, F.; Messman, J. M.; Pratt, R. C.; Hedrick, J. L.; Wade, C. G. Organocatalytic Stereoselective Ring-Opening Polymerization of Lactide with Dimeric Phosphazene Bases. *J. Am. Chem. Soc.* **2007**, *129* (42), 12610–12611.

(41)   Gazeau-Bureau, S.; Delcroix, D.; Martín-Vaca, B.; Bourissou, D.; Navarro, C.; Magnet, S. Organo-Catalyzed ROP of ε-Caprolactone: Methanesulfonic Acid Competes with Trifluoromethanesulfonic Acid. *Macromolecules* **2008**, *41* (11), 3782–3784.

(42)   Makiguchi, K.; Satoh, T.; Kakuchi, T. Diphenyl Phosphate as an Efficient Cationic Organocatalyst for Controlled/Living Ring-Opening Polymerization of δ-Valerolactone and ε-Caprolactone. *Macromolecules* **2011**, *44* (7), 1999–2005.

(43)   Kricheldorf, H. R.; Dunsing, R. Polylactones, 8. Mechanism of the Cationic Polymerization of L,L-dilactide. *Die Makromol. Chemie* **1986**, *187* (7), 1611–1625.

(44)   Connor, E. F.; Nyce, G. W.; Myers, M.; Möck, A.; Hedrick, J. L. First Example of N-Heterocyclic Carbenes as Catalysts for Living Polymerization: Organocatalytic Ring-Opening Polymerization of Cyclic Esters. *J. Am. Chem. Soc.* **2002**, *124* (6), 914–915.

(45)   Zhang, L.; Nederberg, F.; Pratt, R. C.; Waymouth, R. M.; Hedrick, J. L.; Wade, C. G. Phosphazene Bases: A New Category of Organocatalysts for the Living Ring-Opening Polymerization of Cyclic Esters. *Macromolecules* **2007**, *40* (12), 4154–4158.

(46)   Lohmeijer, B. G. G.; Pratt, R. C.; Leibfarth, F.; Logan, J. W.; Long, D. A.; Dove, A. P.;

Nederberg, F.; Choi, J.; Wade, C.; Waymouth, R. M.; et al. Guanidine and Amidine Organocatalysts for Ring-Opening Polymerization of Cyclic Esters. *Macromolecules* **2006**, *39* (25), 8574–8583.

(47) Dove, A. P.; Pratt, R. C.; Lohmeijer, B. G. G. G.; Waymouth, R. M.; Hedrick, J. L. Thiourea-Based Bifunctional Organocatalysis: Supramolecular Recognition for Living Polymerization. *J. Am. Chem. Soc.* **2005**, *127* (40), 13798–13799.

(48) Zhang, X.; Jones, G. O.; Hedrick, J. L.; Waymouth, R. M. Fast and Selective Ring-Opening Polymerizations by Alkoxides and Thioureas. *Nat. Chem.* **2016**, *8* (11), 1047–1053.

(49) Dharmaratne, N. U.; Pothupitiya, J. U.; Kiesewetter, M. K. The Mechanistic Duality of (Thio)Urea Organocatalysts for Ring-Opening Polymerization. *Org. Biomol. Chem.* **2019**, *17* (13), 3305–3313.

(50) Lin, B.; Waymouth, R. M. Urea Anions: Simple, Fast, and Selective Catalysts for Ring-Opening Polymerizations. *J. Am. Chem. Soc.* **2017**, *139* (4), 1645–1652.

(51) Hu, X.; Zhu, N.; Fang, Z.; Guo, K. Continuous Flow Ring-Opening Polymerizations. *React. Chem. Eng.* **2017**, *2* (1), 20–26.

(52) De Risi, C.; Bortolini, O.; Brandolese, A.; Di Carmine, G.; Ragno, D.; Massi, A. Recent Advances in Continuous-Flow Organocatalysis for Process Intensification. *Reaction Chemistry and Engineering*. The Royal Society of Chemistry June 2, 2020, pp 1017–1052.

(53) Reis, M. H.; Leibfarth, F. A.; Pitet, L. M. Polymerizations in Continuous Flow: Recent Advances in the Synthesis of Diverse Polymeric Materials. *ACS Macro Lett.* **2020**, *9* (1), 123–133.

(54) Brooks, B. W. Chemical Reactor Analysis and Design. *Chem. Eng. J.* **1991**, *47* (2), 133.

(55)   Scott Fogler, H. Elements of Chemical Reaction Engineering. *Chem. Eng. Sci.* **1987**, *42* (10), 2493.

(56)   Nagy, K. D.; Shen, B.; Jamison, T. F.; Jensen, K. F. Mixing and Dispersion in Small-Scale Flow Systems. *Org. Process Res. Dev.* **2012**, *16* (5), 976–981.

(57)   Walsh, D. J.; Dutta, S.; Sing, C. E.; Guironnet, D. Engineering of Molecular Geometry in Bottlebrush Polymers. *Macromolecules* **2019**, *52* (13), 4847–4857.

(58)   Zhu, N.; Huang, W.; Hu, X.; Liu, Y.; Fang, Z.; Guo, K. Chemoselective Polymerization Platform for Flow Synthesis of Functional Polymers and Nanoparticles. *Chem. Eng. J.* **2018**, *333*, 43–48.

(59)   Van Den Berg, S. A.; Zuilhof, H.; Wennekes, T. Clickable Polylactic Acids by Fast Organocatalytic Ring-Opening Polymerization in Continuous Flow. *Macromolecules* **2016**, *49* (6), 2054–2062.

(60)   Walsh, D. J.; Dutta, S.; Sing, C. E.; Guironnet, D. Engineering of Molecular Geometry in Bottlebrush Polymers. *Macromolecules* **2019**, *52* (13), 4847–4857.

(61)   Walsh, D. J.; Schinski, D. A.; Schneider, R. A.; Guironnet, D. General Route to Design Polymer Molecular Weight Distributions through Flow Chemistry. *Nat. Commun. 2020 111* **2020**, *11* (1), 1–9.

(62)   Zhu, N.; Feng, W.; Hu, X.; Zhang, Z.; Fang, Z.; Zhang, K.; Li, Z.; Guo, K. Organocatalyzed Continuous Flow Ring-Opening Polymerizations to Homo- and Block-Polylactones. *Polymer (Guildf).* **2016**, *84*, 391–397.

(63)   Huang, W.; Zhu, N.; Liu, Y.; Wang, J.; Zhong, J.; Sun, Q.; Sun, T.; Hu, X.; Fang, Z.; Guo, K. A Novel Microfluidic Enzyme-Organocatalysis Combination Strategy for Ring-Opening Copolymerizations of Lactone, Lactide and Cyclic Carbonate. *Chem. Eng. J.*

2019, *356*, 592–597.

(64) Hu, S.; Zhao, J.; Zhang, G.; Schlaad, H. Macromolecular Architectures through Organocatalysis. *Prog. Polym. Sci.* **2017**, *74*, 34–77.

(65) Reis, M. H.; Varner, T. P.; Leibfarth, F. A. The Influence of Residence Time Distribution on Continuous-Flow Polymerization. *Macromolecules* **2019**, *52* (9), 3551–3557.

(66) Mathers, R. T.; Meier, M. A. R. *Green Polymerization Methods: Renewable Starting Materials, Catalysis and Waste Reduction*; 2011.

(67) Gilbert, M. Plastics Materials. In *Brydson's Plastics Materials*; Elsevier, 2017; pp 1–18.

(68) Hungenberg, K.-D.; Jahns, E. Trends in Emulsion Polymerization Processes from an Industrial Perspective. In *Adv Polym Sci*; 2017; pp 195–214.

(69) Webb, H. K.; Arnott, J.; Crawford, R. J.; Ivanova, E. P. Plastic Degradation and Its Environmental Implications with Special Reference to Poly(Ethylene Terephthalate). *Polymers (Basel).* **2013**, *5* (1), 1–18.

(70) Mecking, S.; Held, A.; Bauers, F. M. Aqueous Catalytic Polymerization of Olefins. *Angew. Chemie Int. Ed.* **2002**, *41* (4), 544–561.

(71) Mecking, S. State-of-the-Art. In *Multiphase Homogeneous Catalysis*; Wiley-VCH Verlag GmbH: Weinheim, Germany, 2008; pp 763–764.

(72) Anderson, C. D.; Daniels, E. S. *Emulsion Polymerisation and Latex Applications*; 2003.

(73) Chern, C.-S. *Principles and Applications of Emulsion Polymerization*; Wiley, 2008.

(74) DeKock, R. L.; Hristov, J. H.; Anderson, G. D. W.; Göttker-Schnetmann, I.; Mecking, S.; Ziegler, T. Possible Side Reactions Due to Water in Emulsion Polymerization by Late Transition Metal Complexes II: Deactivation of the Catalyst by a Wacker-Type Reaction. *Organometallics* **2005**, *24* (11), 2679–2687.

(75)   Christopher, G. F.; Anna, S. L. Microfluidic Methods for Generating Continuous Droplet Streams. *J. Phys. D. Appl. Phys.* **2007**, *40* (19), R319–R336.

(76)   Janiesch, J. W.; Weiss, M.; Kannenberg, G.; Hannabuss, J.; Surrey, T.; Platzman, I.; Spatz, J. P. Key Factors for Stable Retention of Fluorophores and Labeled Biomolecules in Droplet-Based Microfluidics. *Anal. Chem.* **2015**, *87* (4), 2063–2067.

(77)   Liu, K.; Lepin, E. J.; Wang, M. W.; Guo, F.; Lin, W. Y.; Chen, Y. C.; Sirk, S. J.; Olma, S.; Phelps, M. E.; Zhao, X. Z.; et al. Microfluidic-Based 18F-Labeling of Biomolecules for Immuno-Positron Emission Tomography. *Mol. Imaging* **2011**, *10* (3), 168–176.

(78)   Zhu, P.; Wang, L. Passive and Active Droplet Generation with Microfluidics: A Review. *Lab Chip* **2017**, *17* (1), 34–75.

(79)   Stutman, D. R.; Klein, A.; El-Aasser, M. S.; Vanderhoff, J. W. Mechanism of Core/Shell Emulsion Polymerization. *Ind. Eng. Chem. Prod. Res. Dev.* **1985**, *24* (3), 404–412.

(80)   Shah, R. K.; Shum, H. C.; Rowat, A. C.; Lee, D.; Agresti, J. J.; Utada, A. S.; Chu, L. Y.; Kim, J. W.; Fernandez-Nieves, A.; Martinez, C. J.; et al. Designer Emulsions Using Microfluidics. *Materials Today*. April 2008, pp 18–27.

(81)   Bottaro, E.; Nastruzzi, C. "Off-the-Shelf" Microfluidic Devices for the Production of Liposomes for Drug Delivery. *Mater. Sci. Eng. C* **2016**, *64*, 29–33.

(82)   Gu, F.; Farokhzad, O. C.; Kyei-Manu, W.; Cannizzaro, C.; Karnik, R.; Dean, L.; Basto, P.; Langer, R. Microfluidic Platform for Controlled Synthesis of Polymeric Nanoparticles. *Nano Lett.* **2008**, *8* (9), 2906–2912.

(83)   Dorresteijn, R.; Haschick, R.; Klapper, M.; Müllen, K. Poly(L -Lactide) Nanoparticles via Ring-Opening Polymerization in Non-Aqueous Emulsion. *Macromol. Chem. Phys.* **2012**, *213* (19), 1996–2002.

(84) Mei, L.; Jin, M.; Xie, S.; Yan, Z.; Wang, X.; Zhou, G.; Van Den Berg, A.; Shui, L. A Simple Capillary-Based Open Microfluidic Device for Size on-Demand High-Throughput Droplet/Bubble/Microcapsule Generation. *Lab Chip* **2018**, *18* (18), 2806–2815.

(85) Moritz, H. U. Increase in Viscosity and Its Influence on Polymerization Processes. *Chem. Eng. Technol.* **1989**, *12* (1), 71–87.

(86) Chen, C. C.; Nauman, E. B. Verification of a Complex, Variable Viscosity Model for a Tubular Polymerization Reactor. *Chem. Eng. Sci.* **1989**, *44* (1), 179–188.

(87) Panja, S.; Siehr, A.; Sahoo, A.; Siegel, R. A.; Shen, W. Biodegradable Elastomers Enabling Thermoprocessing below 100 °c. *Biomacromolecules* **2022**, *23* (1), 163–173.

(88) Wang, Y.; Ameer, G. A.; Sheppard, B. J.; Langer, R. A Tough Biodegradable Elastomer. *Nat. Biotechnol.* **2002**, *20* (6), 602–606.

(89) Palmgren, R.; Karlsson, S.; Albertsson, A. Synthesis of Degradable Crosslinked Polymers Based on 1,5-dioxepan-2-one and Crosslinker of Bis-ϵ-caprolactone Type. *J. Polym. Sci. Part A Polym. Chem.* **1997**, *35* (9), 1635–1649.

(90) Palmgren, R.; Karlsson, S.; Albertsson, A.-C. Synthesis of Degradable Crosslinked Polymers Based on 1,5-Dioxepan-2-One and Crosslinker of Bis-1-Caprolactone Type. *J Polym Sci A Polym Chem* **1997**, *35*, 1635–1649.

(91) Nijenhuis, A. J.; Grijpma, D. W.; Pennings, A. J. Crosslinked Poly(l-Lactide) and Poly(ε-Caprolactone). *Polymer (Guildf).* **1996**, *37* (13), 2783–2791.

(92) Amsden, B. Curable, Biodegradable Elastomers: Emerging Biomaterials for Drug Delivery and Tissue Engineering. *Soft Matter*. 2007, pp 1335–1348.

(93) Bat, E.; Zhang, Z.; Feijen, J.; Grijpma, D. W.; Poot, A. A. Biodegradable Elastomers for Biomedical Applications and Regenerative Medicine. *Regen. Med.* **2014**, *9* (3), 385–398.

(94)   Convery, N.; Gadegaard, N. 30 Years of Microfluidics. *Micro Nano Eng.* **2019**, *2*, 76–91.

(95)   Berlanda, S. F.; Breitfeld, M.; Dietsche, C. L.; Dittrich, P. S. Recent Advances in Microfluidic Technology for Bioanalysis and Diagnostics. *Anal. Chem.* **2020**, *93* (1), 311–331.

(96)   Wang, X.; Yi, L.; Mukhitov, N.; Schrell, A. M.; Dhumpa, R.; Roper, M. G. Microfluidics-to-Mass Spectrometry: A Review of Coupling Methods and Applications. *J. Chromatogr. A* **2015**, *1382*, 98–116.

(97)   Riahi, R.; Tamayol, A.; Shaegh, S. A. M.; Ghaemmaghami, A. M.; Dokmeci, M. R.; Khademshosseini, A. Microfluidics for Advanced Drug Delivery Systems. *Curr. Opin. Chem. Eng.* **2015**, *7*, 101–112.

(98)   Stadler, B. Preface to Special Topic: Microfluidics in Drug Delivery. *Biomicrofluidics* **2015**, *9* (5).

(99)   Mancera-Andrade, E. I.; Parsaeimehr, A.; Arevalo-Gallegos, A.; Ascencio-Favela, G.; Parra-Saldivar, R. Microfluidics Technology for Drug Delivery: A Review. *Front. Biosci. - Elit.* **2018**, *10* (1), 74–91.

(100)   Galan, E. A.; Zhao, H.; Wang, X.; Dai, Q.; Huck, W. T. S.; Ma, S. Intelligent Microfluidics: The Convergence of Machine Learning and Microfluidics in Materials Science and Biomedicine. *Matter* **2020**, *3* (6), 1893–1922.

(101)   Whitesides, G. M. The Origins and the Future of Microfluidics. *Nature*. July 27, 2006, pp 368–373.

(102)   Song, Y.; Cheng, D.; Zhao, L. Microfluidics: Fundamental, Devices and Applications. *Microfluid. Fundam. Devices Appl.* **2018**.

(103)   Hessel, V.; Renken, A.; Schouten, J. C.; Yoshida, J. I. *Micro Process Engineering: A*

Comprehensive Handbook; Hessel, V., Renken, A., Schouten, J. C., Yoshida, J.-I., Eds.; Wiley-VCH: Weinheim, Germany, 2013; Vol. 1.

(104) Zeng, S.; Liu, X.; Xie, H.; Lin, B. Basic Technologies for Droplet Microfluidics. *Top. Curr. Chem.* **2011**, *304*, 69–90.

(105) Xu, B. Bin; Zhang, Y. L.; Wei, S.; Ding, H.; Sun, H. B. On-Chip Catalytic Microreactors for Modern Catalysis Research. *ChemCatChem* **2013**, *5* (8), 2091–2099.

(106) Nisisako, T.; Hatsuzawa, T. Microfluidic Fabrication of Oil-Filled Polymeric Microcapsules with Independently Controllable Size and Shell Thickness via Janus to Core–Shell Evolution of Biphasic Droplets. *Sensors Actuators B Chem.* **2016**, *223*, 209–216.

(107) Xu, S.; Nie, Z.; Seo, M.; Lewis, P.; Kumacheva, E.; Stone, H. A.; Garstecki, P.; Weibel, D. B.; Gitlin, I.; Whitesides, G. M.; et al. Generation of Monodisperse Particles by Using Microfluidics: Control over Size, Shape, and Composition. *Angew. Chemie Int. Ed.* **2005**, *44* (5), 724–728.

(108) Gelin, P.; Bihi, I.; Ziemecka, I.; Thienpont, B.; Christiaens, J.; Hellemans, K.; Maes, D.; De Malsche, W. Microfluidic Device for High-Throughput Production of Monodisperse Droplets. *ACS Appl. Mater. Interfaces* **2020**, *59*.

(109) Solsona, M.; Vollenbroek, J. C.; Tregouet, C. B. M.; Nieuwelink, A. E.; Olthuis, W.; Van Den Berg, A.; Weckhuysen, B. M.; Odijk, M. Microfluidics and Catalyst Particles. *Lab Chip* **2019**, *19* (21), 3575–3601.

(110) Amoyav, B.; Benny, O. Controlled and Tunable Polymer Particles' Production Using a Single Microfluidic Device. *Appl. Nanosci.* **2018**, *8* (4), 905–914.

(111) Chen, R.; Chen, X.; Jin, X.; Zhu, X. Morphology Design and Control of Polymer Particles

by Regulating the Droplet Flowing Mode in Microfluidic Chips. *Polym. Chem.* **2017**, *8* (19), 2953–2958.

(112) Otor, H. O.; Steiner, J. B.; García-Sancho, C.; Alba-Rubio, A. C. Encapsulation Methods for Control of Catalyst Deactivation: A Review. *ACS Catalysis*. American Chemical Society July 17, 2020, pp 7630–7656.

(113) Boucher-Jacobs, C.; Rabnawaz, M.; Katz, J. S.; Even, R.; Guironnet, D. Encapsulation of Catalyst in Block Copolymer Micelles for the Polymerization of Ethylene in Aqueous Medium. *Nat. Commun.* **2018**, *9* (1), 841.

(114) Cai, G.; Ding, M.; Wu, Q.; Jiang, H. L. Encapsulating Soluble Active Species into Hollow Crystalline Porous Capsules beyond Integration of Homogeneous and Heterogeneous Catalysis. *Natl. Sci. Rev.* **2020**, *7* (1), 37–45.

(115) Zhang, X.; Hou, Y.; Ettelaie, R.; Guan, R.; Zhang, M.; Zhang, Y.; Yang, H. Pickering Emulsion-Derived Liquid-Solid Hybrid Catalyst for Bridging Homogeneous and Heterogeneous Catalysis. *J. Am. Chem. Soc.* **2019**, *141* (13), 5220–5230.

(116) Gao, C.; Lyu, F.; Yin, Y. Encapsulated Metal Nanoparticles for Catalysis. *Chemical Reviews*. American Chemical Society January 27, 2021, pp 834–881.

(117) Mei, Y.; Lu, Y.; Polzer, F.; Ballauff, M.; Drechsler, M. Catalytic Activity of Palladium Nanoparticles Encapsulated in Spherical Poly Electrolyte Brushes and Core-Shell Microgels. *Chem. Mater.* **2007**, *19* (5), 1062–1069.

(118) Cuomo, F.; Ceglie, A.; De Leonardis, A.; Lopez, F. Polymer Capsules for Enzymatic Catalysis in Confined Environments. *Catalysts*. MDPI AG January 1, 2019, p 1.

(119) Teh, S. Y.; Lin, R.; Hung, L. H.; Lee, A. P. Droplet Microfluidics. *Lab on a Chip*. Royal Society of Chemistry 2008, pp 198–220.

(120) Glawdel, T.; Elbuken, C.; Ren, C. L. Droplet Generation in Microfluidics. In *Encyclopedia of Microfluidics and Nanofluidics*; Springer US, 2013; pp 1–12.

(121) Suo, M.; Griffith, P. Two-Phase Flow in Capillary Tubes. *J. Basic Eng.* **1964**, *86* (3), 576–582.

(122) Rezkallah, K. S. Weber Number Based Flow-Pattern Maps for Liquid-Gas Flows at Microgravity. *Int. J. Multiph. Flow* **1996**, *22* (6), 1265–1270.

(123) Wehking, J. D.; Gabany, M.; Chew, L.; Kumar, R. Effects of Viscosity, Interfacial Tension, and Flow Geometry on Droplet Formation in a Microfluidic T-Junction. *Microfluid. Nanofluidics* **2014**, *16* (3), 441–453.

(124) Nunes, J. K.; Tsai, S. S. H.; Wan, J.; Stone, H. A. Dripping and Jetting in Microfluidic Multiphase Flows Applied to Particle and Fibre Synthesis. *J. Phys. D. Appl. Phys.* **2013**, *46* (11), 114002.

(125) Tanthapanichakoon, W.; Aoki, N.; Matsuyama, K.; Mae, K. Design of Mixing in Microfluidic Liquid Slugs Based on a New Dimensionless Number for Precise Reaction and Mixing Operations. *Chem. Eng. Sci.* **2006**, *61* (13), 4220–4232.

(126) Li, Y.; Reddy, R. K.; Kumar, C. S. S. R.; Nandakumar, K. Computational Investigations of the Mixing Performance inside Liquid Slugs Generated by a Microfluidic T-Junction. *Biomicrofluidics* **2014**, *8* (5), 054125.

(127) Harrier, D. D.; Kenis, P. J. A.; Guironnet, D. Ring-Opening Polymerization of Cyclic Esters in an Aqueous Dispersion. *Macromolecules* **2020**, *53* (18), 7767–7773.

(128) Wehking, J. D.; Gabany, M.; Chew, L.; Kumar, R. Effects of Viscosity, Interfacial Tension, and Flow Geometry on Droplet Formation in a Microfluidic T-Junction. *Microfluid. Nanofluidics* **2014**, *16* (3), 441–453.

(129) Nekouei, M.; Vanapalli, S. A. Volume-of-Fluid Simulations in Microfluidic T-Junction Devices: Influence of Viscosity Ratio on Droplet Size. *Phys. Fluids* **2017**, *29* (3), 032007.

(130) Urbanski, M.; Reyes, C. G.; Noh, J.; Sharma, A.; Geng, Y.; Subba Rao Jampani, V.; Lagerwall, J. P. F. Liquid Crystals in Micron-Scale Droplets, Shells and Fibers. *Journal of Physics Condensed Matter*. 2017.

(131) Adams, L. L. A.; Kodger, T. E.; Kim, S. H.; Shum, H. C.; Franke, T.; Weitz, D. A. Single Step Emulsification for the Generation of Multi-Component Double Emulsions. *Soft Matter* **2012**, *8* (41).

(132) Li, W.; Zhang, L.; Ge, X.; Xu, B.; Zhang, W.; Qu, L.; Choi, C. H.; Xu, J.; Zhang, A.; Lee, H.; et al. Microfluidic Fabrication of Microparticles for Biomedical Applications. *Chemical Society Reviews*. Royal Society of Chemistry August 7, 2018, pp 5646–5683.

(133) Lee, W.; Walker, L. M.; Anna, S. L. Role of Geometry and Fluid Properties in Droplet and Thread Formation Processes in Planar Flow Focusing. *Phys. Fluids* **2009**, *21* (3), 032103.

(134) Wang, Y.; Wu, P.; Luo, Z.; Li, Y.; Liao, M.; Li, Y.; He, L. Controllable Geometry-Mediated Droplet Fission Using "off-the-Shelf" Capillary Microfluidics Device. *RSC Adv.* **2014**, *4* (59), 31184–31187.

(135) Erb, R. M.; Obrist, D.; Chen, P. W.; Studer, J.; Studart, A. R. Predicting Sizes of Droplets Made by Microfluidic Flow-Induced Dripping. *Soft Matter* **2011**, *7* (19), 8757–8761.

(136) Geyer, R.; Jambeck, J. R.; Law, K. L. Production, Use, and Fate of All Plastics Ever Made. *Sci. Adv.* **2017**, *3* (7), e1700782.

(137) Song, R.; Murphy, M.; Li, C.; Ting, K.; Soo, C.; Zheng, Z. Current Development of Biodegradable Polymeric Materials for Biomedical Applications. *Drug Des. Devel. Ther.*

2018, *Volume 12*, 3117–3145.

(138) Armentano, I.; Dottori, M.; Fortunati, E.; Mattioli, S.; Kenny, J. M. Biodegradable

Polymer Matrix Nanocomposites for Tissue Engineering: A Review. *Polym. Degrad.*

Stab. **2010**, *95* (11), 2126–2146.

(139) Lovell, P. A. (Peter A. .; El-Aasser, M. S. *Emulsion Polymerization and Emulsion*

Polymers; J. Wiley, 1997.

(140) Nomura, M.; Tobita, H.; Suzuki, K. Emulsion Polymerization: Kinetic and Mechanistic

Aspects. *Adv. Polym. Sci.* **2005**, *175*, 1–128.

(141) Chern, C. S. Emulsion Polymerization Mechanisms and Kinetics. *Prog. Polym. Sci.* **2006**,

31 (5), 443–486.

(142) Synthetic Latex Polymers: Capacity and Manufacturing Economics Assessment. *Kline Gr.*

2017, *#Y821*.

(143) Deniau, G.; Azoulay, L.; Bougerolles, L.; Palacin, S. Surface Electroinitiated Emulsion

Polymerization: Grafted Organic Coatings from Aqueous Solutions. *Chem. Mater.* **2006**,

18 (23), 5421–5428.

(144) Tsavalas, J. G.; Sundberg, D. C. Hydroplasticization of Polymers: Model Predictions and

Application to Emulsion Polymers. *Langmuir* **2010**, *26* (10), 6960–6966.

(145) Sakdapipanich, J.; Thananusont, N.; Pukkate, N. Synthesis of Acrylate Polymers by a

Novel Emulsion Polymerization for Adhesive Applications. *J. Appl. Polym. Sci.* **2006**, *100*

(1), 413–421.

(146) Khromiak, U.; Levytskyi, V.; Stepova, K.; Tarnawsky, A. Synthesis and Properties of

Adhesive Polymer-Methylmethacrylate Materials. *Int. J. Polym. Sci.* **2018**, *2018*, 1–9.

(147) Reverchon, E.; Adami, R.; Cardea, S.; Porta, G. Della. Supercritical Fluids Processing of

Polymers for Pharmaceutical and Medical Applications. *Journal of Supercritical Fluids*. January 2009, pp 484–492.

(148) Colombo, C.; Morosi, L.; Bello, E.; Ferrari, R.; Licandro, S. A.; Lupi, M.; Ubezio, P.; Morbidelli, M.; Zucchetti, M.; DIncalci, M.; et al. PEGylated Nanoparticles Obtained through Emulsion Polymerization as Paclitaxel Carriers. *Mol. Pharm.* **2016**, *13* (1), 40–46.

(149) Soppimath, K. S.; Aminabhavi, T. M.; Kulkarni, A. R.; Rudzinski, W. E. Biodegradable Polymeric Nanoparticles as Drug Delivery Devices. *J. Control. Release* **2001**, *70* (1), 1–20.

(150) Freiberg, S.; Zhu, X. X. Polymer Microspheres for Controlled Drug Release. *International Journal of Pharmaceutics*. September 10, 2004, pp 1–18.

(151) Madhavan Nampoothiri, K.; Nair, N. R.; John, R. P. An Overview of the Recent Developments in Polylactide (PLA) Research. *Bioresour. Technol.* **2010**, *101* (22), 8493–8501.

(152) Okada, M. Chemical Syntheses of Biodegradable Polymers. *Prog. Polym. Sci.* **2002**, *27* (1), 87–133.

(153) Hopewell, J.; Dvorak, R.; Kosior, E. Plastics Recycling: Challenges and Opportunities. *Philos. Trans. R. Soc. Lond. B. Biol. Sci.* **2009**, *364* (1526), 2115–2126.

(154) Amass, W.; Amass, A.; Tighe, B. A Review of Biodegradable Polymers: Uses, Current Developments in the Synthesis and Characterization of Biodegradable Polyesters, Blends of Biodegradable Polymers and Recent Advances in Biodegradation Studies. *Polym. Int.* **1998**, *47* (2), 89–144.

(155) Tiwari, A.; Titinchi, S. *Advanced Catalytic Materials*; John Wiley & Sons, Inc.: Hoboken, NJ, USA, 2015.

(156) Siparsky, G. L.; Voorhees, K. J.; Miao, F. Hydrolysis of Polylactic Acid (PLA) and Polycaprolactone (PCL) in Aqueous Acetonitrile Solutions: Autocatalysis. *J. Polym. Environ.* **1998**, *6* (1), 31–41.

(157) Zhao, H.; Nathaniel, G. A.; Merenini, P. C. Enzymatic Ring-Opening Polymerization (ROP) of Lactides and Lactone in Ionic Liquids and Organic Solvents: Digging the Controlling Factors. *RSC Adv.* **2017**, *7* (77), 48639–48648.

(158) Mecking, S. Polymer Dispersions from Catalytic Polymerization in Aqueous Systems. *Colloid and Polymer Science*. Springer March 8, 2007, pp 605–619.

(159) Maitre, C.; Ganachaud, F.; Ferreira, O.; Lutz, J. F.; Paintoux, Y.; Hémery, P. Anionic Polymerization of Phenyl Glycidyl Ether in Miniemulsion. *Macromolecules* **2000**, *33* (21), 7730–7736.

(160) Kamber, N. E.; Jeong, W.; Waymouth, R. M.; Pratt, R. C.; Lohmeijer, B. G. G.; Hedrick, J. L. Organocatalytic Ring-Opening Polymerization. *Chem. Rev.* **2007**, *107* (12), 5813–5840.

(161) Lin, B.; Waymouth, R. M. Organic Ring-Opening Polymerization Catalysts: Reactivity Control by Balancing Acidity. *Macromolecules* **2018**, *51* (8), 2932–2938.

(162) Eckardt, O.; Wenn, B.; Biehl, P.; Junkers, T.; Schacher, F. H. Facile Photo-Flow Synthesis of Branched Poly(Butyl Acrylate)S. *React. Chem. Eng.* **2017**, *2* (4), 479–486.

(163) Seemann, R.; Brinkmann, M.; Pfohl, T.; Herminghaus, S. Droplet Based Microfluidics. *Reports Prog. Phys.* **2012**, *75* (1), 016601.

(164) Yoon, D.; Tanaka, D.; Sekiguchi, T.; Shoji, S. Structural Formation of Oil-in-Water (O/W) and Water-in-Oil-in-Water (W/O/W) Droplets in PDMS Device Using Protrusion Channel without Hydrophilic Surface Treatment. *Micromachines* **2018**, *9* (9), 468.

(165) Piccin, E.; Ferraro, D.; Sartori, P.; Chiarello, E.; Pierno, M.; Mistura, G. Generation of Water-in-Oil and Oil-in-Water Microdroplets in Polyester-Toner Microfluidic Devices. *Sensors Actuators, B Chem.* **2014**, *196*, 525–531.

(166) Pitt, C. G.; Hendren, R. W.; Schindler, A.; Woodward, S. C. The Enzymatic Surface Erosion of Aliphatic Polyesters. *J. Control. Release* **1984**, *1* (1), 3–14.

(167) Maul, J.; Frushour, B. G.; Kontoff, J. R.; Eichenauer, H.; Ott, K.-H.; Schade, C. Polystyrene and Styrene Copolymers. *Ullmann's Encycl. Ind. Chem.* **2007**.

(168) Vivaldo-Lima, E.; Wood, P. E.; Hamielec, A. E.; Penlidis, A. An Updated Review on Suspension Polymerization. *Ind. Eng. Chem. Res.* **1997**, *36* (4), 939–965.

(169) Brooks, B. Suspension Polymerization Processes. *Chem. Eng. Technol.* **2010**, *33* (11), 1737–1744.

(170) Häckl, K.; Kunz, W. Some Aspects of Green Solvents. *Comptes Rendus Chim.* **2018**, *21* (6), 572–580.

(171) Cunningham, M. F. Controlled/Living Radical Polymerization in Aqueous Dispersed Systems. *Prog. Polym. Sci.* **2008**, *33* (4), 365–398.

(172) Herzberger, J.; Niederer, K.; Pohlit, H.; Seiwert, J.; Worm, M.; Wurm, F. R.; Frey, H. Polymerization of Ethylene Oxide, Propylene Oxide, and Other Alkylene Oxides: Synthesis, Novel Polymer Architectures, and Bioconjugation. *Chem. Rev.* **2015**, *116* (4), 2170–2243.

(173) Duda, A. *ROP of Cyclic Esters: Mechanisms of Ionic and Coordination Processes*; Elsevier B.V., 2012; Vol. 4.

(174) Harrier, D. D.; Guironnet, D. Design Rules for Performing Water-Sensitive Ring-Opening Polymerizations in an Aqueous Dispersion. *Polym. Chem.* **2022**.

(175) Dinh, T.; Cubaud, T. Role of Interfacial Tension on Viscous Multiphase Flows in Coaxial Microfluidic Channels. *Langmuir* **2021**, *37* (24), 7420–7429.

(176) Zhu, P.; Wang, L. Passive and Active Droplet Generation with Microfluidics: A Review. *Lab Chip* **2017**, *17* (1), 34–75.

(177) Liu, X.; Wu, L.; Zhao, Y.; Chen, Y. Study of Compound Drop Formation in Axisymmetric Microfluidic Devices with Different Geometries. *Colloids Surfaces A Physicochem. Eng. Asp.* **2017**, *533*, 87–98.

(178) Lei, L.; Zhao, Y.; Chen, W.; Li, H.; Wang, X.; Zhang, J. Experimental Studies of Droplet Formation Process and Length for Liquid–Liquid Two-Phase Flows in a Microchannel. *Energies* **2021**, *14* (5), 1–17.

(179) Tice, J. D.; Song, H.; Lyon, A. D.; Ismagilov, R. F. Formation of Droplets and Mixing in Multiphase Microfluidics at Low Values of the Reynolds and the Capillary Numbers. *Langmuir* **2003**, *19* (22), 9127–9133.

(180) Wang, J.; Wang, J.; Feng, L.; Lin, T. Fluid Mixing in Droplet-Based Microfluidics with a Serpentine Microchannel. *RSC Adv.* **2015**, *5* (126), 104138–104144.

(181) Baret, J.-C. Surfactants in Droplet-Based Microfluidics. *Lab Chip* **2012**, *12* (3), 422–433.

(182) Harikrishnan, A. R.; Dhar, P.; Agnihotri, P. K.; Gedupudi, S.; Das, S. K. Effects of Interplay of Nanoparticles, Surfactants and Base Fluid on the Surface Tension of Nanocolloids. *Eur. Phys. J. E* **2017**, *40* (5), 1–14.

(183) Riechers, B.; Maes, F.; Akoury, E.; Semin, B.; Gruner, P.; Baret, J. C. Surfactant Adsorption Kinetics in Microfluidics. *Proc. Natl. Acad. Sci. U. S. A.* **2016**, *113* (41), 11465–11470.

(184) Pan, D.; Zhang, Y.; Zhang, T.; Li, B. Flow Regimes of Polymeric Fluid Droplet

Formation in a Co-Flowing Microfluidic Device. *Colloids Interface Sci. Commun.* **2021**, *42*, 100392.

(185) Azouz, L.; Dahmoune, F.; Rezgui, F.; G'Sell, C. Full Factorial Design Optimization of Anti-Inflammatory Drug Release by PCL-PEG-PCL Microspheres. *Mater. Sci. Eng. C* **2016**, *58*, 412–419.

(186) Maikawa, C. L.; Sevit, A.; Lin, B.; Wallstrom, R. J.; Mann, J. L.; Yu, A. C.; Waymouth, R. M.; Appel, E. A. Block Copolymer Composition Drives Function of Self-Assembled Nanoparticles for Delivery of Small-Molecule Cargo. *J. Polym. Sci. Part A Polym. Chem.* **2019**, *57* (12), 1322–1332.

(187) Walsh, D. J.; Wade, M. A.; Rogers, S. A.; Guironnet, D. Challenges of Size-Exclusion Chromatography for the Analysis of Bottlebrush Polymers. *Macromolecules* **2020**, *53* (19), 8610–8620.

(188) Pasquali, R. C.; Taurozzi, M. P.; Bregni, C. Some Considerations about the Hydrophilic-Lipophilic Balance System. *Int. J. Pharm.* **2008**, *356* (1–2), 44–51.

(189) Ohba, N. Hydrophile-Lipophile Balance Values for O/W Emulsions Stabilized by Nonionic Surfactants. I. Hydrophile-Lipophile Balance Values of Nonionic Surfactants Determined by Emulsification. *Bull. Chem. Soc. Jpn.* **1962**, *35* (6), 1016–1020.

(190) Muranaka, M.; Hirota, K.; Ono, T. PEG–PLA Nanoparticles Prepared by Emulsion Solvent Diffusion Using Oil-Soluble and Water-Soluble PEG–PLA. *Mater. Lett.* **2010**, *64* (8), 969–971.

(191) Chen, Y.; Shen, J.; Liu, S.; Zhao, J.; Wang, Y.; Zhang, G. High Efficiency Organic Lewis Pair Catalyst for Ring-Opening Polymerization of Epoxides with Chemoselectivity. *Macromolecules* **2018**, *51* (20), 8286–8297.

(192) Zhao, J.; Hadjichristidis, N.; Gnanou, Y. Phosphazene-Promoted Anionic Polymerization. *Polimery* **2014**, *59* (01), 49–59.

(193) Yang, J.-L.; Wu, H.-L.; Li, Y.; Zhang, X.-H.; Darensbourg, D. J. Perfectly Alternating and Regioselective Copolymerization of Carbonyl Sulfide and Epoxides by Metal-Free Lewis Pairs. *Angew. Chemie* **2017**, *129* (21), 5868–5873.

(194) Boileau, S.; Illy, N. Activation in Anionic Polymerization: Why Phosphazene Bases Are Very Exciting Promoters. *Prog. Polym. Sci.* **2011**, *36* (9), 1132–1151.

(195) Herzberger, J.; Niederer, K.; Pohlit, H.; Seiwert, J.; Worm, M.; Wurm, F. R.; Frey, H. Polymerization of Ethylene Oxide, Propylene Oxide, and Other Alkylene Oxides: Synthesis, Novel Polymer Architectures, and Bioconjugation. *Chem. Rev.* **2016**, *116* (4), 2170–2243.

(196) Uhrich, K. E.; Cannizzaro, S. M.; Langer, R. S.; Shakesheff, K. M. Polymeric Systems for Controlled Drug Release. *Chem. Rev.* **1999**, *99* (11), 3181–3198.

(197) Lee, J. H.; Yeo, Y. Controlled Drug Release from Pharmaceutical Nanocarriers. *Chem. Eng. Sci.* **2015**, *125*, 75–84.

(198) Huynh, C. T.; Lee, D. S. Controlled Release. In *Encyclopedia of Polymeric Nanomaterials*; Springer Berlin Heidelberg: Berlin, Heidelberg, 2015; pp 439–449.

(199) Sinha, V. R.; Trehan, A. Biodegradable Microspheres for Protein Delivery. *Journal of Controlled Release*. Elsevier July 31, 2003, pp 261–280.

(200) Tiwari, G.; Tiwari, R.; Sriwastawa, B.; Bhati, L.; Pandey, S.; Pandey, P.; Bannerjee, S. K. Drug Delivery Systems: An Updated Review. *Int. J. Pharm. Investig.* **2012**, *2* (1), 2.

(201) Adepu, S.; Ramakrishna, S.; Costa-Pinto, R.; Oliveira, A. L. Controlled Drug Delivery Systems: Current Status and Future Directions. *Mol. 2021, Vol. 26, Page 5905* **2021**, *26*

(19), 5905.

(202) Zhu, M.; Whittaker, A. K.; Han, F. Y.; Smith, M. T. Journey to the Market: The Evolution of Biodegradable Drug Delivery Systems. *Appl. Sci. 2022, Vol. 12, Page 935* **2022**, *12* (2), 935.

(203) Pillai, O.; Panchagnula, R. Polymers in Drug Delivery. *Current Opinion in Chemical Biology*. Elsevier Current Trends August 1, 2001, pp 447–451.

(204) Abasian, P.; Ghanavati, S.; Rahebi, S.; Nouri Khorasani, S.; Khalili, S. Polymeric Nanocarriers in Targeted Drug Delivery Systems: A Review. *Polymers for Advanced Technologies*. 2020, pp 2939–2954.

(205) Kamaly, N.; Yameen, B.; Wu, J.; Farokhzad, O. C. Degradable Controlled-Release Polymers and Polymeric Nanoparticles: Mechanisms of Controlling Drug Release. *Chemical Reviews*. NIH Public Access February 24, 2016, pp 2602–2663.

(206) Sonam, S.; Chaudhary, H.; Arora, V.; Kholi, K.; Kumar, V. Effect of Physicochemical Properties of Biodegradable Polymers on Nano Drug Delivery. *Polym. Rev.* **2013**, *53* (4), 546–567.

(207) Trucillo, P. Drug Carriers: Classification, Administration, Release Profiles, and Industrial Approach. *Processes* **2021**, *9* (3), 470.

(208) Srivastava, A.; Yadav, T.; Sharma, S.; Nayak, A.; Kumari, A. A.; Mishra, N.; Srivastava, A.; Yadav, T.; Sharma, S.; Nayak, A.; et al. Polymers in Drug Delivery. *J. Biosci. Med.* **2015**, *4* (1), 69–84.

(209) Idrees, H.; Zaidi, S. Z. J.; Sabir, A.; Khan, R. U.; Zhang, X.; Hassan, S. U. A Review of Biodegradable Natural Polymer-Based Nanoparticles for Drug Delivery Applications. *Nanomaterials*. Multidisciplinary Digital Publishing Institute (MDPI) October 1, 2020, pp

1–22.

(210) Pang, X.; Yang, X.; Zhai, G. Polymer-Drug Conjugates: Recent Progress on Administration Routes. *Expert Opin. Drug Deliv.* **2014**, *11* (7), 1075–1086.

(211) Liechty, W. B.; Kryscio, D. R.; Slaughter, B. V.; Peppas, N. A. Polymers for Drug Delivery Systems. *Annu. Rev. Chem. Biomol. Eng.* **2010**, *1*, 149–173.

(212) Leenslag, J. W.; Pennings, A. J.; Bos, R. R. M.; Rozema, F. R.; Boering, G. Resorbable Materials of Poly(l-Lactide). VI. Plates and Screws for Internal Fracture Fixation. *Biomaterials* **1987**, *8* (1), 70–73.

(213) Freed, L. E.; Marquis, J. C.; Nohria, A.; Emmanual, J.; Mikos, A. G.; Langer, R. Neocartilage Formation in Vitro and in Vivo Using Cells Cultured on Synthetic Biodegradable Polymers. *J. Biomed. Mater. Res.* **1993**, *27* (1), 11–23.

(214) Holland, S. J.; Tighe, B. J.; Gould, P. L. Polymers for Biodegradable Medical Devices. 1. The Potential of Polyesters as Controlled Macromolecular Release Systems. *J. Control. Release* **1986**, *4* (3), 155–180.

(215) Dai, H.; Kramer, E. J.; J Frechet, J. M.; Creton, C.; Xiao, F.; Hui, C. Y.; Powers, W.; Wang, H. C.; Handy, D. C.; Fusco, J. V; et al. New Challenges in Biomaterials. *Science (80-.).* **1994**, *263* (5154), 1715–1720.

(216) Benicewicz, B. C.; Hopper, P. K. Review : Polymers for Absorbable Surgical Sutures— Part II. *J. Bioact. Compat. Polym.* **1991**, *6* (1), 64–94.

(217) Sung, Y. K.; Kim, S. W. Recent Advances in Polymeric Drug Delivery Systems. *Biomater. Res. 2020 241* **2020**, *24* (1), 1–12.

(218) Kreua-ongarjnukool, N.; Soomherun, N.; Thumsing Niyomthai, S.; Chumnanvej, S. Aliphatic Polyester Nanoparticles for Drug Delivery Systems. In *Smart Drug Delivery*;

IntechOpen, 2021.

(219) Urbánek, T.; Jäger, E.; Jäger, A.; Hrubý, M. Selectively Biodegradable Polyesters: Nature-Inspired Construction Materials for Future Biomedical Applications. *Polymers*. Multidisciplinary Digital Publishing Institute June 19, 2019, p 1061.

(220) Brannigan, R. P.; Dove, A. P. Synthesis, Properties and Biomedical Applications of Hydrolytically Degradable Materials Based on Aliphatic Polyesters and Polycarbonates. *Biomaterials Science*. Royal Society of Chemistry December 20, 2017, pp 9–21.

(221) Urbánek, T.; Jäger, E.; Jäger, A.; Hrubý, M. Selectively Biodegradable Polyesters: Nature-Inspired Construction Materials for Future Biomedical Applications. *Polymers (Basel).* **2019**, *11* (6), 1061.

(222) Stewart, S. A.; Domínguez-Robles, J.; Donnelly, R. F.; Larrañeta, E. Implantable Polymeric Drug Delivery Devices: Classification, Manufacture, Materials, and Clinical Applications. *Polymers*. Multidisciplinary Digital Publishing Institute December 12, 2018, p 1379.

(223) Indurkhya, A.; Patel, M.; Sharma, P.; Abed, S. N.; Shnoudeh, A.; Maheshwari, R.; Deb, P. K.; Tekade, R. K. Influence of Drug Properties and Routes of Drug Administration on the Design of Controlled Release System. *Dos. Form Des. Considerations Vol. I* **2018**, 179–223.

(224) Bhattacharjee, S. Understanding the Burst Release Phenomenon: Toward Designing Effective Nanoparticulate Drug-Delivery Systems. *Therapeutic Delivery*. Newlands Press Ltd London, UK January 23, 2021, pp 21–36.

(225) Borowy, C. S.; Ashurst, J. V. *Physiology, Zero and First Order Kinetics*; StatPearls Publishing, 2019.

(226) Laracuente, M. L.; Yu, M. H.; McHugh, K. J. Zero-Order Drug Delivery: State of the Art and Future Prospects. *J. Control. Release* **2020**, *327*, 834–856.

(227) Son, G. H.; Lee, B. J.; Cho, C. W. Mechanisms of Drug Release from Advanced Drug Formulations Such as Polymeric-Based Drug-Delivery Systems and Lipid Nanoparticles. *Journal of Pharmaceutical Investigation*. Springer Netherlands July 1, 2017, pp 287–296.

(228) Siepmann, J.; Siepmann, F. Modeling of Diffusion Controlled Drug Delivery. *Journal of Controlled Release*. J Control Release July 20, 2012, pp 351–362.

(229) Siepmann, J.; Lecomte, F.; Bodmeier, R. Diffusion-Controlled Drug Delivery Systems: Calculation of the Required Composition to Achieve Desired Release Profiles. *J. Control. Release* **1999**, *60* (2–3), 379–389.

(230) Siepmann, J.; Siegel, R. A.; Siepmann, F. Diffusion Controlled Drug Delivery Systems. In *Fundamentals and Applications of Controlled Release Drug Delivery*; Springer US: Boston, MA, 2012; pp 127–152.

(231) Fan, L.; Singh, S. K. Diffusion-Controlled Release. In *Controlled Release*; Springer, Berlin, Heidelberg, 1989; pp 9–88.

(232) Carbinatto, F. M.; de Castro, A. D.; Evangelista, R. C.; Cury, B. S. F. Insights into the Swelling Process and Drug Release Mechanisms from Cross-Linked Pectin/High Amylose Starch Matrices. *Asian J. Pharm. Sci.* **2014**, *9* (1), 27–34.

(233) Keraliya, R. A.; Patel, C.; Patel, P.; Keraliya, V.; Soni, T. G.; Patel, R. C.; Patel, M. M. Osmotic Drug Delivery System as a Part of Modified Release Dosage Form. *ISRN Pharm.* **2012**, *2012*, 1–9.

(234) Behzadi, S.; Rosenauer, C.; Kappl, M.; Mohr, K.; Landfester, K.; Crespy, D. Osmotic Pressure-Dependent Release Profiles of Payloads from Nanocontainers by Co-

Encapsulation of Simple Salts. *Nanoscale* **2016**, *8* (26), 12998–13005.

(235) Babasola, I. O.; Zhang, W.; Amsden, B. G. Osmotic Pressure Driven Protein Release from Viscous Liquid, Hydrophobic Polymers Based on 5-Ethylene Ketal ε-Caprolactone: Potential and Mechanism. *Eur. J. Pharm. Biopharm.* **2013**, *85* (3 PART A), 765–772.

(236) Zhang, W.; Qu, L.; Pei, H.; Qin, Z.; Didier, J.; Wu, Z.; Bobe, F.; Ingber, D. E.; Weitz, D. A. Controllable Fabrication of Inhomogeneous Microcapsules for Triggered Release by Osmotic Pressure. *Small* **2019**, *15* (42), 1903087.

(237) Zhang, A.; Jung, K.; Li, A.; Liu, J.; Boyer, C. Recent Advances in Stimuli-Responsive Polymer Systems for Remotely Controlled Drug Release. *Progress in Polymer Science*. Pergamon December 1, 2019, p 101164.

(238) Wells, C. M.; Harris, M.; Choi, L.; Murali, V. P.; Guerra, F. D.; Jennings, J. A. Stimuli-Responsive Drug Release from Smart Polymers. *Journal of Functional Biomaterials*. Multidisciplinary Digital Publishing Institute July 31, 2019, p 34.

(239) Wang, Y.; Shim, M. S.; Levinson, N. S.; Sung, H. W.; Xia, Y. Stimuli-Responsive Materials for Controlled Release of Theranostic Agents. *Adv. Funct. Mater.* **2014**, *24* (27), 4206–4220.

(240) Priya James, H.; John, R.; Alex, A.; Anoop, K. R. Smart Polymers for the Controlled Delivery of Drugs – a Concise Overview. *Acta Pharm. Sin. B* **2014**, *4* (2), 120–127.

(241) Faÿ, F.; Linossier, I.; Langlois, V.; Renard, E.; Vallée-Réhel, K. Degradation and Controlled Release Behavior ε-Caprolactone Copolymers in Biodegradable Antifouling Coatings. *Biomacromolecules* **2006**, *7* (3), 851–857.

(242) Woodard, L. N.; Grunlan, M. A. Hydrolytic Degradation and Erosion of Polyester Biomaterials. *ACS Macro Lett.* **2018**, *7* (8), 976–982.

(243) Cha, Y.; Pitt, C. G. The Acceleration of Degradation-Controlled Drug Delivery from Polyester Microspheres. *J. Control. Release* **1989**, *8* (3), 259–265.

(244) Mohamed, F.; Van Der Walle, C. F. Engineering Biodegradable Polyester Particles With Specific Drug Targeting and Drug Release Properties. *J. Pharm. Sci.* **2008**, *97* (1), 71–87.

(245) Pandey, S. P.; Shukla, T.; Dhote, V. K.; Mishra, D. K.; Maheshwari, R.; Tekade, R. K. Use of Polymers in Controlled Release of Active Agents. In *Basic Fundamentals of Drug Delivery*; Academic Press, 2018; pp 113–172.

(246) Burkersroda, F. Von; Schedl, L.; Göpferich, A. Why Degradable Polymers Undergo Surface Erosion or Bulk Erosion. *Biomaterials* **2002**, *23* (21), 4221–4231.

(247) Rothstein, S. N.; Federspiel, W. J.; Little, S. R. A Unified Mathematical Model for the Prediction of Controlled Release from Surface and Bulk Eroding Polymer Matrices. *Biomaterials* **2009**, *30* (8), 1657–1664.

(248) Göpferich, A. Polymer Bulk Erosion. *Macromolecules* **1997**, *30* (9), 2598–2604.

(249) Tamada, J. A.; Langer, R. Erosion Kinetics of Hydrolytically Degradable Polymers. *Proc. Natl. Acad. Sci. U. S. A.* **1993**, *90* (2), 552–556.

(250) Göpferich, A.; Langer, R. Modeling of Polymer Erosion in Three Dimensions: Rotationally Symmetric Devices. *AIChE J.* **1995**, *41* (10), 2292–2299.

(251) Göpferich, A. Mechanisms of Polymer Degradation and Erosion1. In *The Biomaterials: Silver Jubilee Compendium*; Elsevier Science, 1996; pp 117–128.

(252) Shi, Z.; Zhou, Y.; Yan, D. Preparation of Robust Poly(ε-Caprolactone) Hollow Spheres with Controlled Biodegradability. *Macromol. Rapid Commun.* **2006**, *27* (15), 1265–1270.

(253) Erdal, N. B.; Lando, G. A.; Yadav, A.; Srivastava, R. K.; Hakkarainen, M. Hydrolytic Degradation of Porous Crosslinked Poly(ε-Caprolactone) Synthesized by High Internal

Phase Emulsion Templating. *Polymers (Basel)*. **2020**, *12* (8), 1849.

(254) Andronova, N.; Srivastava, R. K.; Albertsson, A.-C. Potential Tissue Implants from the Networks Based on 1,5-Dioxepan-2-One and ε-Caprolactone. *Polymer (Guildf)*. **2005**, *46* (18), 6746–6755.

(255) Palmgren, R.; Karlsson, S.; Albertsson, A. C. Synthesis of Degradable Crosslinked Polymers Based on 1,5-Dioxepan-2-One and Crosslinker of Bis-ε-Caprolactone Type. *J. Polym. Sci. Part A Polym. Chem.* **1997**, *35* (9), 1635–1649.

(256) Tong, R.; Cheng, J. Paclitaxel-Initiated, Controlled Polymerization of Lactide for the Formulation of Polymeric Nanoparticulate Delivery Vehicles. *Angew. Chemie Int. Ed.* **2008**, *47* (26), 4830–4834.

(257) Tong, R.; Cheng, J. Drug-Initiated, Controlled Ring-Opening Polymerization for the Synthesis of Polymer–Drug Conjugates. *Macromolecules* **2012**, *45* (5), 2225–2232.

(258) Nakielski, P.; Kowalczyk, T.; Zembrzycki, K.; Kowalewski, T. A. Experimental and Numerical Evaluation of Drug Release from Nanofiber Mats to Brain Tissue. *J. Biomed. Mater. Res. - Part B Appl. Biomater.* **2015**, *103* (2), 282–291.

(259) Sindhwani, N.; Ivanchenko, O.; Lueshen, E.; Prem, K.; Linninger, A. A. Methods for Determining Agent Concentration Profiles in Agarose Gel during Convection-Enhanced Delivery. *IEEE Trans. Biomed. Eng.* **2011**, *58* (3 PART 1), 626–632.

(260) Chen, Z. J.; Broaddus, W. C.; Viswanathan, R. R.; Raghavan, R.; Gillies, G. T. Intraparenchymal Drug Delivery via Positive-Pressure Infusion: Experimental and Modeling Studies of Poroelasticity in Brain Phantom Gels. *IEEE Trans. Biomed. Eng.* **2002**, *49* (2), 85–96.

(261) Bąk, A.; Podgórska, W. Interfacial and Surface Tensions of Toluene/Water and Air/Water

Systems with Nonionic Surfactants Tween 20 and Tween 80. *Colloids Surfaces A Physicochem. Eng. Asp.* **2016**, *504*, 414–425.

(262) Lombardo, D.; Kiselev, M. A.; Magazù, S.; Calandra, P. Amphiphiles Self-Assembly: Basic Concepts and Future Perspectives of Supramolecular Approaches. *Adv. Condens. Matter Phys.* **2015**, *2015*, 1–22.

(263) Cui, X.; Mao, S.; Liu, M.; Yuan, H.; Du, Y. Mechanism of Surfactant Micelle Formation. *Langmuir* **2008**, *24* (19), 10771–10775.

(264) Glotzer, S. C.; Solomon, M. J. Anisotropy of Building Blocks and Their Assembly into Complex Structures. *Nat. Mater.* **2007**, *6* (8), 557–562.

(265) Dong, Y.; Liu, P. Amphiphilic Triblock Copolymer Prodrug for Tumor-Specific PH/Reduction Dual-Triggered Drug Delivery: Effect of Self-Assembly Behaviors. *Langmuir* **2021**, *37* (24), 7356–7363.

(266) Chen, P. C.; Lai, J. J.; Huang, C. J. Bio-Inspired Amphoteric Polymer for Triggered-Release Drug Delivery on Breast Cancer Cells Based on Metal Coordination. *ACS Appl. Mater. Interfaces* **2021**, *13* (22), 25663–25673.

(267) Adams, M. L.; Lavasanifar, A.; Kwon, G. S. Amphiphilic Block Copolymers for Drug Delivery. *Journal of Pharmaceutical Sciences*. Elsevier July 1, 2003, pp 1343–1355.

(268) Gaucher, G.; Dufresne, M. H.; Sant, V. P.; Kang, N.; Maysinger, D.; Leroux, J. C. Block Copolymer Micelles: Preparation, Characterization and Application in Drug Delivery. In *Journal of Controlled Release*; Elsevier, 2005; Vol. 109, pp 169–188.

(269) Allen, C.; Maysinger, D.; Eisenberg, A. Nano-Engineering Block Copolymer Aggregates for Drug Delivery. *Colloids Surfaces B Biointerfaces* **1999**, *16* (1–4), 3–27.

(270) Bhatt, P.; Trehan, S.; Inamdar, N.; Mourya, V. K.; Misra, A. Polymers in Drug Delivery:

An Update. In *Applications of Polymers in Drug Delivery*; Elsevier, 2021; pp 1–42.

(271) Zhang, Q.; Wang, R.; Chen, Y.; Zhang, L.; Tan, J. Block Copolymer Vesicles with Tunable Membrane Thicknesses and Compositions Prepared by Aqueous Seeded Photoinitiated Polymerization-Induced Self-Assembly at Room Temperature. *Langmuir* **2022**, *38* (8), 2699–2710.

(272) Gigmes, D.; Trimaille, T. Advances in Amphiphilic Polylactide/Vinyl Polymer Based Nano-Assemblies for Drug Delivery. *Advances in Colloid and Interface Science*. Elsevier August 1, 2021, p 102483.

(273) Li, Z.; Lin, Z. Self-Assembly of Block Copolymers for Biological Applications. *Polym. Int.* **2022**, *71* (4), 366–370.

(274) Karayianni, M.; Pispas, S. Block Copolymer Solution Self-Assembly: Recent Advances, Emerging Trends, and Applications. *Journal of Polymer Science*. John Wiley & Sons, Ltd September 1, 2021, pp 1874–1898.

(275) Oliveira, A. S. R.; Mendonça, P. V.; Simões, S.; Serra, A. C.; Coelho, J. F. J. Amphiphilic Well-Defined Degradable Star Block Copolymers by Combination of Ring-Opening Polymerization and Atom Transfer Radical Polymerization: Synthesis and Application as Drug Delivery Carriers. *Journal of Polymer Science*. John Wiley & Sons, Ltd February 1, 2021, pp 211–229.

(276) Ray, P.; Kale, N.; Quadir, M. New Side Chain Design for PH-Responsive Block Copolymers for Drug Delivery. *Colloids Surfaces B Biointerfaces* **2021**, *200*, 111563.

(277) Du, J.; Fan, L.; Liu, Q. PH-Sensitive Block Copolymer Vesicles with Variable Trigger Points for Drug Delivery. *Macromolecules* **2012**, *45* (20), 8275–8283.

(278) Ohta, S.; Kikuchi, E.; Ishijima, A.; Azuma, T.; Sakuma, I.; Ito, T. Investigating the

Optimum Size of Nanoparticles for Their Delivery into the Brain Assisted by Focused Ultrasound-Induced Blood–Brain Barrier Opening. *Sci. Reports 2020 101* **2020**, *10* (1), 1–13.

(279) Patra, J. K.; Das, G.; Fraceto, L. F.; Campos, E. V. R.; Rodriguez-Torres, M. D. P.; Acosta-Torres, L. S.; Diaz-Torres, L. A.; Grillo, R.; Swamy, M. K.; Sharma, S.; et al. Nano Based Drug Delivery Systems: Recent Developments and Future Prospects. *J. Nanobiotechnology 2018 161* **2018**, *16* (1), 1–33.

(280) Gaumet, M.; Vargas, A.; Gurny, R.; Delie, F. Nanoparticles for Drug Delivery: The Need for Precision in Reporting Particle Size Parameters. *Eur. J. Pharm. Biopharm.* **2008**, *69* (1), 1–9.

(281) Sen Gupta, A. Role of Particle Size, Shape, and Stiffness in Design of Intravascular Drug Delivery Systems: Insights from Computations, Experiments, and Nature. *Wiley Interdiscip. Rev. Nanomedicine Nanobiotechnology* **2016**, *8* (2), 255–270.

(282) Chen, W.; Palazzo, A.; Hennink, W. E.; Kok, R. J. Effect of Particle Size on Drug Loading and Release Kinetics of Gefitinib-Loaded PLGA Microspheres. *Mol. Pharm.* **2017**, *14* (2), 459–467.

(283) Langer, R. New Methods of Drug Delivery. *Science.* **1990**, *249* (4976), 1527–1533.

(284) Nakamura, H.; Watano, S. Direct Permeation of Nanoparticles across Cell Membrane: A Review. *KONA Powder Part J.* **2018**, *35* (35), 49–65.

(285) J, C. T.; Shikha, S.; Ramesh, R. Nanotechnology: Interdisciplinary Science of Applications. *Afr J Biotechnol.* **2013**, *12* (3), 219–226.

(286) De Jong, W. H.; Hagens, W. I.; Krystek, P.; Burger, M. C.; Sips, A. J. A. M.; Geertsma, R. E. Particle Size-Dependent Organ Distribution of Gold Nanoparticles after Intravenous

Administration. *Biomaterials.* **2008**, *29* (12), 1912–1919.

(287) Chenthamara, D.; Subramaniam, S.; Ramakrishnan, S. G.; Krishnaswamy, S.; Essa, M. M.; Lin, F. H.; Qoronfleh, M. W. Therapeutic Efficacy of Nanoparticles and Routes of Administration. *Biomater. Res. 2019 231* **2019**, *23* (1), 1–29.

(288) Danaei, M.; Dehghankhold, M.; Ataei, S.; Hasanzadeh Davarani, F.; Javanmard, R.; Dokhani, A.; Khorasani, S.; Mozafari, M. R. Impact of Particle Size and Polydispersity Index on the Clinical Applications of Lipidic Nanocarrier Systems. *Pharmaceutics* **2018**, *10* (2).

(289) Dreifuss, T.; Betzer, O.; Barnoy, E.; Motiei, M.; Popovtzer, R. The Effect of Nanoparticle Size on Theranostic Systems: The Optimal Particle Size for Imaging Is Not Necessarily Optimal for Drug Delivery. *https://doi.org/10.1117/12.2287392* **2018**, *10506*, 130–137.

(290) Hoshyar, N.; Gray, S.; Han, H.; Bao, G. The Effect of Nanoparticle Size on in Vivo Pharmacokinetics and Cellular Interaction. *Nanomedicine* **2016**, *11* (6), 673.

(291) Makgwane, P. R.; Ray, S. S. Synthesis of Nanomaterials by Continuous-Flow Microfluidics: A Review. *J. Nanosci. Nanotechnol.* **2014**, *14* (2), 1338–1363.

(292) Salafi, T.; Zeming, K. K.; Zhang, Y. Advancements in Microfluidics for Nanoparticle Separation. *Lab Chip* **2016**, *17* (1), 11–33.

(293) Dev, S.; Iyer, K. S.; Raston, C. L. Nanosized Drug Formulations under Microfluidic Continuous Flow. *Lab Chip* **2011**, *11* (19), 3214–3217.

(294) Hamdallah, S. I.; Zoqlam, R.; Erfle, P.; Blyth, M.; Alkilany, A. M.; Dietzel, A.; Qi, S. Microfluidics for Pharmaceutical Nanoparticle Fabrication: The Truth and the Myth. *Int. J. Pharm.* **2020**, *584*, 119408.

(295) Kim, H.; Sung, J.; Chang, Y.; Alfeche, A.; Leal, C. Microfluidics Synthesis of Gene

Silencing Cubosomes. *ACS Nano* **2018**, *12* (9), 9196–9205.

(296) Satish, C.; Satish, K.; Shivakumar, H. Hydrogels as Controlled Drug Delivery Systems: Synthesis, Crosslinking, Water and Drug Transport Mechanism. *Indian J. Pharm. Sci.* **2006**, *68* (2), 133–140.

(297) Uddin, M. S.; Ju, J. Effect of Crosslinking Agents on Drug Distribution in Chitosan Hydrogel for Targeted Drug Delivery to Treat Cancer. *J. Polym. Res.* **2020**, *27* (3), 1–10.

(298) Fan, W.; Zhang, L.; Li, Y.; Wu, H. Recent Progress of Crosslinking Strategies for Polymeric Micelles with Enhanced Drug Delivery in Cancer Therapy. *Curr. Med. Chem.* **2017**, *26* (13), 2356–2376.

(299) Thakur, G.; Rodrigues, F. C.; Singh, K. Crosslinking Biopolymers for Advanced Drug Delivery and Tissue Engineering Applications. *Adv. Exp. Med. Biol.* **2018**, *1078*, 213–231.

(300) Bhattacharjee, P.; Ahearne, M. Significance of Crosslinking Approaches in the Development of next Generation Hydrogels for Corneal Tissue Engineering. *Pharmaceutics*. Multidisciplinary Digital Publishing Institute February 28, 2021, pp 1–24.

(301) Sood, A.; Gupta, A.; Agrawal, G. Recent Advances in Polysaccharides Based Biomaterials for Drug Delivery and Tissue Engineering Applications. *Carbohydr. Polym. Technol. Appl.* **2021**, *2*, 100067.

(302) Le Devedec, F.; Boucher, H.; Dubins, D.; Allen, C. Factors Controlling Drug Release in Cross-Linked Poly(Valerolactone) Based Matrices. *Mol. Pharm.* **2018**, *15* (4), 1565–1577.

(303) Bao, Z.; Jung, S.; Bufton, J.; Evans, J. C.; Aguiar, D. J.; Allen, C. Poly(δ-Valerolactone-Co-Allyl-δ-Valerolactone) Cross-Linked Microparticles: Formulation, Characterization and Biocompatibility. *J. Pharm. Sci.* **2021**, *110* (7), 2771–2777.

(304) Bufton, J.; Jung, S.; Evans, J. C.; Bao, Z.; Aguiar, D.; Allen, C. Cross-Linked Valerolactone Copolymer Implants with Tailorable Biodegradation, Loading and in Vitro Release of Paclitaxel. *Eur. J. Pharm. Sci.* **2021**, *162*, 105808.

(305) Tsoi, K. M.; Macparland, S. A.; Ma, X. Z.; Spetzler, V. N.; Echeverri, J.; Ouyang, B.; Fadel, S. M.; Sykes, E. A.; Goldaracena, N.; Kaths, J. M.; et al. Mechanism of Hard-Nanomaterial Clearance by the Liver. *Nat. Mater.* **2016**, *15* (11), 1212–1221.

(306) Yang, Y.; Chen, Q.; Lin, J.; Cai, Z.; Liao, G.; Wang, K.; Bai, L.; Zhao, P.; Yu, Z. Recent Advance in Polymer Based Microspheric Systems for Controlled Protein and Peptide Delivery. *Curr. Med. Chem.* **2019**, *26* (13), 2285–2296.

(307) Sung, Y. K.; Kim, S. W. Recent Advances in Polymeric Drug Delivery Systems. *Biomater. Res.* **2020**, *24* (1).

(308) Liechty, W. B.; Kryscio, D. R.; Slaughter, B. V.; Peppas, N. A. Polymers for Drug Delivery Systems. *Annu. Rev. Chem. Biomol. Eng.* **2010**, *1*, 149–173.

(309) Srivastava, A.; Yadav, T.; Sharma, S.; Nayak, A.; Akanksha Kumari, A.; Mishra, N. Polymers in Drug Delivery. *J. Biosci. Med.* **2016**, *04* (01), 69–84.

(310) Bari, E.; Perteghella, S.; Torre, M. L. CHAPTER 1 Micro and Nano-Drug Delivery Systems. *Silk-based Drug Deliv. Syst.* **2020**, 1–24.

(311) Di, J.; Gao, X.; Du, Y.; Zhang, H.; Gao, J.; Zheng, A. Size, Shape, Charge and "Stealthy" Surface: Carrier Properties Affect the Drug Circulation Time in Vivo. *Asian J. Pharm. Sci.* **2021**, *16* (4), 444–458.

(312) Qin, X.; Li, Y. Strategies To Design and Synthesize Polymer-Based Stimuli-Responsive Drug-Delivery Nanosystems. *ChemBioChem*. John Wiley & Sons, Ltd May 4, 2020, pp 1236–1253.

(313) Sun, W.; Jiang, H.; Wu, X.; Xu, Z.; Yao, C.; Wang, J.; Qin, M.; Jiang, Q.; Wang, W.; Shi, D.; et al. Strong Dual-Crosslinked Hydrogels for Ultrasound-Triggered Drug Delivery. *Nano Res.* **2019**, *12* (1), 115–119.

(314) Dharmaratne, N. U.; Pothupitiya, J. U.; Kiesewetter, M. K. C. *Org. Biomol. Chem.* **2019**, *17* (13), 3305–3313.

(315) Huang, X.; Zhuang, T.; Kates, P. A.; Gao, H.; Chen, X.; Groves, J. T. Alkyl Isocyanates via Manganese-Catalyzed C–H Activation for the Preparation of Substituted Ureas. *J. Am. Chem. Soc.* **2017**, *139* (43), 15407–15413.

(316) Sugiura, S.; Nakajima, M.; Iwamoto, S.; Seki, M. Interfacial Tension Driven Monodispersed Droplet Formation from Microfabricated Channel Array. *Langmuir* **2001**, *17* (18), 5562–5566.

(317) Shen, C.; Liu, F.; Wu, L.; Yu, C.; Yu, W. Dripping, Jetting and Regime Transition of Droplet Formation in a Buoyancy-Assisted Microfluidic Device. *Micromachines* **2020**, *11* (11), 962.

(318) Gupta, M. K.; Walthall, J. M.; Venkataraman, R.; Crowder, S. W.; Jung, D. K.; Yu, S. S.; Feaster, T. K.; Wang, X.; Giorgio, T. D.; Hong, C. C.; et al. Combinatorial Polymer Electrospun Matrices Promote Physiologically-Relevant Cardiomyogenic Stem Cell Differentiation. *PLoS One* **2011**, *6* (12), e28935.